R75AEG504
NASA CR-135254

QUIET CLEAN SHORT-HAUL EXPERIMENTAL ENGINE (QCSEE)

Acoustic and Aerodynamic Tests on a Scale Model Over-the-Wing Thrust Reverser and Forward Thrust Nozzle

January 18, 1978

by

D.L. Stimpert

GENERAL ELECTRIC COMPANY

National Aeronautics and Space Administration

NASA Lewis Research Center
Contract NAS3-18021

FOREWORD

The assistance of Messrs. M.R. Woodruff and R.G. Siegfried during the course of this test program is appreciated. M.R. Woodruff was responsible for the design of the hardware and coordinated with the vendor during its manufacture. R.G. Siegfried was responsible for the analysis of the aerodynamic results which are presented in Section VI.

TABLE OF CONTENTS

Section		Page
I	SUMMARY	1
II	INTRODUCTION	2
III	TEST FACILITY	3
IV	TEST VEHICLE AND HARDWARE	6
V	DATA ACQUISITION AND REDUCTION	16
	A. Aerodynamic	16
	B. Acoustic	16
VI	AERODYNAMIC RESULTS	22
VII	ACOUSTIC RESULTS	37
	A. Forward Thrust	37
	1. Cruise Nozzle	37
	2. Takeoff Nozzle	37
	3. Takeoff and Cruise Nozzle Comparison	42
	B. Reverse Thrust	42
	1. Spacing Effects	42
	2. Blocker Height Effects	51
	3. Lip Angle and Length Effects	51
	4. Summary of Geometry Effects	51
	5. Thrust Reverser Orientation	64
VIII	CONCLUSIONS	74
IX	NOMENCLATURE	75
X	REFERENCES	76

LIST OF ILLUSTRATIONS

Figure		Page
1.	Schematic of Coannular Flow JENOTS Facility.	4
2.	Photograph of the Coannular Flow JENOTS Facility.	5
3.	OTW Model Forward Thrust Cruise Nozzle Installation.	8
4.	Forward Thrust Cruise Nozzle Schematic.	9
5.	Forward Thrust Cruise Nozzle.	10
6.	Forward Thrust Takeoff Nozzle Schematic.	11
7.	Takeoff Nozzle Test Configurations.	12
8.	OTW Model Thrust Reverser Schematic.	13
9.	OTW Model Thrust Reverser.	14
10.	OTW Model Thrust Reverser Parameters.	15
11.	Model Pressure and Temperature Instrumentation.	17
12.	Schematic of Instrumentation Frame.	18
13.	Forward Thrust Nozzle Exit Instrumentation Plane.	19
14.	Reverse Thrust Charging Station Instrumentation Plane.	20
15.	JENOTS Data Acquisition System.	21
16.	Forward Thrust Nozzle Flow as a function of Pressure Ratio.	23
17.	Effect of Thrust Reverser Spacing on Flow as a Function of Pressure Ratio.	24
18.	Thrust Reverser Blocker Height Effect on Flow as a Function of Pressure Ratio.	25
19.	Effect of Lip Angle on Flow as a Function of Pressure Ratio.	26
20.	Effect of Thrust Reverser Lip Length on Flow as a Function of Pressure Ratio.	27

LIST OF ILLUSTRATIONS (Continued)

Figure		Page
21.	Reverse Thrust Charging Station Velocity Profiles (Nominal Configuration).	28
22.	Forward Thrust Cruise Nozzle Velocity Profiles.	29
23.	Forward Thrust Takeoff Nozzle Velocity Profiles.	30
24.	Typical Reverser Efflux Lampblack Pattern (Nominal Configuration).	31
25.	OTW Model Thrust Reverser Performance Estimates.	35
26.	Cruise Nozzle PNL Directivity with and without Long Stub Wing.	38
27.	Cruise Nozzle Spectra with and without Long Stub Wing.	39
28.	Cruise Nozzle Peak PNL Variation with Pressure Ratio.	40
29.	Takeoff Nozzle PNL Directivity with and without Short Stub Wing.	41
30.	Takeoff Nozzle Spectra with and without Short Stub Wing.	43
31.	Takeoff Nozzle Peak PNL Variation with Pressure Ratio.	44
32.	Cruise and Takeoff Nozzle PNL Directivity Comparison.	45
33.	Cruise and Takeoff Nozzle Spectral Comparison at 120 Degrees.	46
34.	Cruise and Takeoff Nozzle Peak PNL Comparison as a Function of Pressure Ratio.	47
35.	Reverse Thrust Spacing Variation.	48
36.	Reverse Thrust PNL Variation with Blocker Spacing.	49
37.	Reverse Thrust SPL Spectral Variation with Blocker Spacing at 60 Degrees.	50
38.	Reverse Thrust SPL Spectral Variation with Blocker Spacing at 80 Degrees.	52
39.	Reverse Thrust Peak PNL Variation with Blocker Spacing as a Function of Pressure Ratio.	53

LIST OF ILLUSTRATIONS (Continued)

Figure		Page
40.	Reverse Thrust Blocker Height Variation.	54
41.	Reverse Thrust PNL Variation with Increased Blocker Height.	55
42.	Reverse Thrust SPL Spectral Variation with Increased Blocker Height.	56
43.	Reverse Thrust Peak PNL Variation with Increased Blocker Height as a Function of Pressure Ratio.	57
44.	Reverse Thrust Lip Variation.	58
45.	Reverse Thrust PNL Directivity Variation with Lip Geometry Changes.	59
46.	Reverse Thrust SPL Spectral Variation with Lip Geometry Changes at 70 Degrees.	60
47.	Reverse Thrust SPL Spectral Variation with Lip Geometry Changes at 80 Degrees.	61
48.	Reverse Thrust Peak PNL Variation with Lip Geometry Changes as a Function of Pressure Ratio.	62
49.	Summary of the Effect of Thrust Reverser Variations on Peak PNL as a Function of Pressure Ratio.	63
50.	Empirical Curve for Adding Constituent PNL's with Non-similar Spectra.	65
51.	Upward and Downward Exhausting Reverse Thrust Configurations.	66
52.	Photograph of Downward Exhausting Reverse Thrust Configuration.	67
53.	Reverse Thrust PNL Directivity for Upward and Downward Exhaust.	68
54.	Reverse Thrust SPL Spectral Variation for Upward and Downward Exhaust.	70
55.	Reverse Thrust Peak PNL Variation for Upward and Downward Exhaust as a Function of Pressure Ratio.	71

LIST OF ILLUSTRATIONS (Concluded)

Figure		Page
56.	Horizontal Exhausting Reverse Thrust Configuration.	72
57.	Reverser Thrust PNL Directivity Variation with Upward and Horizontal Exhaust.	73

SECTION I

SUMMARY

As part of the NASA/General Electric Company Quiet, Clean Short-Haul Experimental Engine (QCSEE) Program, a test program was conducted on a 1/6.25 scale model of an Over-the-Wing (OTW) forward thrust nozzle and thrust reverser. Both acoustic and aerodynamic performance of the models were monitored. In reverse thrust, the effect of thrust reverser geometry was studied by parametric variations in blocker spacing, blocker height, lip angle, and lip length. The aeroacoustic objectives of the reverse thrust tests were to achieve a total system noise level of 100 PNdB or less on a 152.4 m (500 ft) sideline at a reverse thrust which is 35 percent of the thrust required for takeoff. Forward thrust nozzle tests determined the jet noise levels of the nozzle, the effect of opening side doors to achieve takeoff thrust, and scrubbing noise of the jet over a simulated wing surface.

Velocity profiles were measured for the forward thrust nozzle and the thrust reverser. An estimate of the achieved reverse thrust was made utilizing the centerline turning angle observed with lampblack smears on a flow splitter.

A configuration was defined which best satisfies the acoustic and aerodynamic goals in reverse thrust. However, the instrumentation and procedures used were capable of providing only approximate weight flow and reverse thrust values.

SECTION II

INTRODUCTION

The General Electric Company is currently engaged in the Quiet, Clean Short-Haul, Experimental Engine (QCSEE) Program under Contract NAS3-18021 to NASA Lewis Research Center. The QCSEE program has as one of its major objectives the development and demonstration of the technology required to meet stringent noise requirements anticipated for commercial turbofan short-haul aircraft. The QCSEE engine must achieve a total system noise level of 100 PNdB or less on a 152.4 m (500 ft) sideline at a reverse thrust which is 35 percent of the thrust required for takeoff. More details of the QCSEE objectives and design rationale are available in Reference 1.

A component test was conducted on a scale model of the Over-the-Wing (OTW) engine thrust reverser and forward thrust nozzle at the General Electric Company Jet Engine Noise Outdoor Test Stand (JENOTS). One objective of the reverse thrust tests was to determine the effect of thrust reverser geometry on noise and aerodynamic performance by a parametric variation in blocker spacing, blocker height, lip angle, and lip length. A second objective was to determine the effect of thrust reverser orientation on noise so that possible static test mountings of the full-scale engine could be evaluated. Tests with the forward thrust nozzle were designed to determine the jet noise levels of the nozzle, the effect on noise of opening side doors for takeoff thrust, and scrubbing noise of the jet over a simulated wing surface.

Total pressure surveys were taken at the charging station plane for the nominal thrust reverser configuration and at the nozzle exit plane in forward thrust to provide velocity profiles at these locations.

Lampblack smears on a flow splitter were used to observe the turning angle achieved with the various thrust reverser configurations.

SECTION III

TEST FACILITY

The model tests were conducted on the General Electric Company Jet Engine Noise Outdoor Test Stand (JENOTS) which was developed for turbojet noise and suppressor studies. A schematic of the coannular flow JENOTS facility is shown in Figure 1; a photograph of the facility is shown in Figure 2. The coannular plenum chamber, to which the test models are attached, serves to give the flow a uniform velocity profile and to eliminate any high frequency system noise through the use of acoustically treated baffles. Only secondary flow air was used for this model test with the primary flow completely blocked off. Airflow for the secondary flow was measured upstream using an orifice plate system coupled with pressure and thermocouple rakes. The stream was heated to 389 K (700° R) for all tests to approximate engine cycle conditions.

The acoustic sound field consisted of 13 microphones located on an arc from 40 to 160 degrees in 10 degree increments (See Figure 1). For the forward thrust tests, these microphones were mounted 4.9 m (16 ft) above the ground and were on a 12.2 m (40 ft) radius. The mounts were specially designed "gooseneck" mounts to minimize the influence of reflections. For reverse thrust tests, the microphones were mounted at engine centerline height [140 cm (55 in.)] with the microphones from 40 to 120 degrees on a 11.3 m (37 ft) arc while the microphones from 130 to 160 degrees were on a 12.2 m (40 ft) radius.

The ground plane is composed of concrete to about 6.1 m (20 ft) from the nozzle exit and then crushed rock to a 12.2 m (40 ft) radius. A grassy field exists beyond the acoustic arena. Specially designed acoustic barriers are located approximately 18.3 m (60 ft) from the sound field to protect the neighboring community from high noise levels. These barriers are designed such that there are no measurable reflections back into the sound field.

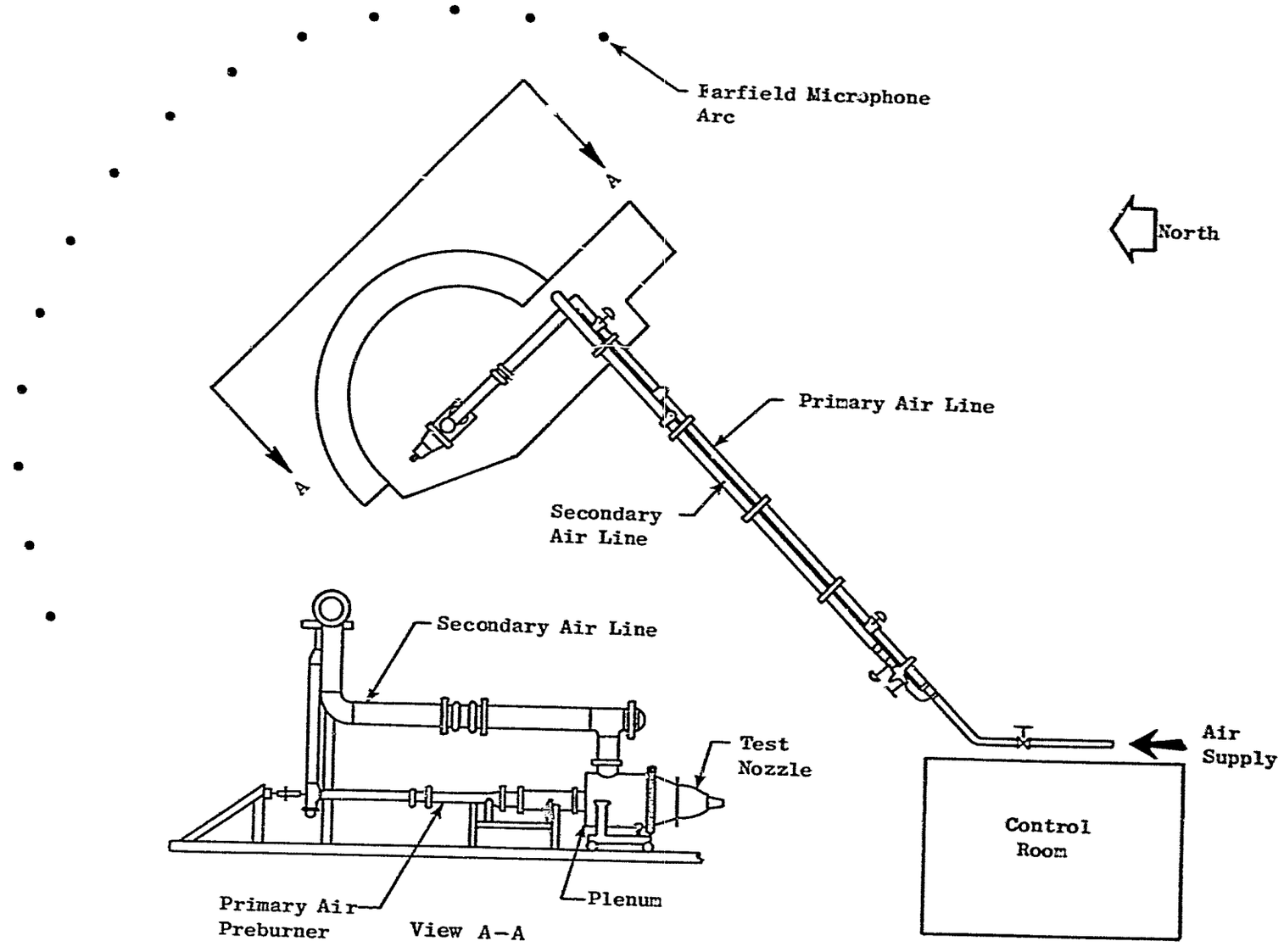

Figure 1. Schematic of Coannular Flow JENOTS Facility.

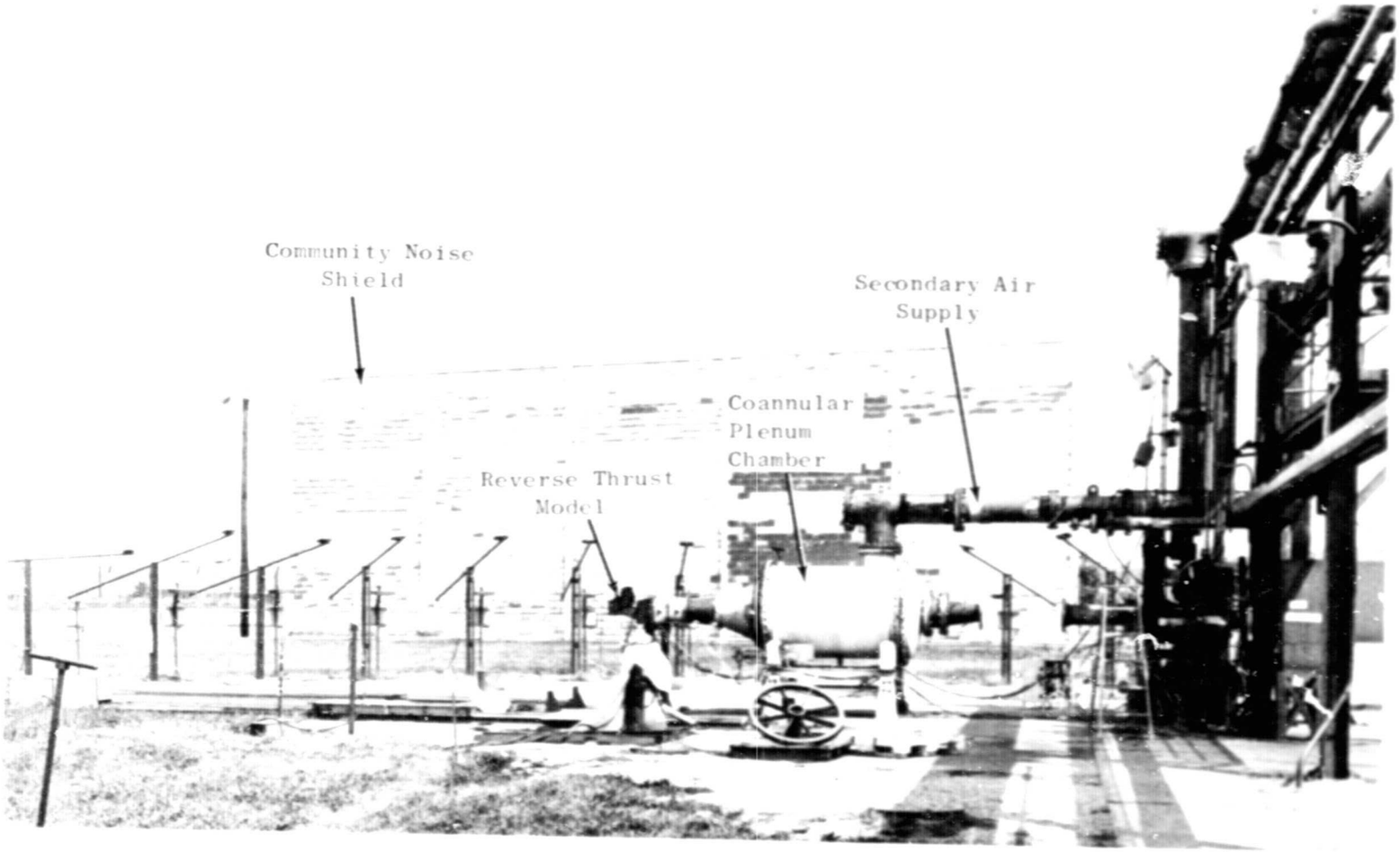

Figure 2. Photograph of the Coannular Flow JENOTS Facility.

SECTION IV

TEST VEHICLE AND HARDWARE

The model thrust reverser and forward thrust nozzles were 1/6.25 linear scale models of the full-size OTW engine. This means, for example, that at the charging station in reverse thrust, the flowpath height and width were exact scales of the full-size engine. However, the full-size engine has a D-shaped cross section while the models were rectangular. Thus the scale factor based upon the square root of the area ratio of the model to full size is 1 to 5.9. The scale factor of 5.9 was used in all acoustic scaling operations. Tables I and II present the test matrix for both the forward and reverse thrust tests, respectively.

A. Forward Thrust

A schematic of the forward thrust hardware is presented in Figure 3. Tests were made with and without the long stub wing, the extent of which is shown in Figure 4, and which is used to turn the flow to achieve axial thrust. The cruise nozzle is shown in Figure 5. Note the static pressure taps which are located in the total pressure survey plane.

To achieve the increased nozzle area and operating line required for takeoff, side doors were opened to 35°. The takeoff nozzle as shown schematically in Figure 6 was tested with and without a short stub wing which terminated at the nozzle exit plane. The stub wing turns the spreading flow from the side doors axial. Figure 7 shows the takeoff nozzle with and without the short stub wing. There were no static taps on the side doors.

B. Reverse Thrust

A schematic of the reverse thrust model and its installation to the coannular plenum is shown in Figure 8. Figure 9 is a photograph of the installation. The reverse thrust model was designed with the flexibility to vary geometric parameters such as blocker spacing, blocker height, lip angle, and lip length. These parameters are shown in Figure 10 along with their values for each configuration.

Table I. OTW Forward Thrust Model Test Matrix.

Configuration Number	Nozzle	Simulated Stub Wing
1	Cruise	Long
2*	Cruise	None
4*	Takeoff	Short
14	Takeoff	None

*Includes aerodynamic probe data for velocity profiles.

Table II. OTW Reverse Thrust Model Test Matrix.

Configuration Number	Blocker		Lip		Exhaust Direction
	Spacing, (X/D_{TH})	Height, (H/D_{TH})	Angle	Length, (L/D_{TH})	
8*	Nominal, 1.02	Nominal, 1.77	30°	Nominal, 0.24	Up
9	Close, 0.89	Nominal, 1.77	30°	Nominal, 0.24	Up
10	Wide, 1.15	Nominal, 1.77	30°	Nominal, 0.24	Up
11	Nominal, 1.02	Increased, 1.87	30°	Nominal, 0.24	Up
12	Nominal, 1.02	Nominal, 1.77	20°	Nominal, 0.26	Up
13	Nominal, 1.02	Nominal, 1.77	30°	Nominal, 0.24	Down
15	Nominal, 1.02	Nominal, 1.77	20°	Double, 0.52	Up
16	Nominal, 1.02	Nominal, 1.77	20°	Double, 0.52	Horizontal

*Includes aerodynamic probe data for velocity profiles.

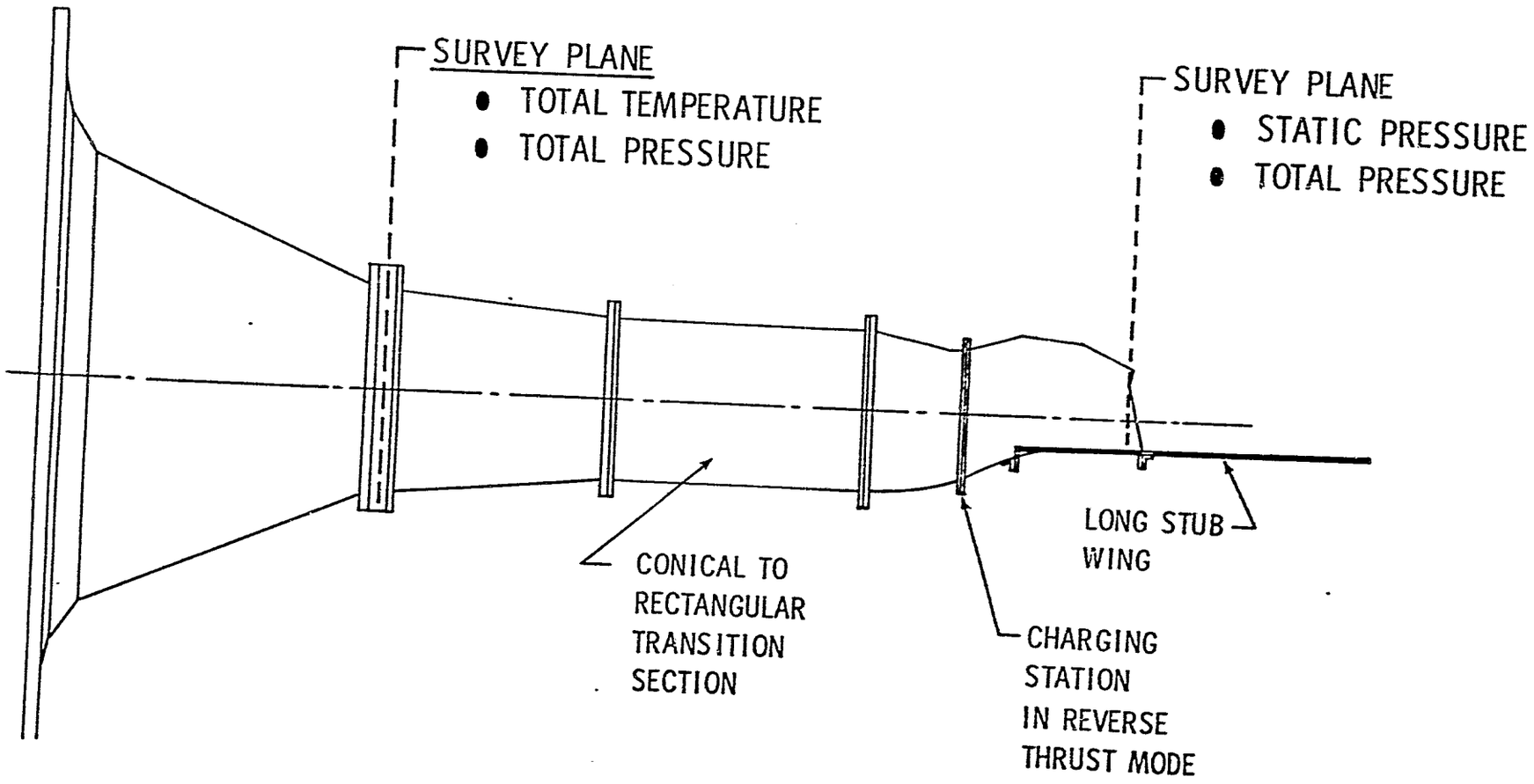

Figure 3. OTW Model Forward Thrust Cruise Nozzle Installation.

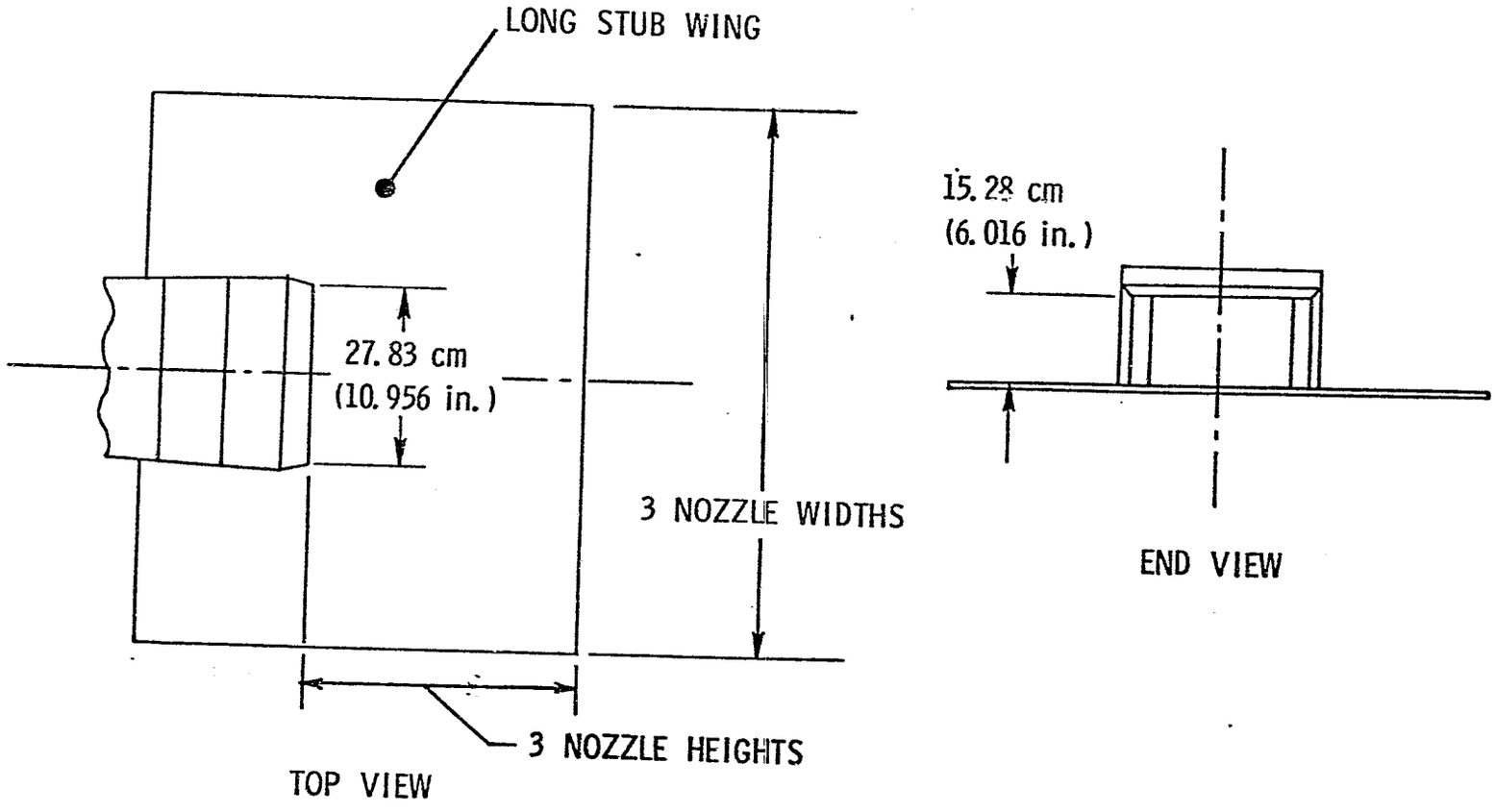

Figure 4. Forward Thrust Cruise Nozzle Schematic.

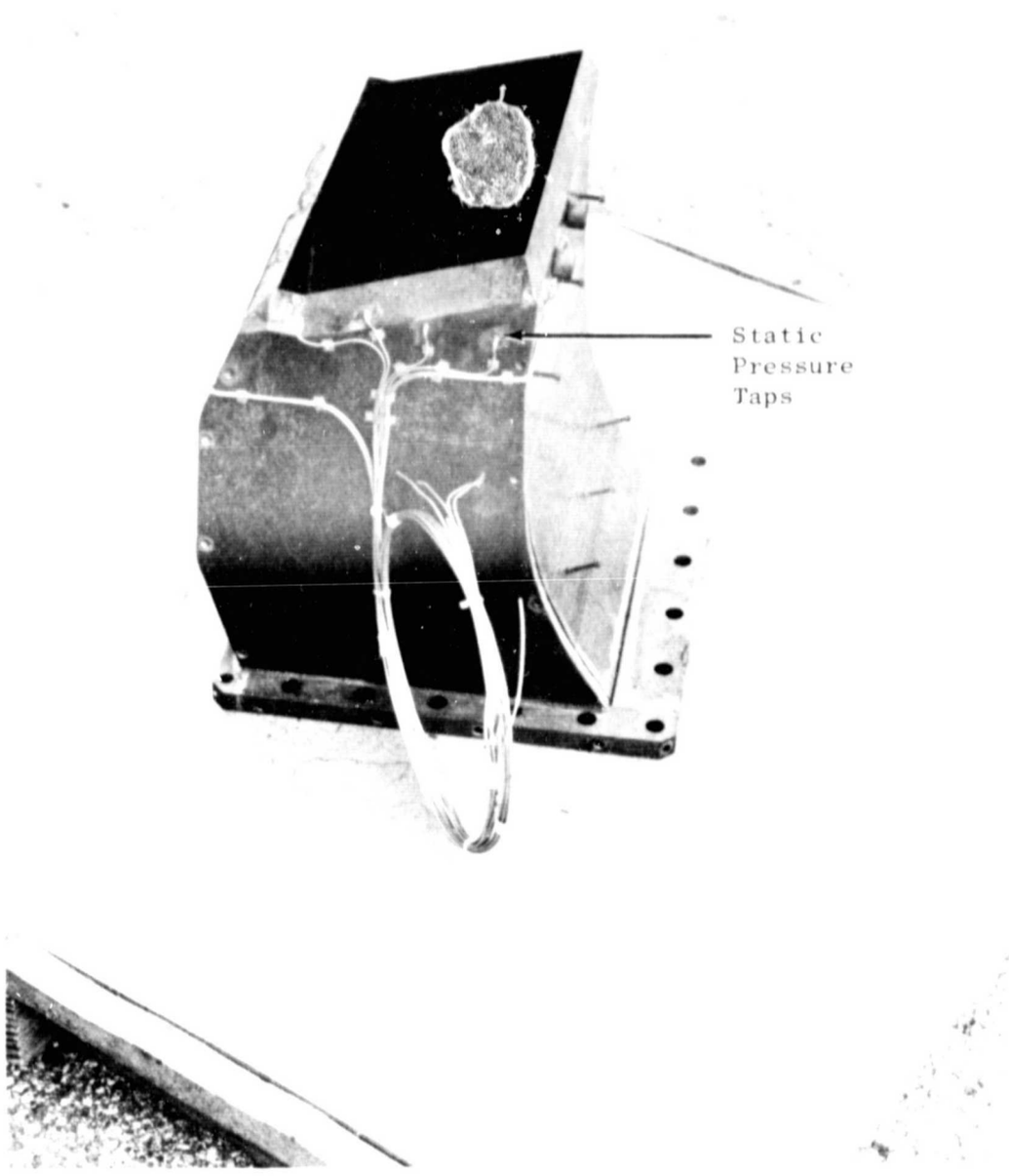

Figure 5. Forward Thrust Cruise Nozzle.

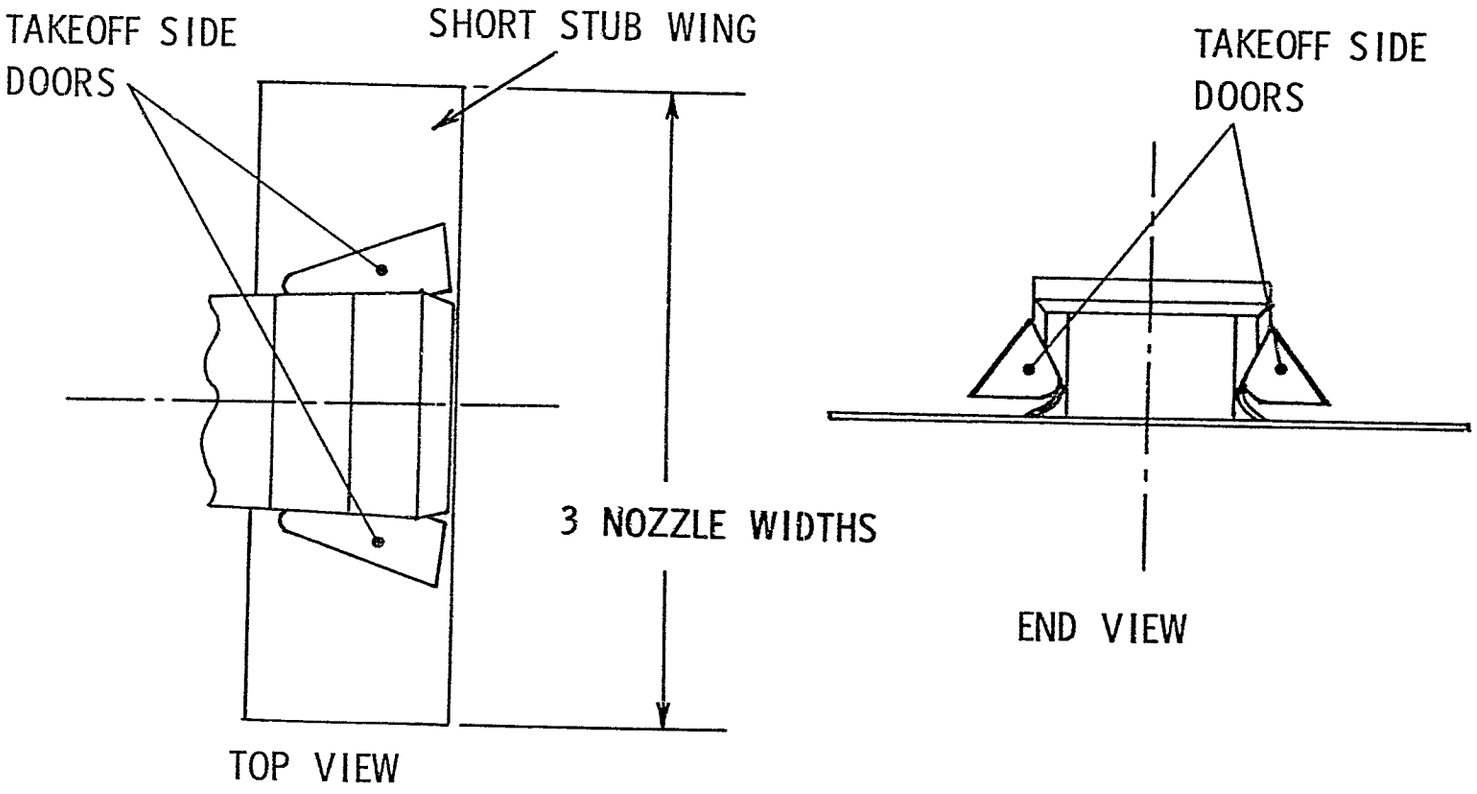

Figure 6. Forward Thrust Takeoff Nozzle Schematic.

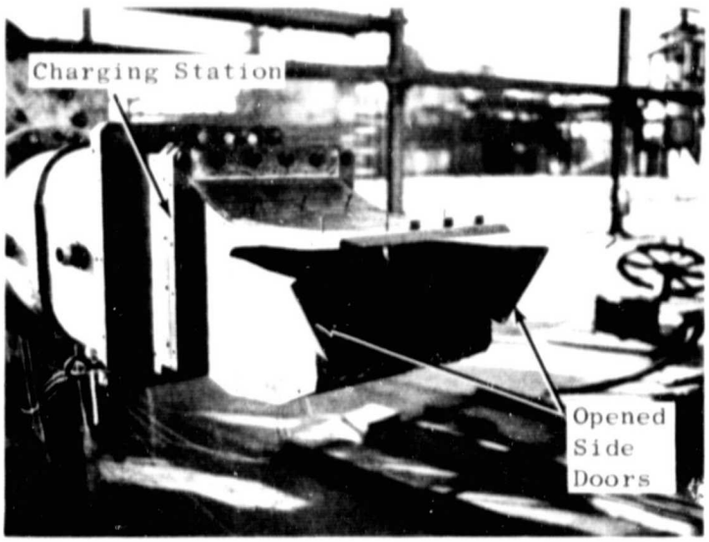

Configuration 14

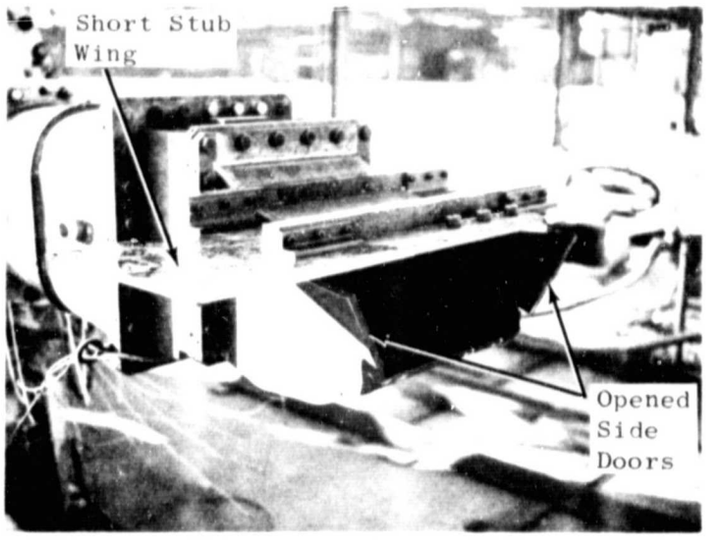

Configuration 4

Figure 7. Takeoff Nozzle Test Configurations.

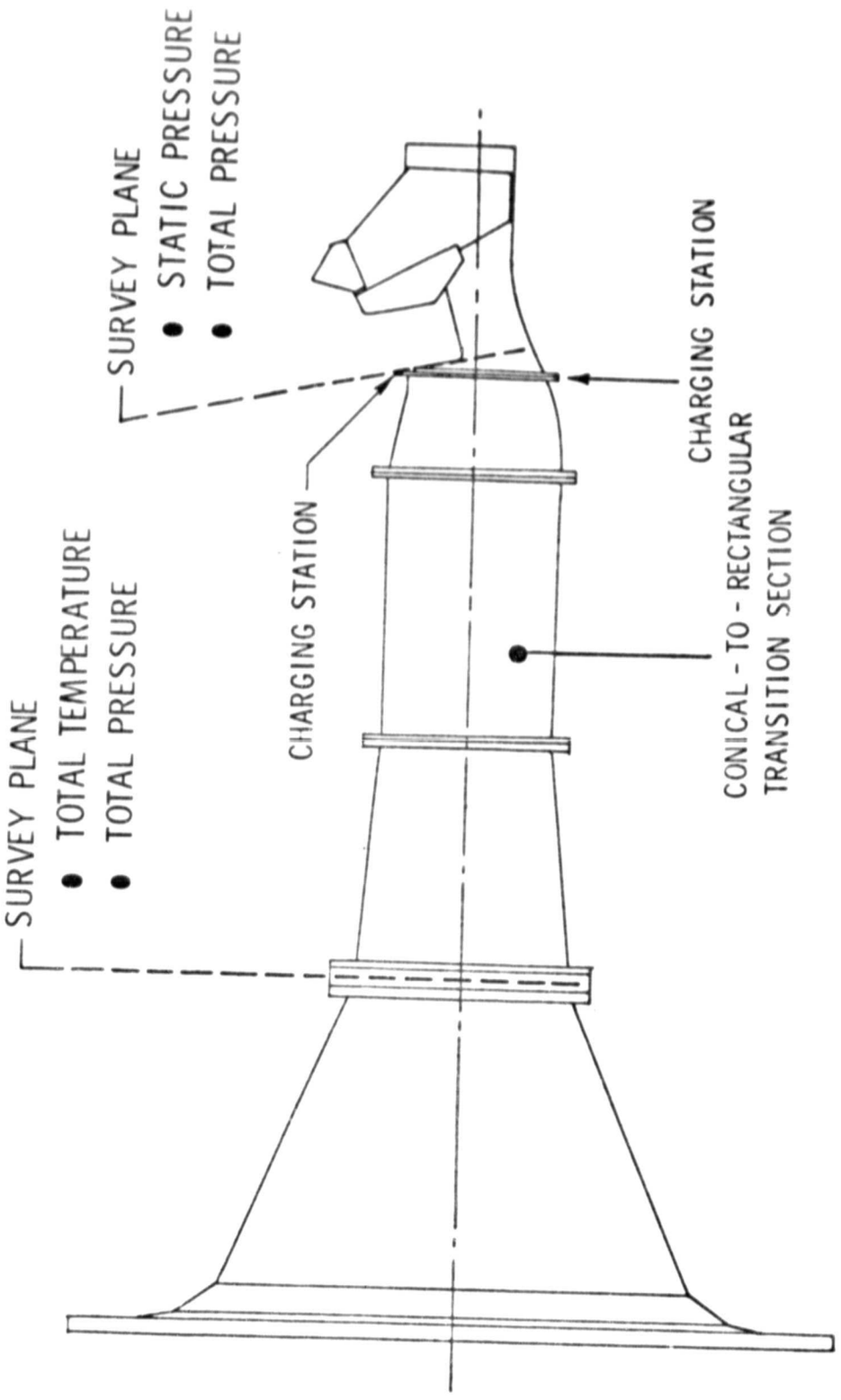

Figure 8. OTW Model Thrust Reverser Schematic.

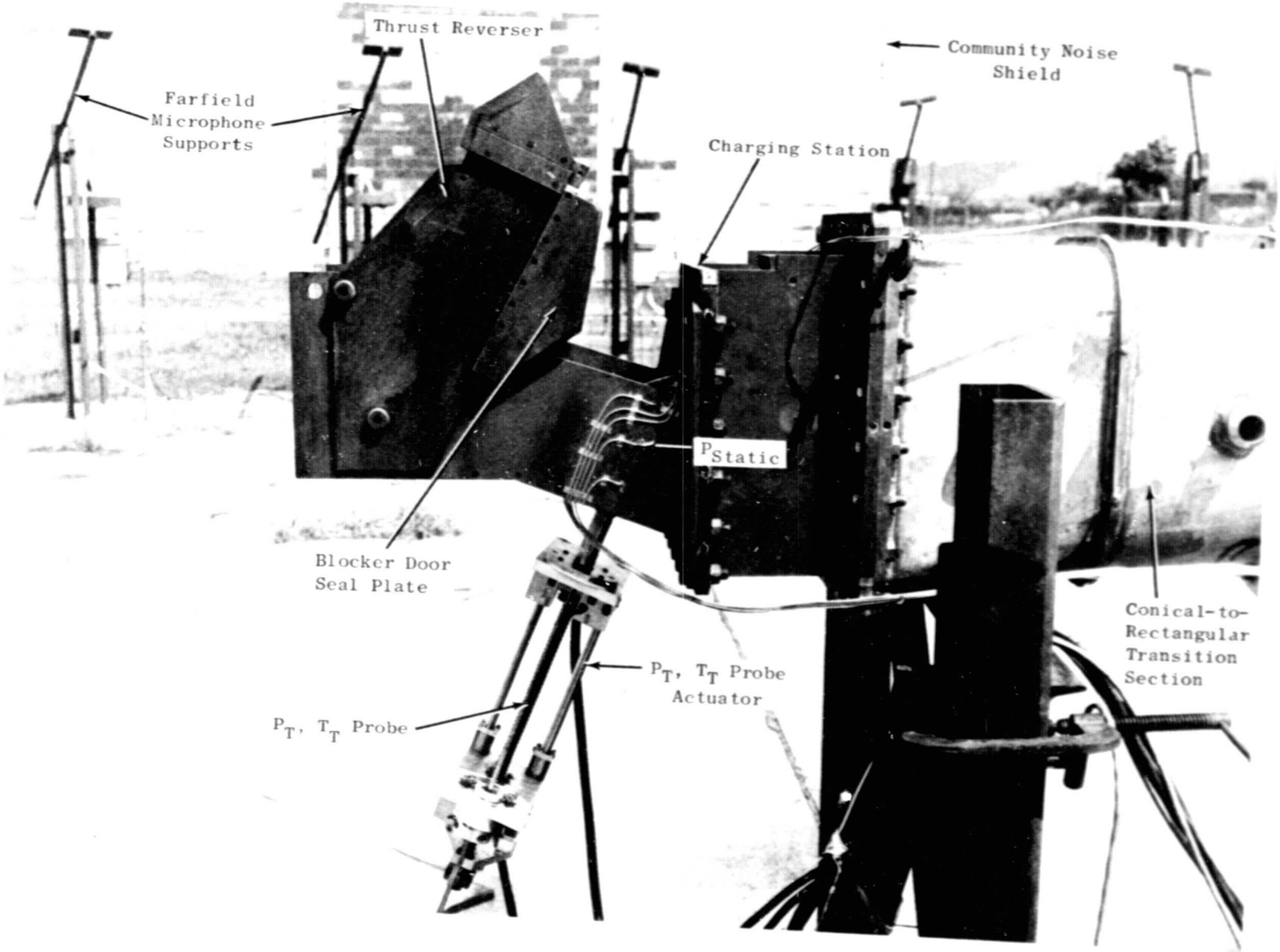

Figure 9. OTW Model Thrust Reverser.

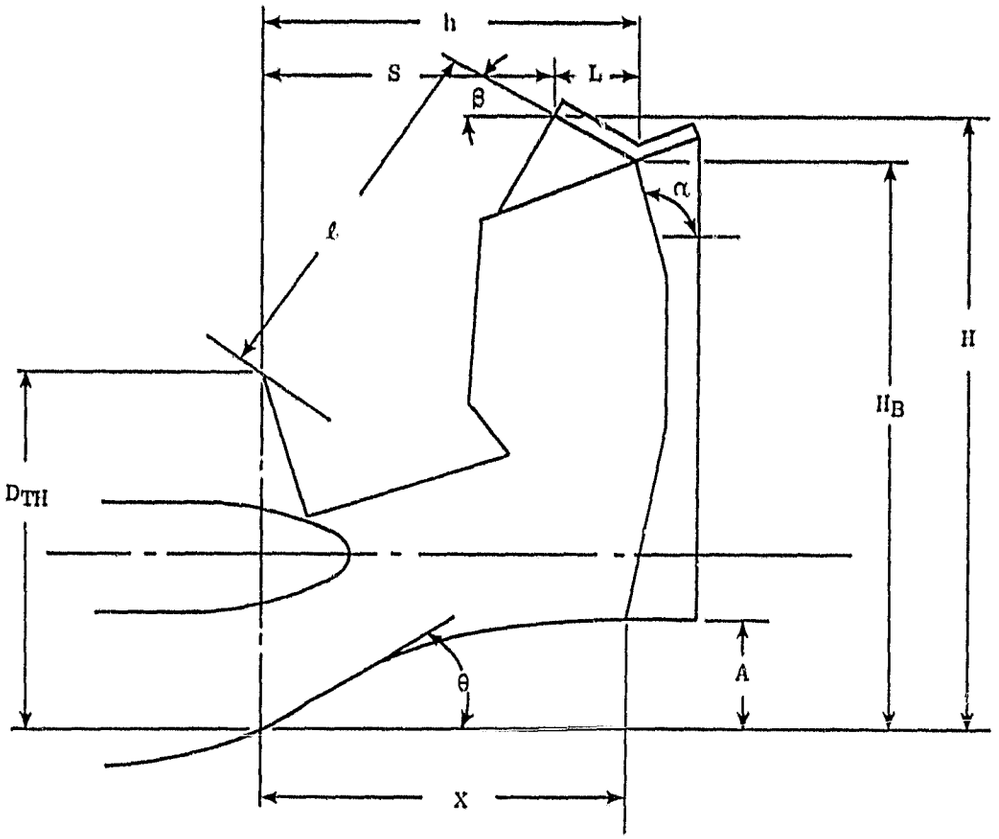

Configuration	$\frac{X}{D_{TH}}$	$\frac{H}{D_{TH}}$	$\frac{H_B}{D_{TH}}$	$\frac{S}{D_{TH}}$	$\frac{h}{D_{TH}}$	$\frac{\ell}{D_{TH}}$	$\frac{A}{D_{TH}}$	β°	α°	θ°	$\frac{L}{D_{TH}}$
8, 13, Nominal	1.02	1.77	1.63	0.69	0.93	1.04	0.28	30	109	29	0.24
9, Decreased Spacing	0.89	1.77	1.63	0.56	0.80	0.95	0.28	30	109	29	0.24
10, Increased Spacing	1.15	1.77	1.63	0.79	1.03	1.11	0.28	30	109	29	0.24
11. Increased Height	1.02	1.87	1.73	0.66	0.90	1.09	0.28	30	109	29	0.24
12, 20° Lip	1.02	1.73	1.63	0.67	0.93	0.99	0.28	20	109	29	0.26
15, 16, Increased Lip Length	1.02	1.83	1.63	0.41	0.93	0.92	0.28	20	109	29	0.52

Figure 10. OTW Model Thrust Reverser Parameters.

SECTION V

DATA ACQUISITION AND REDUCTION

A. Aerodynamic

Pressure, temperature, and weight flow measurements were made at the locations shown in Figure 11. Nine total pressures and nine total temperatures were recorded in the instrumentation frame upstream of the model charging station. Immersion depths in the instrumentation frame are shown in Figure 12. Total pressure and total temperature traverses were made at the nozzle exit for the forward mode model and at the charging station for the reverse mode model. A Cobra total pressure and total temperature probe was used for these traverses. The probe is shown in Figure 9 installed on the thrust reverser model. Traverse profiles at the three spanwise locations shown in Figure 13 were recorded on strip charts.

Static pressure measurements were made at the nozzle exit plane for the forward thrust model and at the charging station for the reverse mode model. Tap locations are indicated on Figures 13 and 14 and can be seen in the photographs in Figures 5 and 9.

Model weight flow was measured with a calibrated orifice plate located upstream of the test rig.

Flow visualization of the reverse thrust configuration was achieved by lampblack smears on a flow splitter. Polaroid photographs were taken and the centerline turning angle measured on the photograph.

B. Acoustic

The data collection system at JENOTS is shown schematically in Figure 15. It is composed of a B&K microphone/cathode follower powered and conditioned by a B&K 2801 power supply followed by 0.9 m (3 ft) of line to a specially designed 10 dB fixed-gain preamplifier which drives 45.7 m (150 ft) of cable terminating at the variable gain differential input amplifiers to the Sangamo Sabre IV tape recorder. The signal is recorded on magnetic tape for future playback.

Standard data reduction was conducted in the General Electric Data Systems Operation. All 1/3-octave band analysis was performed on a General Radio 1921 1/3-octave analyzer. Integration time was 32 seconds to ensure good iteration for the low frequency content. All data were processed through the Full-Scale Data Reduction (FSDR) program which corrected the data to 298 K (77° F), 70 percent relative humidity standard acoustic day conditions (per Reference 2) and corrected for ground reflections (high microphones only), scaled to full size, and extrapolated the SPL's to 61 m (200 ft) and 152 m (500 ft) sidelines.

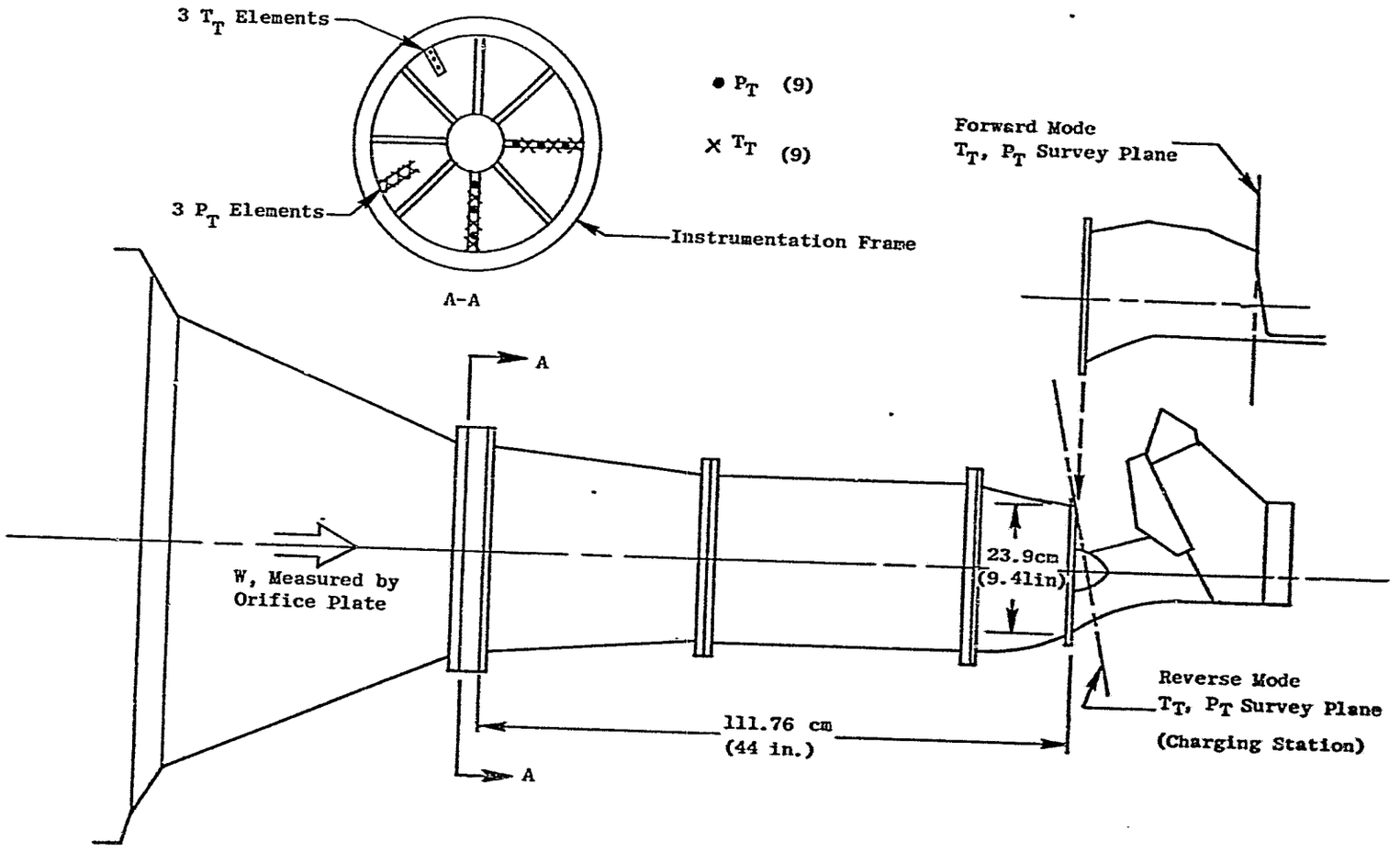

Figure 11. Model Pressure and Temperature Instrumentation.

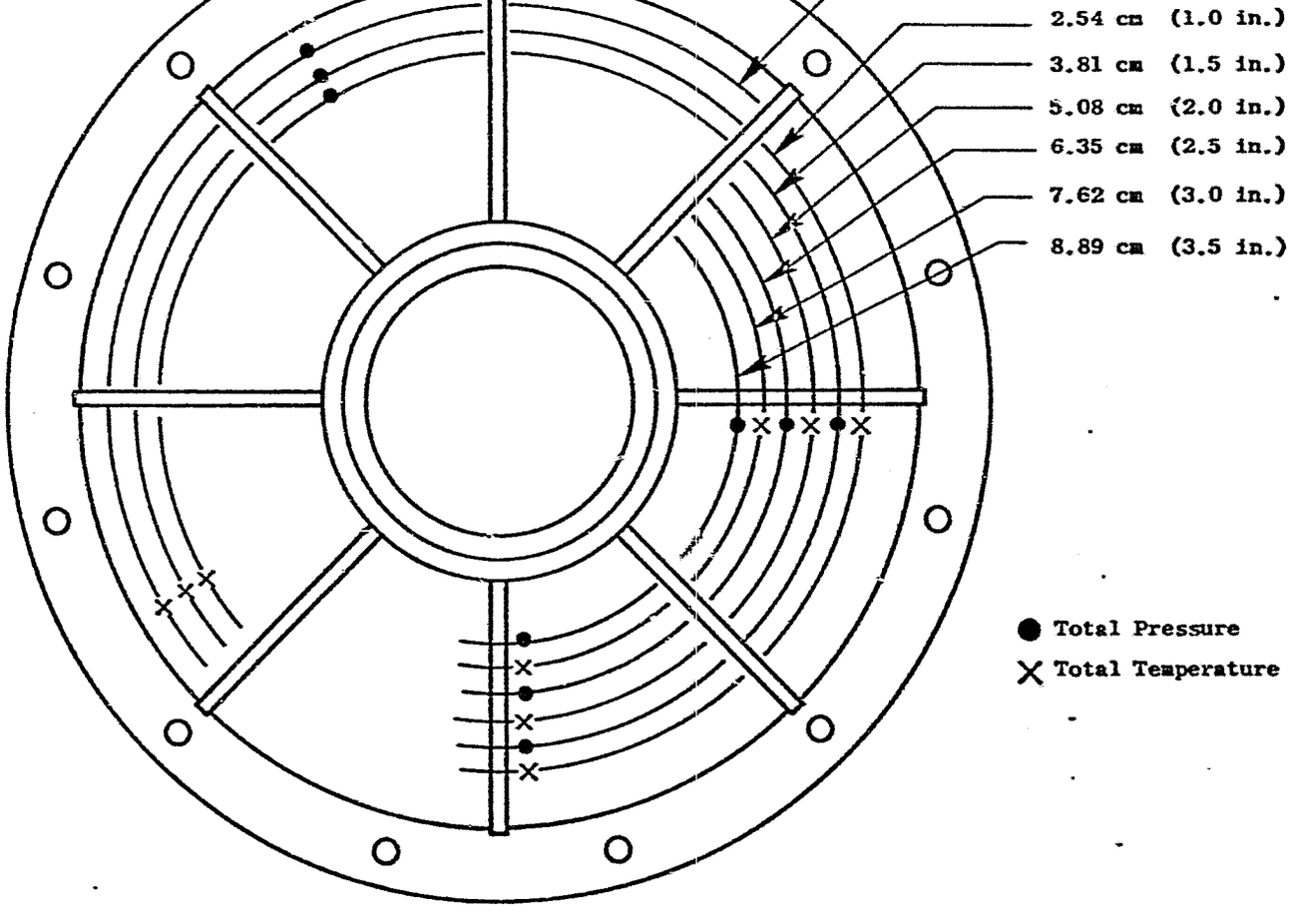

Figure 12. Schematic of Instrumentation Frame.

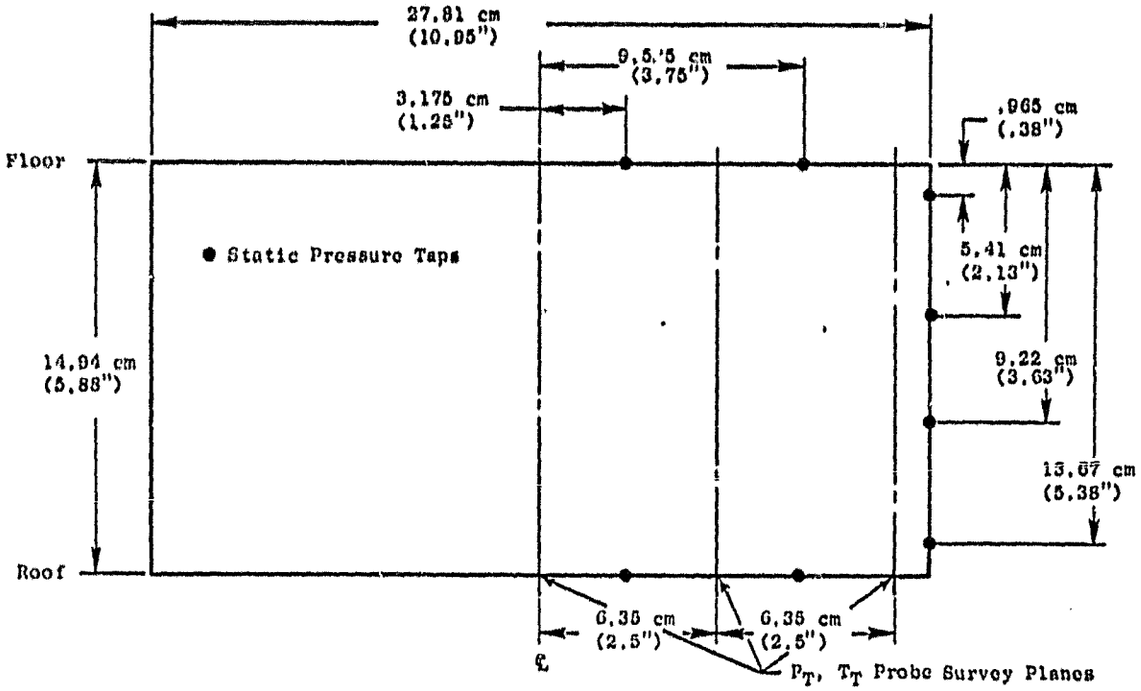

Aft Looking Forward

Figure 13. Forward Thrust Nozzle Exit Instrumentation Plane.

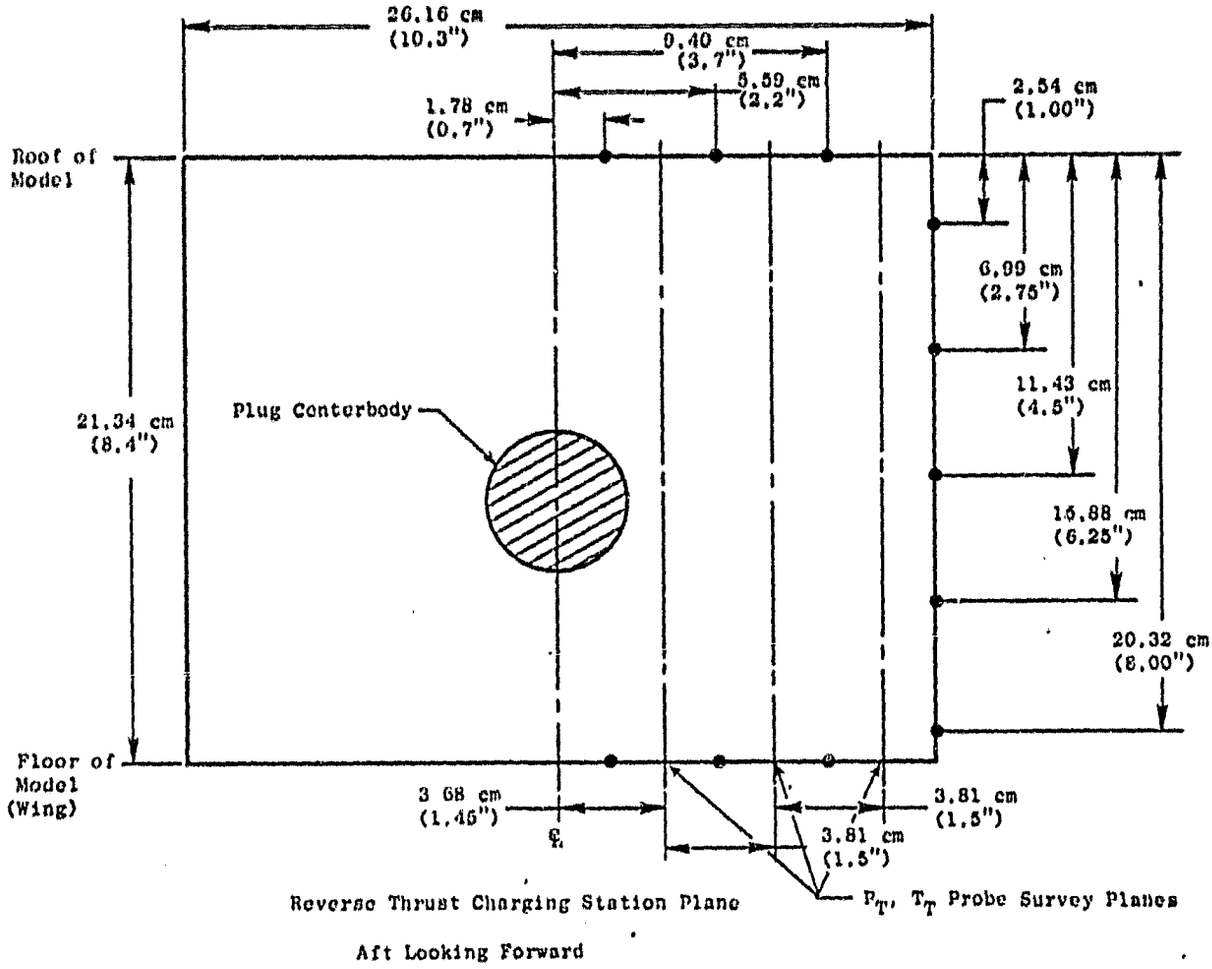

Aft Looking Forward

Figure 14. Reverse Thrust Charging Station Instrumentation Plane.

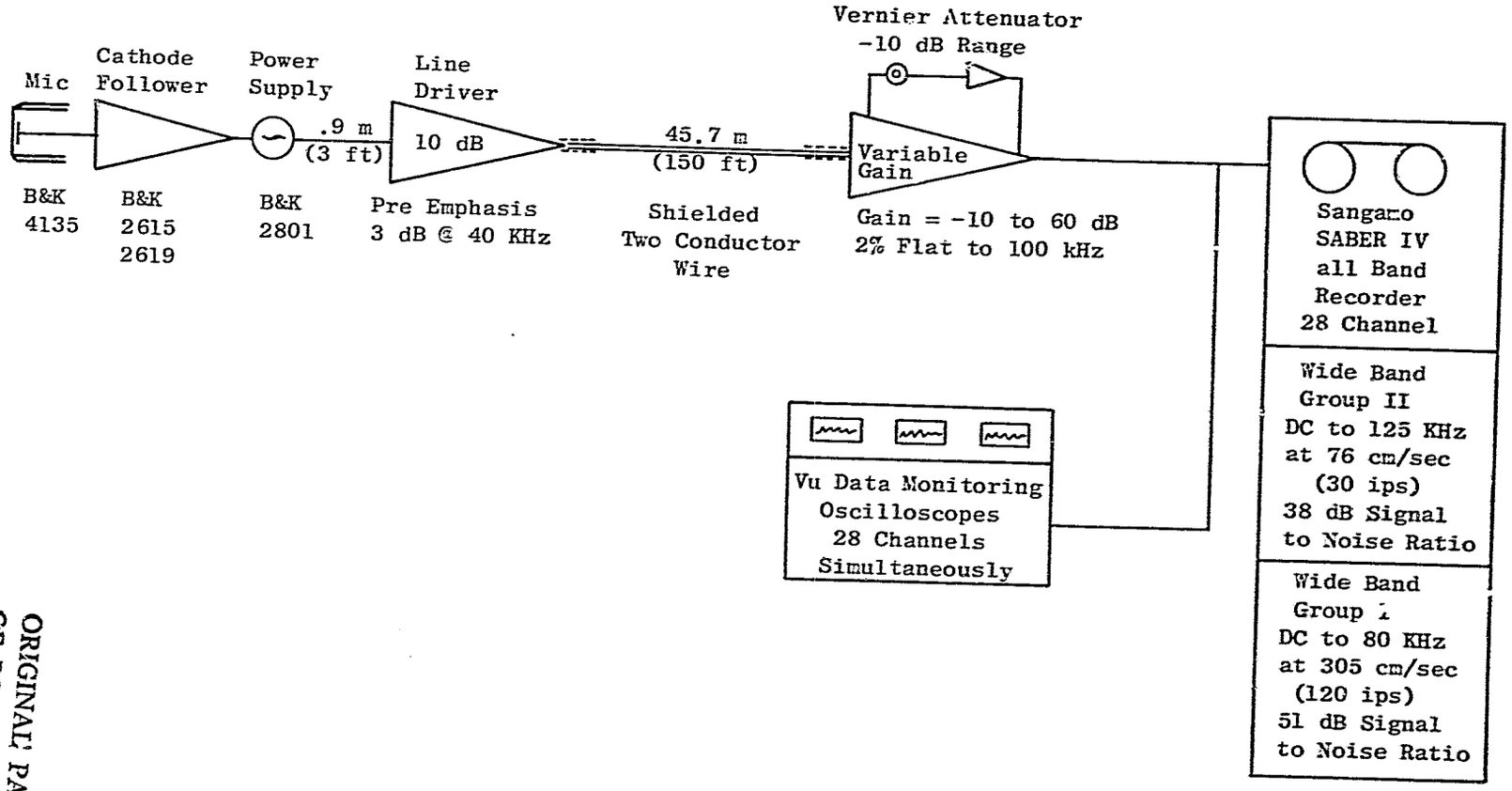

Figure 15. JENOTS Data Acquisition System.

SECTION VI

AERODYNAMIC RESULTS

Model weight flow as a function of pressure ratio is presented in Figure 16, 17, 18, and 19 for all configurations tested. Forward thrust flow data, Figure 16, showed that at the predicted takeoff pressure ratio of 1.29, the takeoff nozzle had 17.5 percent greater flow than the cruise nozzle without a simulated wing and 19.2 percent more flow than the cruise nozzle with a simulated wing. These flow changes are in agreement with expected results.

Reverse thrust data in Figures 17, 18, and 19 indicated that axial blocker spacing had the greatest effect on flowrate. Increasing the blocker spacing, X/D_{TH}, from 0.89 to 1.15 increased the flow by 10.8 percent relative to the takeoff flow. This is shown in Figure 17. However, the reverse thrust flow was appreciably less than the forward thrust takeoff flow at all axial spacings. For the nominal axial spacing, 1.02, a 21.1 percent reduction in reverse thrust flow relative to the takeoff nozzle flow was observed. Blocker height and lip angle variations had small effects on flow as shown in Figures 18 and 19. Increasing the lip length, L/D_{TH}, from 0.26 to 0.52 decreased the flow by 3 percent as shown in Figure 20.

Velocity profiles are presented in Figures 21, 22, and 23 for the reverse and forward thrust models. Reverse thrust profiles are presented for the charging station while forward thrust profiles are at the nozzle exit plane. Static pressures, total pressures, and total temperatures at these axial locations were used to calculate the velocity profiles. The reverse thrust velocity profiles for the nominal configuration are presented in Figure 21 and showed that the velocities near the roof are higher than the floor velocities. The reduced velocities in the floor region are caused by the blocker door flow stagnation region which locally increases the static pressures. In Figure 21, the forward thrust cruise nozzle has a velocity profile which is skewed and has the highest velocity near the roof of the nozzle while the takeoff nozzle in Figure 22 has a more uniform profile.

Reverse thrust performance estimates were made analytically. This analysis required the following information to determine reverse thrust: reverser lip flow angle, spillage flow between the blocker door seal plate and the charging station (see Figure 9), spillage flow angle, and the total pressure drop from the instrumentation frame to the reverser exit. Lamp-black photographs provided an estimate of the reverser lip flow angle and the spillage flow angle was approximated from hand held wand/tuft surveys. As shown in Figure 24, the reverse flow angle was measured directly from the flow picture. Reverser exit flow was calculated from a knowledge of the reverse flow area, total temperature near the lip exit (assumed equal to the instrumentation frame measurement) and the total pressure near the lip exit as described later. The spillage flow rate was then determined from the calculated reverser exit flow and the total measured flow. Because of the complex flow fields and minimal instrumentation, the calculated

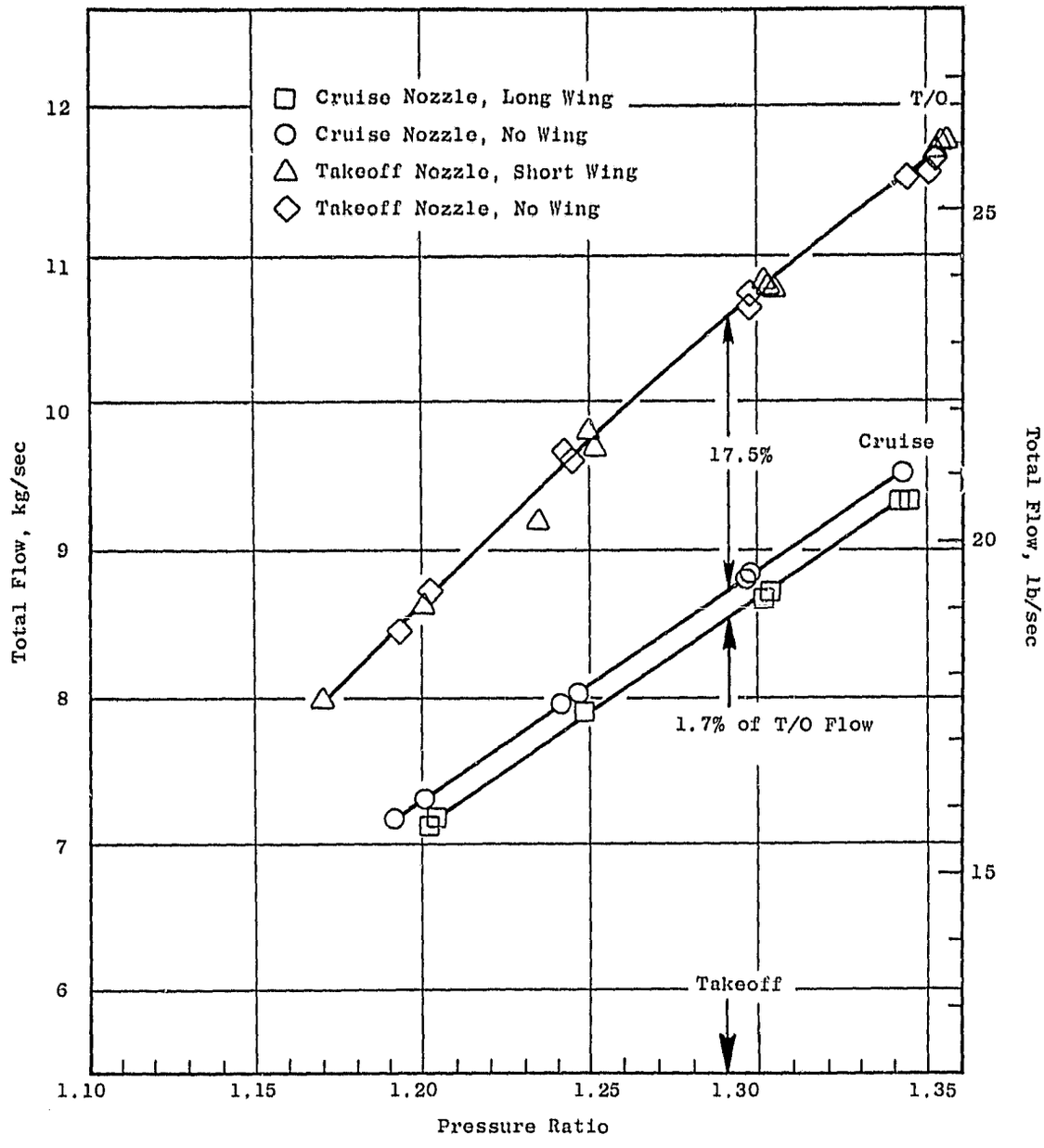

Figure 16. Forward Thrust Nozzle Flow as a Function of Pressure Ratio.

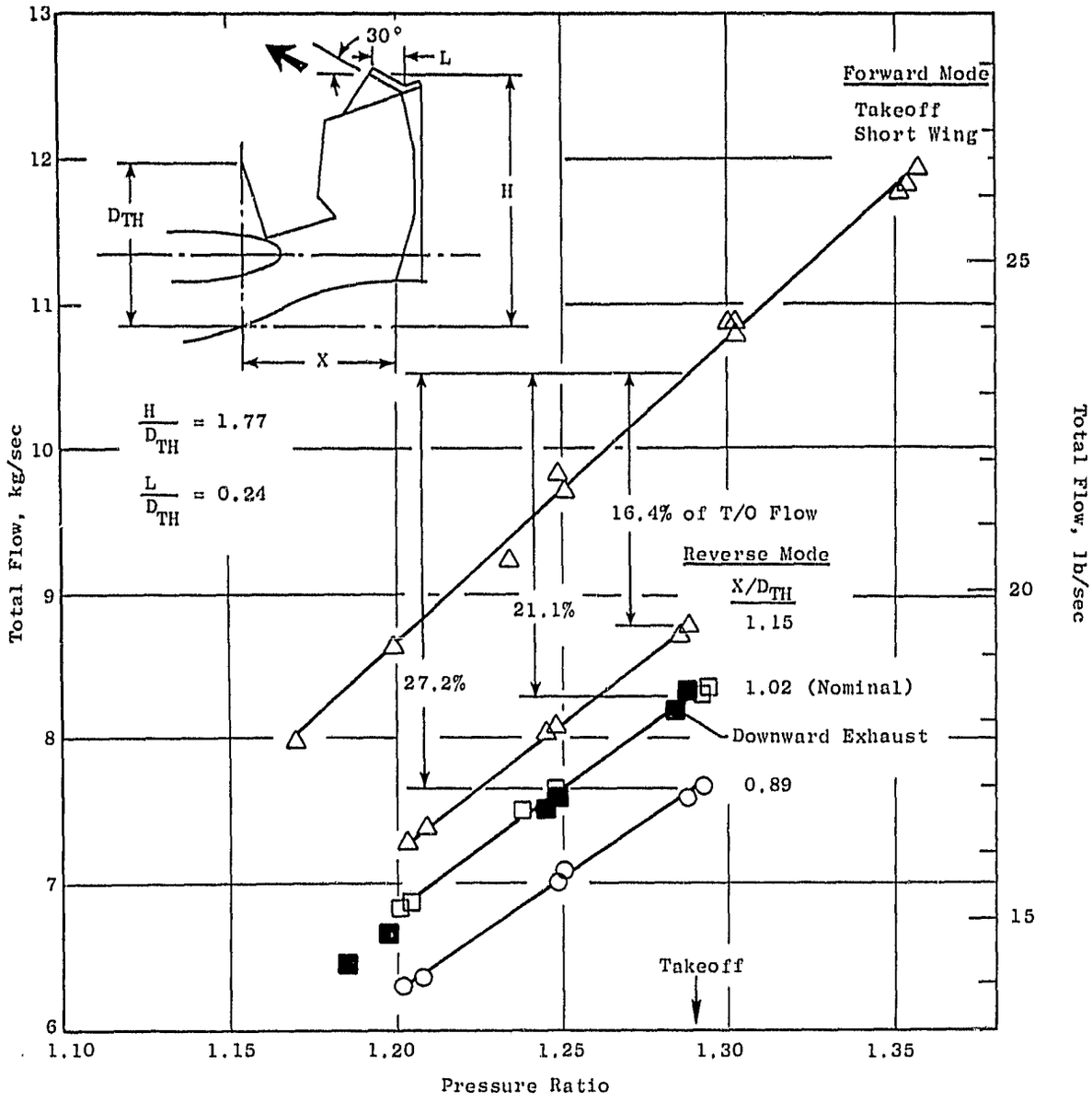

Figure 17. Effect of Thrust Reverser Spacing on Flow as a Function of Pressure Ratio.

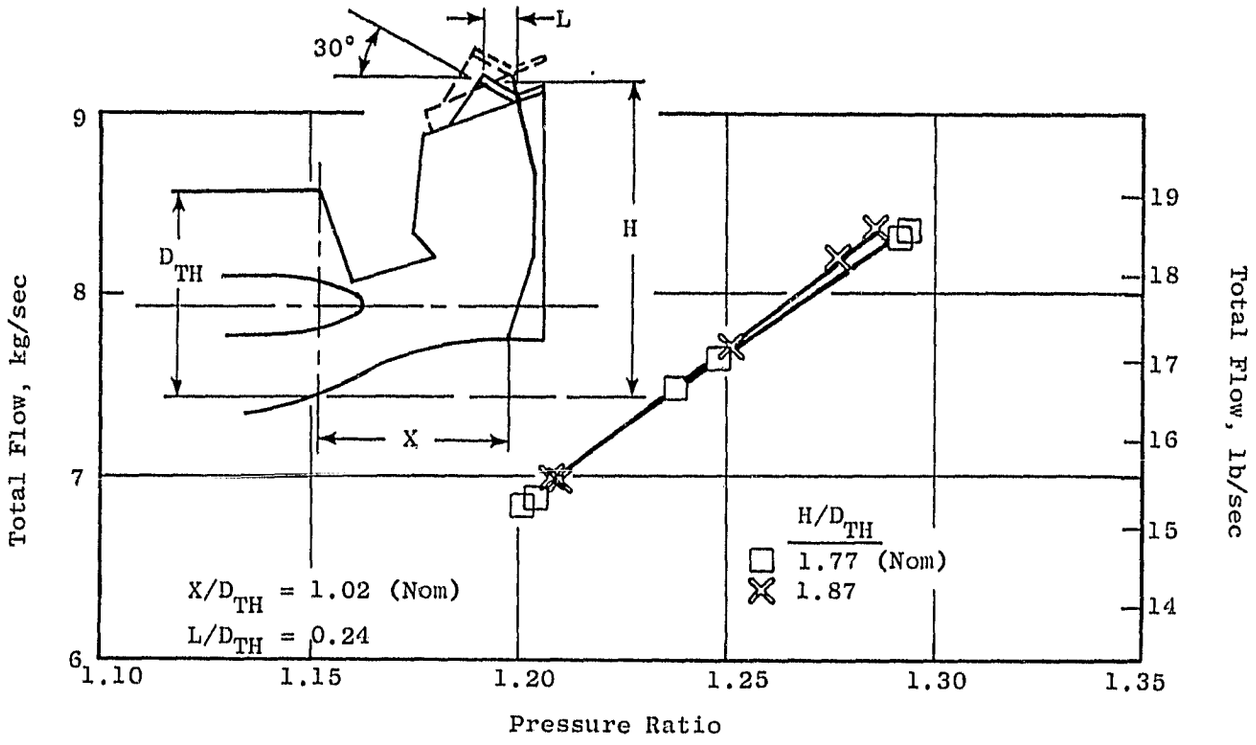

Figure 18. Thrust Reverser Blocker Height Effect on Flow as a Function of Pressure Ratio.

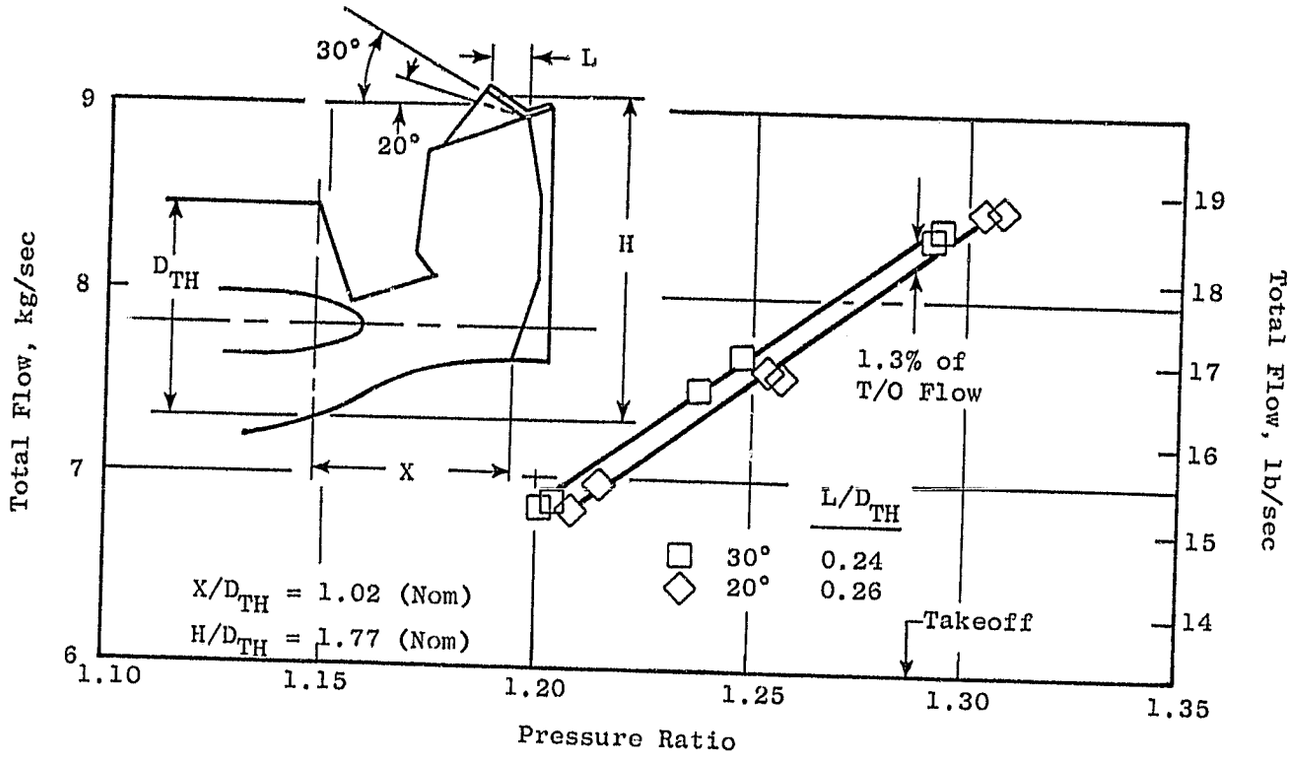

Figure 19. Effect of Lip Angle on Flow as a Function of Pressure Ratio.

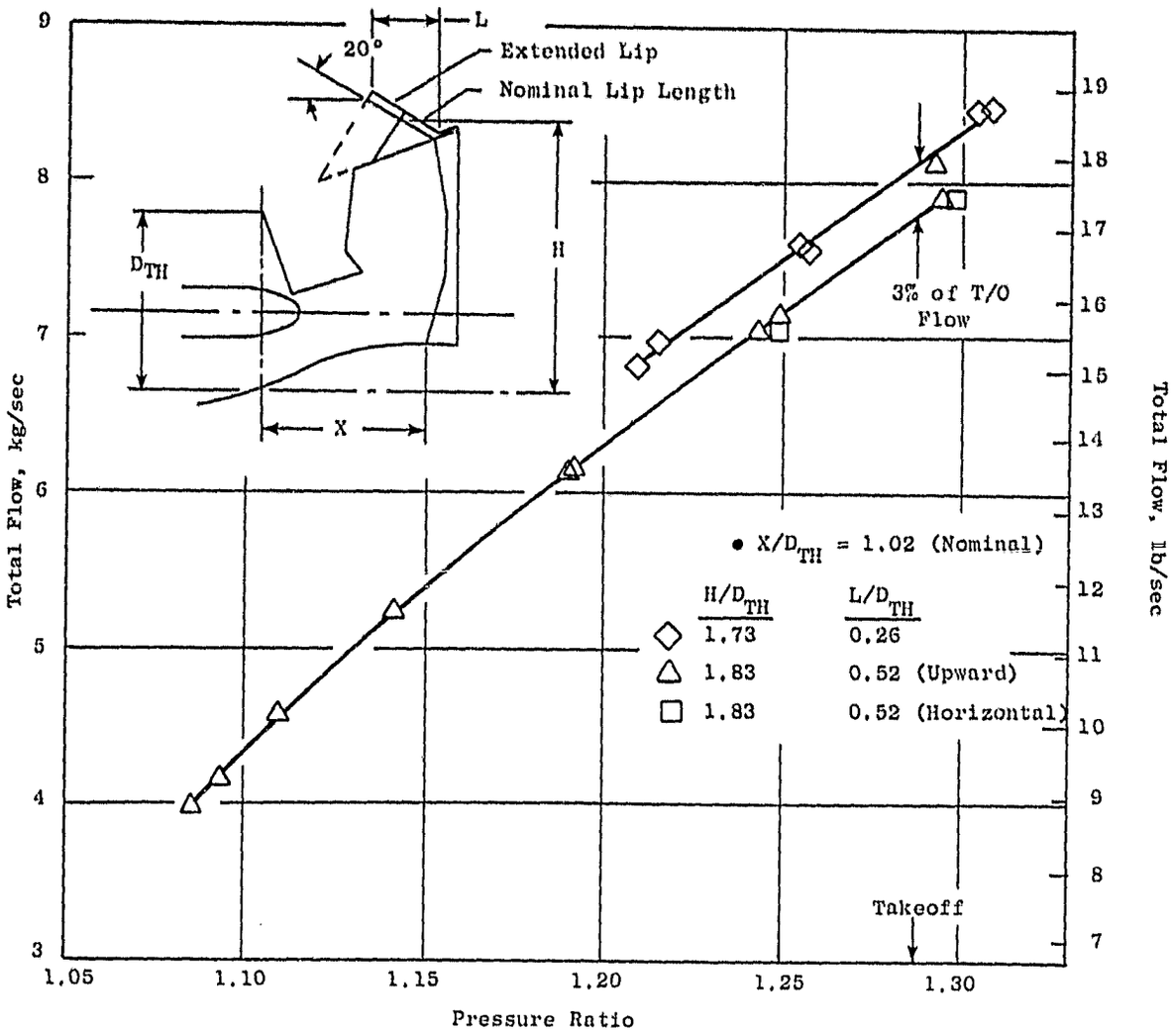

Figure 20. Effect of Thrust Reverser Lip Length on Flow as a Function of Pressure Ratio.

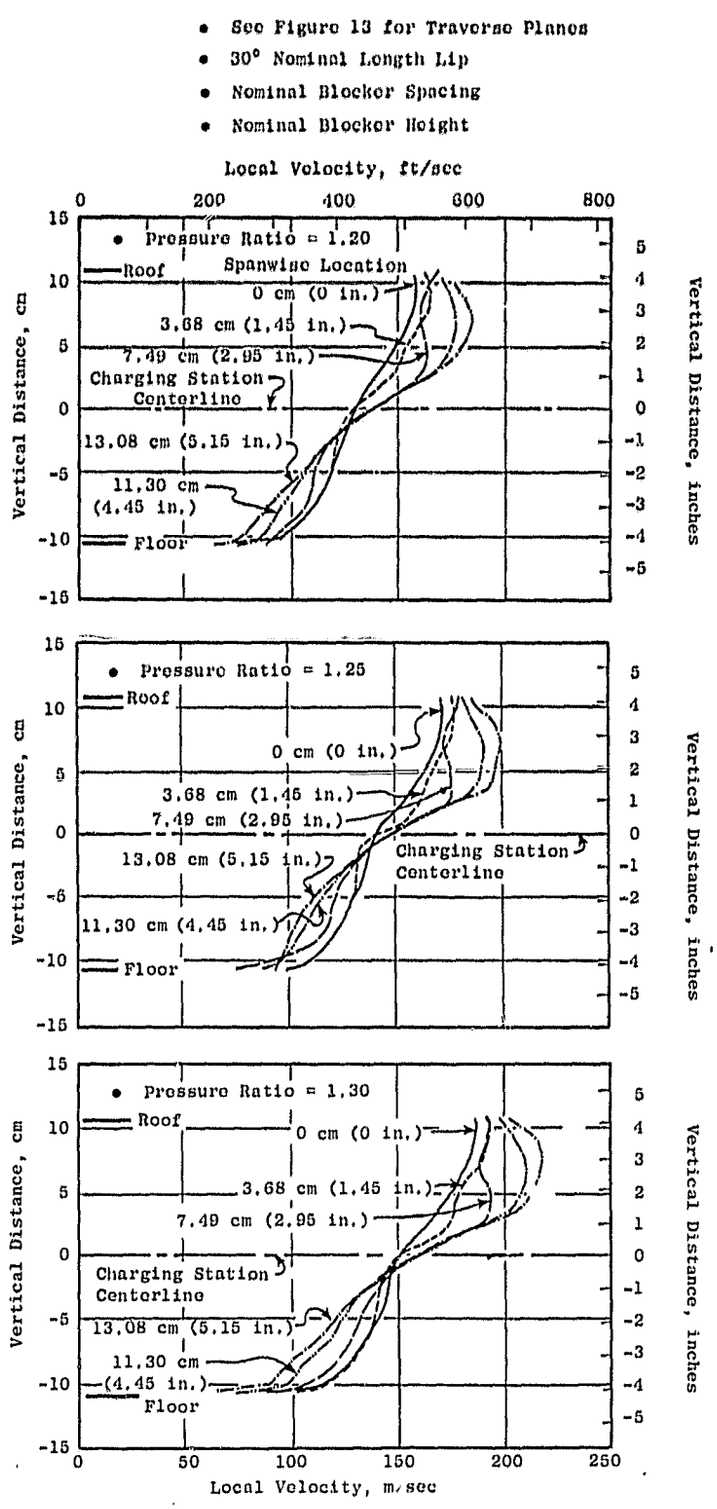

Figure 21. Reverse Thrust Charging Station Velocity Profiles (Nominal Configuration).

• See Figure 13 for Traverse Planes

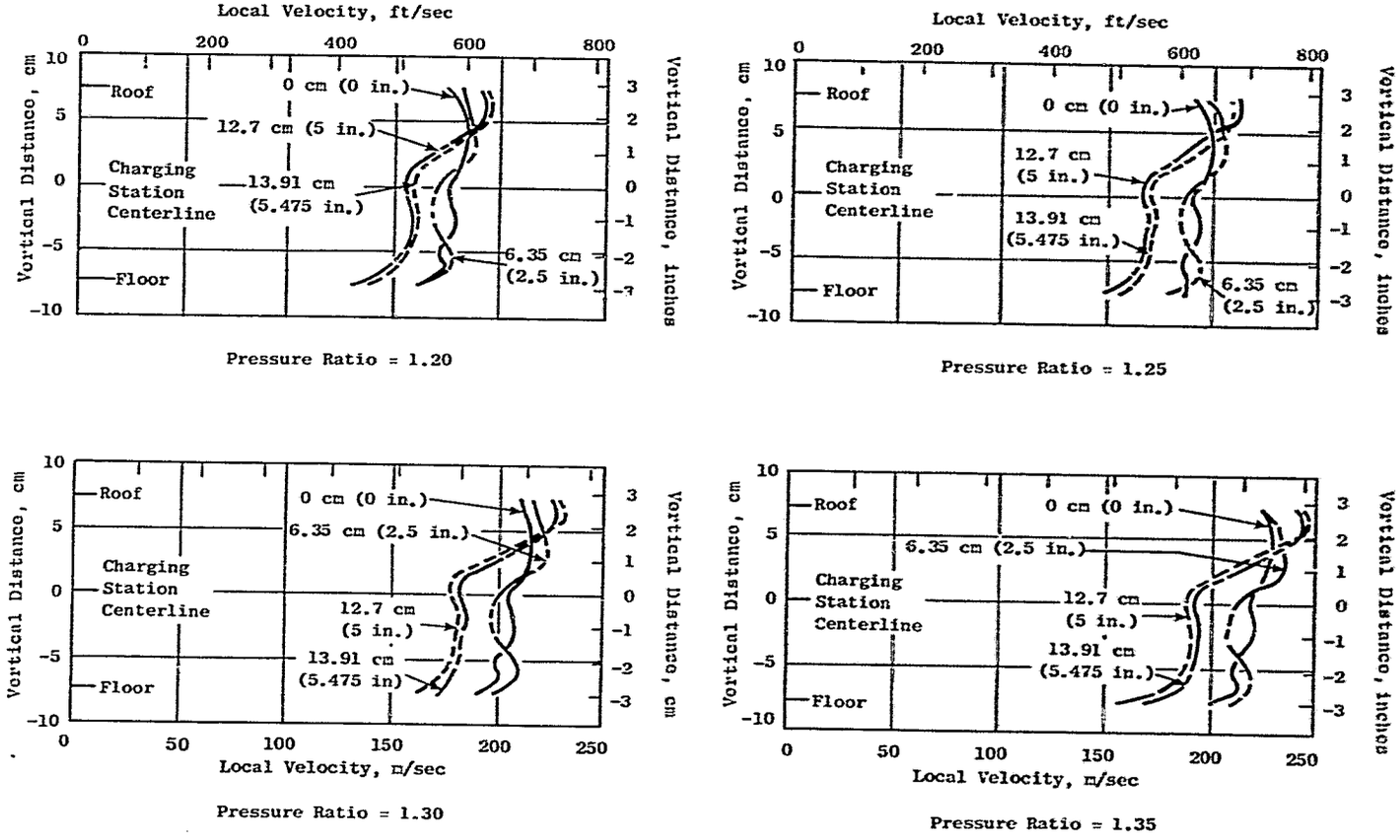

Figure 22. Forward Thrust Cruise Nozzle Velocity Profiles.

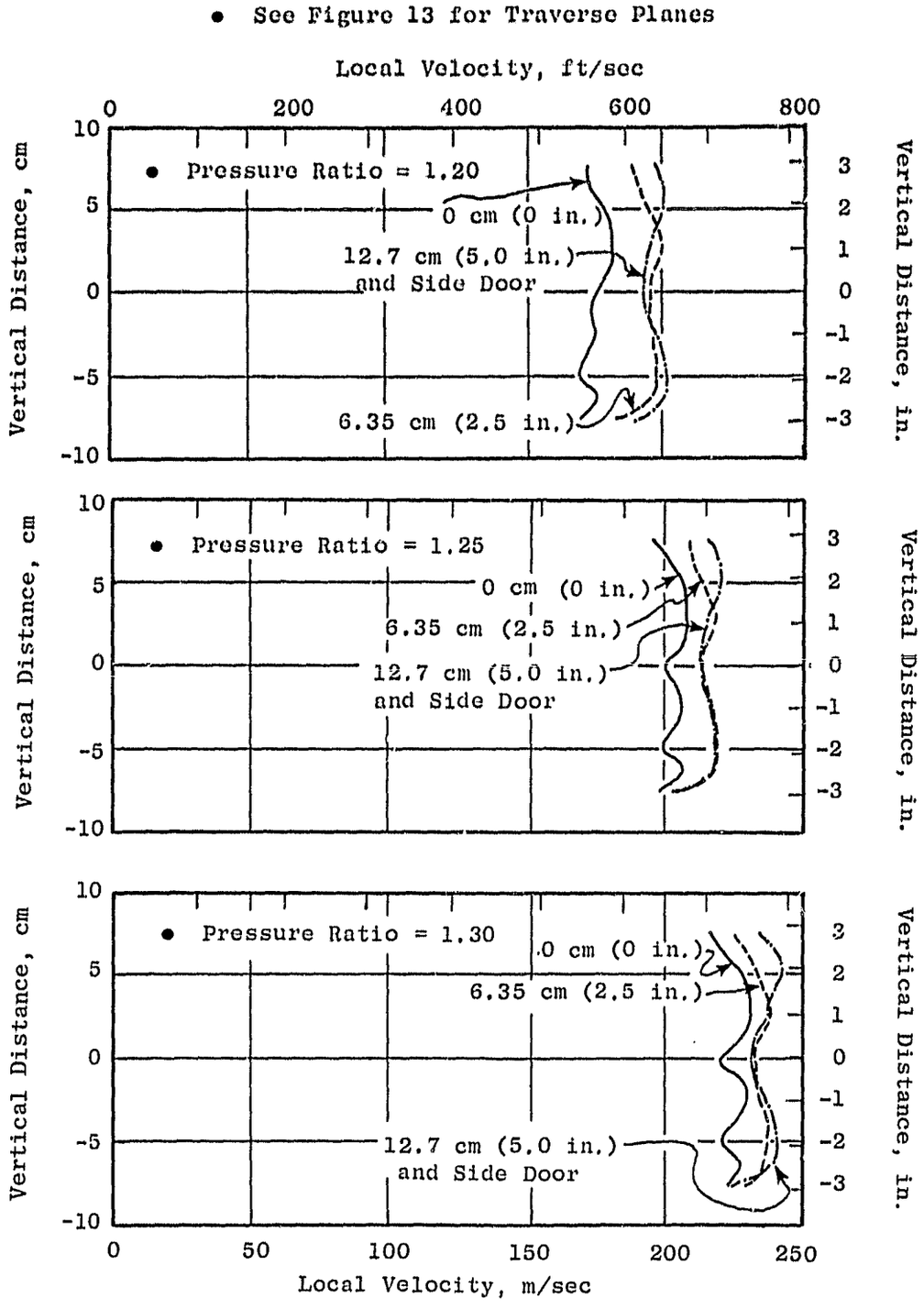

Figure 23. Forward Thrust Takeoff Nozzle Velocity Profiles.

- Nominal Blocker Spacing
- Nominal Blocker Height
- 30° Nominal Length Lip

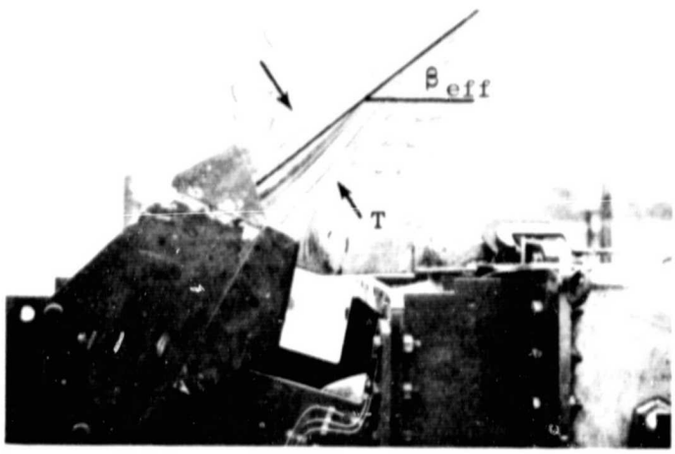

β_{eff} = Effective Blocker Door Discharge Angle
T = Jet Thickness

Figure 24. Typical Reverser Efflux Pattern - Nominal Configuration.

reverser exit and spillage flow values are only rough estimates. A summary of the calculated spillage flow rates and observed reverser lip flow angles for the reverse thrust configurations is shown in Table III.

The total pressure drop from the instrumentation frame to the reverser charging station was estimated using wall friction and strut loss calculations. $\Delta P_T/q$ for this loss was estimated to be 0.25. The turning loss from the charging station to the reverser exit was estimated to be 0.25 ($\Delta P_T/q$) based upon 90 degree pipe bend data which gives a $\Delta P_T/q$ of 0.5. Because the blocker system does not totally envelop the flow as a pipe would, and the Mach number in the blocker turn is lower than the blocker exit (contrary to constant area pipe flow), the blocker turning loss should be less than the indicated pipe flow value.

The spillage flow angle estimates obtained during testing were used to estimate reverse thrust losses associated with this flow. These flow angles are summarized in Table IV.

Reverse thrust performance referenced to forward takeoff thrust at 1.29 pressure ratio is presented in Figure 25 for all reverse thrust models. The extended blocker height configuration with nominal blocker spacing and nominal length 30 degree lip gave the best performance and achieved the goal of 35 percent of takeoff thrust at a pressure ratio of 1.20. All other configurations required a higher pressure ratio to achieve the same level of reverse thrust performance.

Subsequent thrust reverser tests at the NASA Langley Research Center with a 1/12 scale model of the QCSEE OTW thrust reverser (Reference 3) gave reverse thrust levels considerably lower than those shown in Figure 25.

Table III. Model Flow Characteristics Obtained from Lampblack Photographs.

Configuration	Description	W Spillage / W Total	Reverse Flow Angle, $\beta_{effective}$ (degrees)
9	Close Spacing, 30° Lip	.10	45
8	Nominal Spacing, 30° Lip	.17	50
10	Wide Spacing, 30° Lip	.18	48
11	Extended Height, 30° Lip	.11	42
12	Nominal Spacing, 20° Lip	.14	45
15	Extended Lip, 20° Lip	.23	23

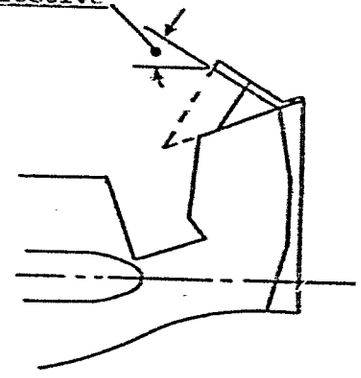

Table IV. Spillage Flow Angle Estimates.

Configuration	Effective Side Flow Angle From Engine Centerline, Degrees
9	70-80
8	62-71
10	73-82
11	70-80
12	62-71
15	52-62

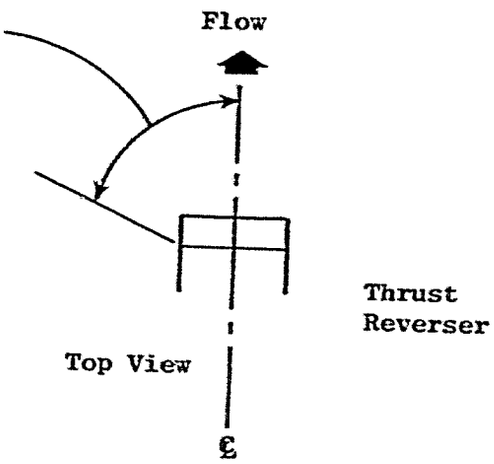

NOTE: The spillage flow was in the aft direction giving forward thrust for this part of the flow.

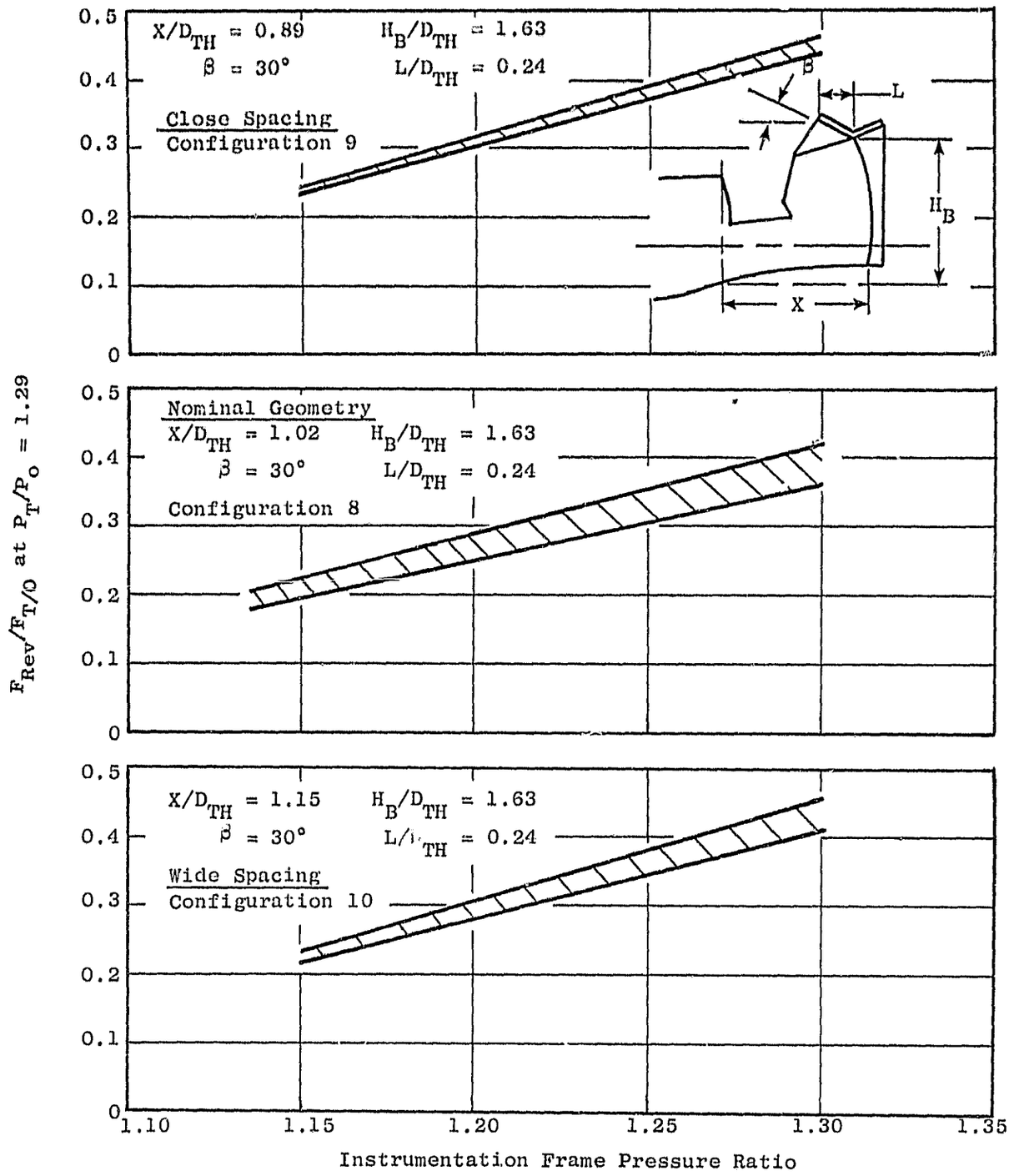

Figure 25. OTW Model Thrust Reverser Performance Estimates.

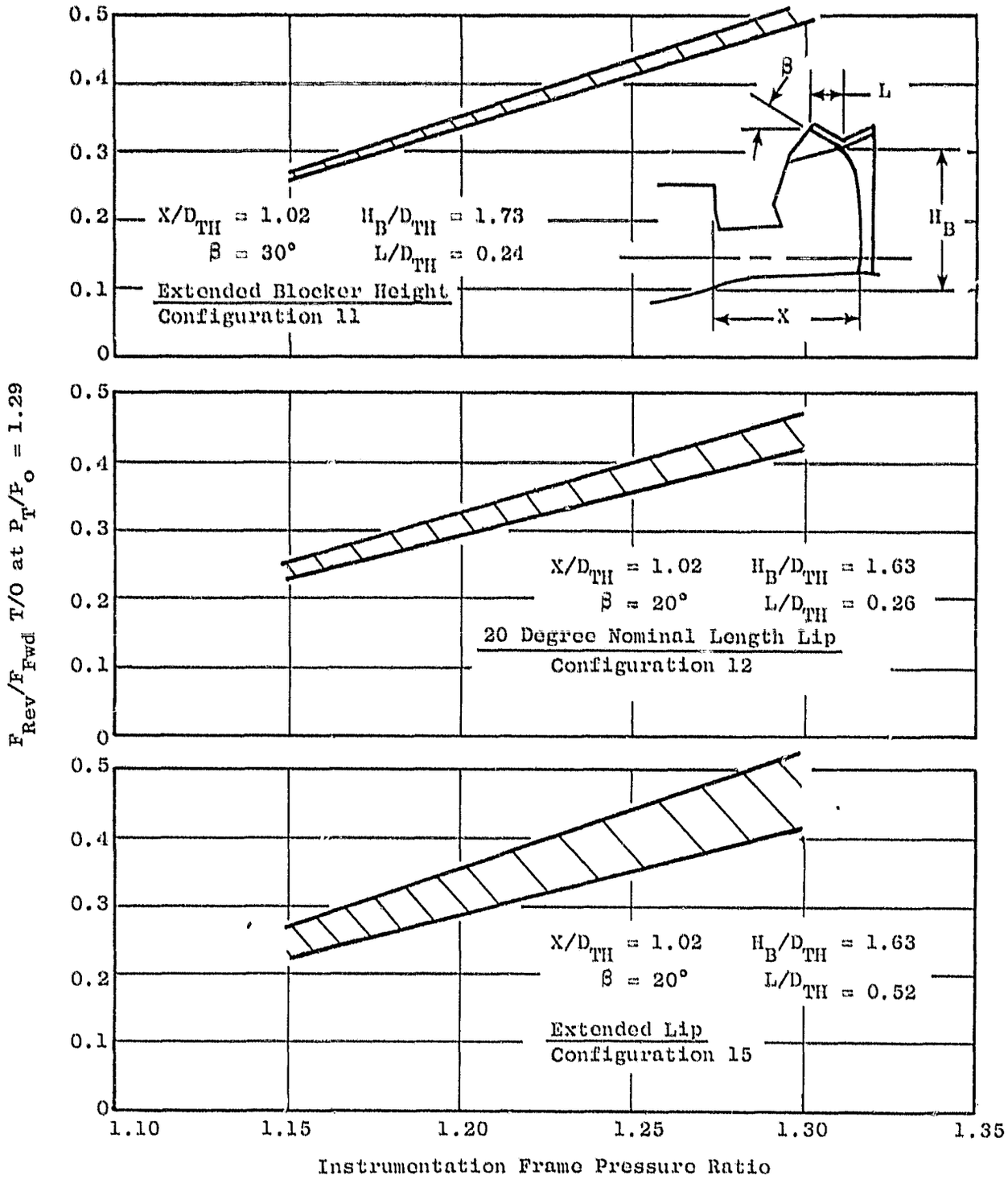

Figure 25. OTW Model Thrust Reverser Performance Estimates (Concluded).

SECTION VII

ACOUSTIC RESULTS

A. FORWARD THRUST

OTW model forward thrust configurations included a cruise and a takeoff nozzle both of which were tested with and without a simulated stub wing. A range of nozzle pressure ratios were run from 1.20 to 1.35. This pressure ratio is the total pressure measured at the instrumentation frame shown in Figure 3 relative to ambient pressure.

The discussion in this section will pertain to sound levels that have been scaled to the QCSEE OTW engine size.

1. Cruise Nozzle

The cruise nozzle which was tested has been discussed earlier in Figures 3, 4, and 5. Installation of the long stub wing resulted in about a 1.7 percent decrease in model flow. This is shown in Figure 16.

Acoustically, the long stub wing increased the 152 m (500 ft) sideline PNL's by 2 to 3 PNdB at all angles. This is shown in Figure 26 at a pressure ratio of 1.35. Although not shown, similar differences are observed at lower pressure ratios. A comparison of the SPL spectra at the angle of maximum noise is shown in Figure 27. The effect of the long stub wing is evident in the low frequencies with the difference decreasing from 4 dB at frequencies from 50 to 100 Hz to zero at 1000 Hz. Similar differences were observed at other angles and pressure ratios. Figure 28 shows the effect of the long stub wing on peak PNL as a function of pressure ratio. The long wing increases the peak PNL by 2 PNdB at all pressure ratios.

2. Takeoff Nozzle

The OTW model takeoff nozzle is shown schematically in Figure 6 and pictorially in Figure 7. Side doors were opened to provide the correct takeoff nozzle area and operating line for the fan. The stub wing was shortened axially to match the configuration contemplated for static tests of the full-size OTW engine.

Tests were made with and without the short stub wing to determine the effect of the wing on both aerodynamic and acoustic performance. There was no change in model flow due to the presence of the short stub wing as shown in Figure 16.

Acoustically, installation of the short stub wing had no effect on the 152 m (500 ft) sideline PNL's near the angle of maximum noise. This is shown in Figure 29 at a pressure ratio of 1.35 and is also representative of the lower pressure ratio results. Away from the angle of maximum noise there is a slight increase due to the short stub wing at the forward angles

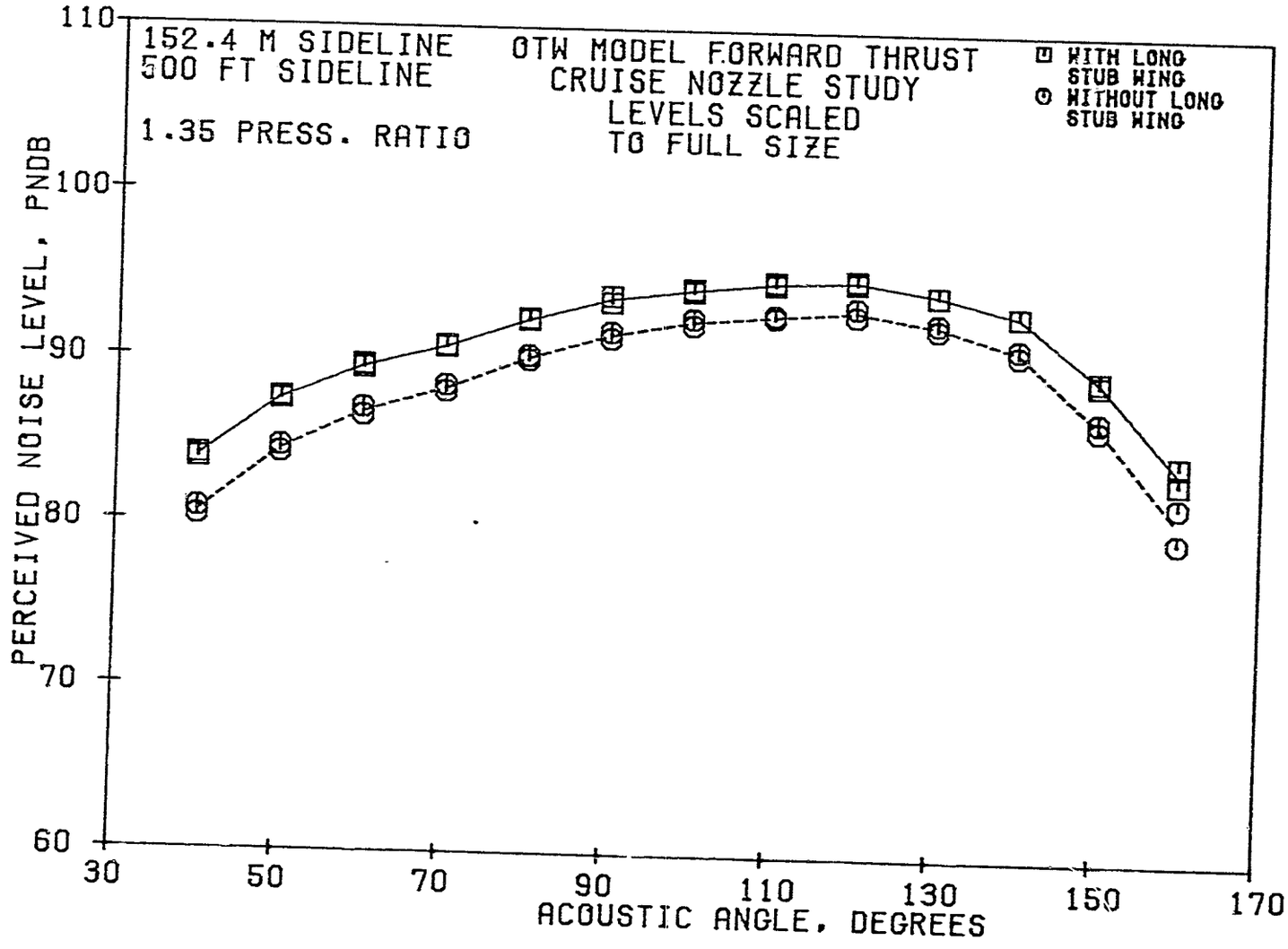

Figure 26. Cruise Nozzle PNL Directivity with and without Long Stub Wing.

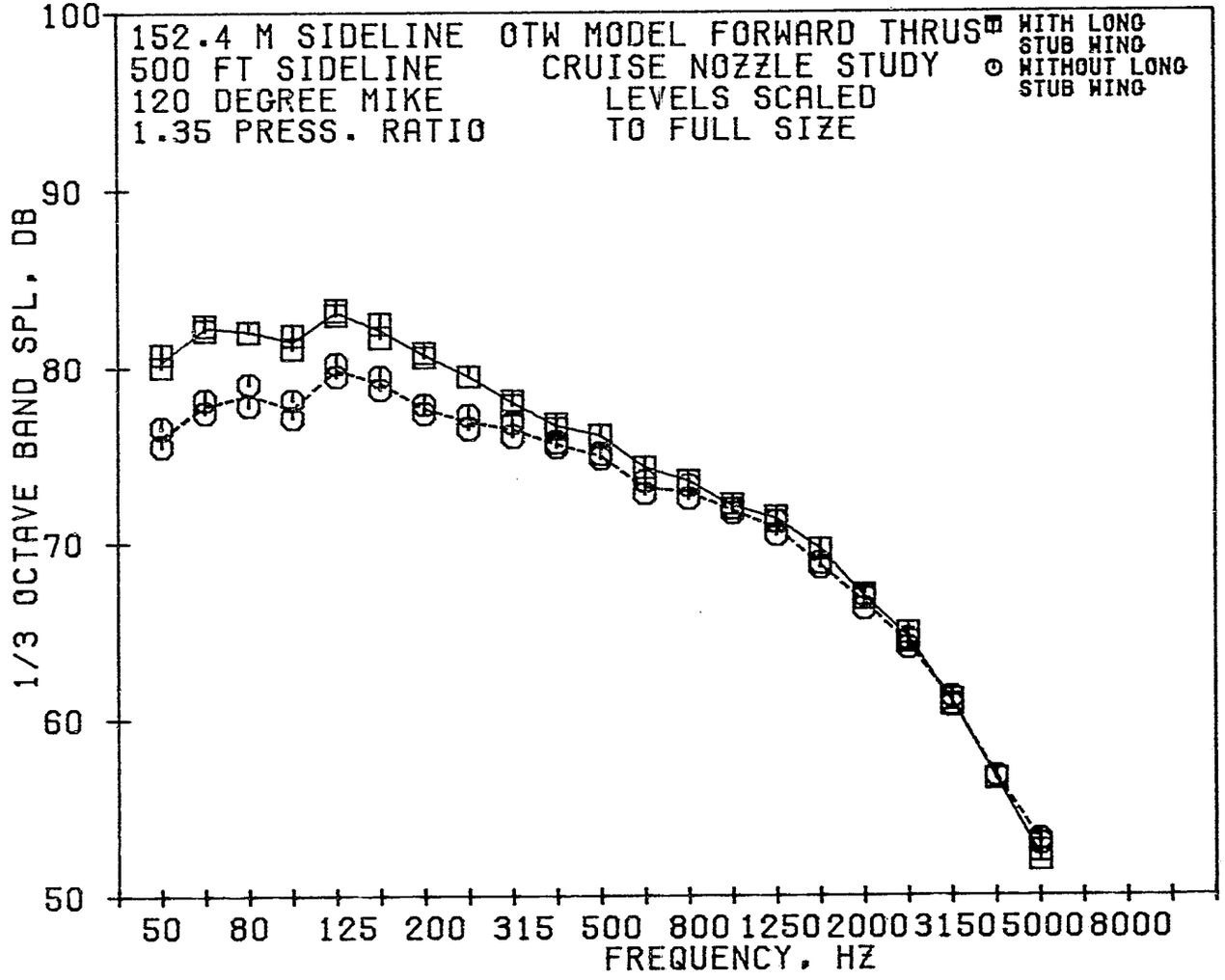

Figure 27. Cruise Nozzle Spectra with and without Long Stub Wing.

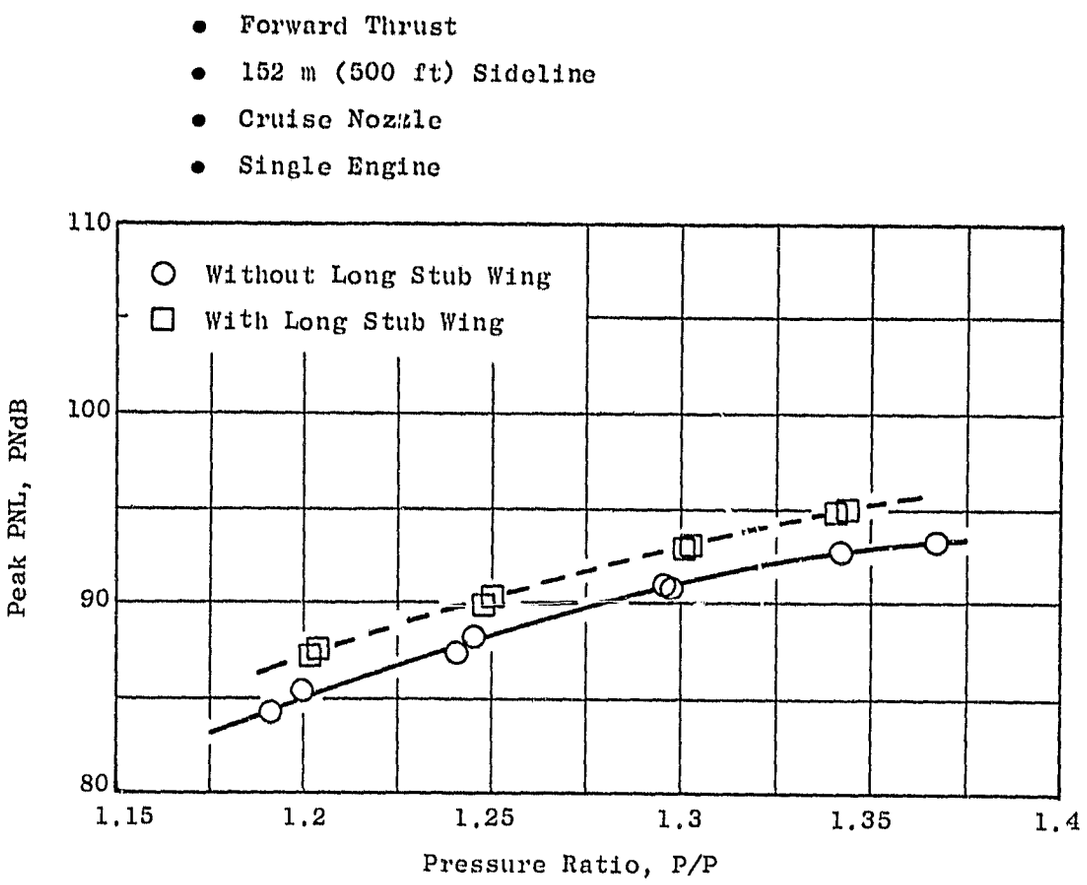

Figure 28. Cruise Nozzle Peak PNL Variation with Pressure Ratio.

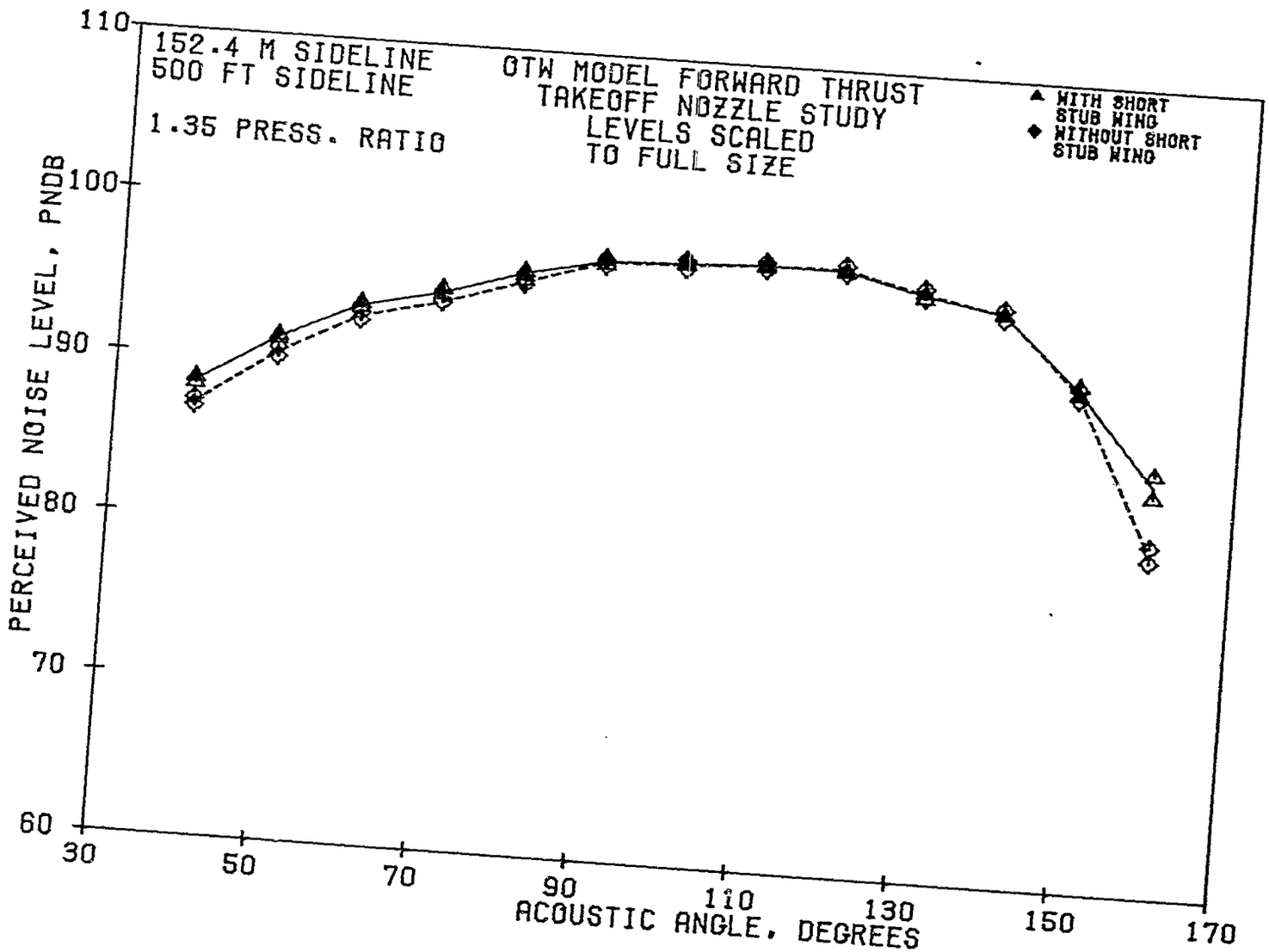

Figure 29. Takeoff Nozzle PNL Directivity with and without Short Stub Wing.

of 40 to 80 degrees and at 160 degrees. At the angle of maximum noise of 120 degrees, there is no significant difference in the spectra. This is shown in Figure 30. There is also no effect on the peak PNL's as a function of pressure ratio as indicated by the comparison in Figure 31. These data indicate that the short stub wing when installed on the takeoff nozzle does not generate any noise which would need to be accounted for in the full-size engine tests or in system noise estimates.

3. Takeoff and Cruise Nozzle Comparison

To obtain the increased nozzle area at the takeoff cycle point, side doors were opened to one fixed position of 35° open. A comparison of the cruise and takeoff nozzle weight flow without the stub wing is given in Figure 16. There is 17.5 percent less flow with the cruise nozzle.

The noise of the takeoff nozzle is greater than one would expect from the flow increase at a given pressure ratio. For example, in Figure 32 at 1.30 pressure ratio (most representative of takeoff cycle conditions) and 120 degrees, the PNL difference between the takeoff and cruise nozzles is 4.0 PNdB. The expected difference due to 10 times the log of the weight flow ratio at 1.3 pressure ratio would be 0.9 PNdB. This implies that the side doors generated noise which increased the sideline level by 3 PNdB. On a spectral basis, the noise increase is primarily low frequency. This is shown in Figure 33 which also includes an estimated spectrum obtained by adding 10 times the log of the weight flow ratio at each frequency to the cruise nozzle. The PNL difference between takeoff and cruise nozzles remains constant with pressure ratio as shown in Figure 34.

B. Reverse Thrust

An investigation of reverse thrust geometrical parameters was conducted on the OTW model. The parameters which were varied included axial spacing of the blocker, blocker height, lip angle, and lip length.

As with the forward thrust configurations, total pressure was measured at the instrumentation frame shown in Figure 8 and ratioed to ambient pressure.

1. Spacing Effects

A schematic of the thrust reverser spacing variations is shown in Figure 35. The spacing to the blocker, X, is referenced to the flowpath height at the charging station, D_{TH}. Nominal spacing had an X/D_{TH} of 1.02 while the close spacing was 0.89 and the wide spacing was 1.15. Lip angle, lip length, and blocker height were nominal for this spacing variation study (see Figure 10).

Blocker spacing effect on 152 m (500 ft) sideline PNL's are shown in Figure 36. The wide spacing has consistently higher levels with the peak PNL occurring at 90 degrees. Decreasing spacing decreases the peak PNL and shifts the peak angle forward. At 60 degrees, in Figure 37, the effect of spacing occurs primarily in the low frequencies which accounts for the small

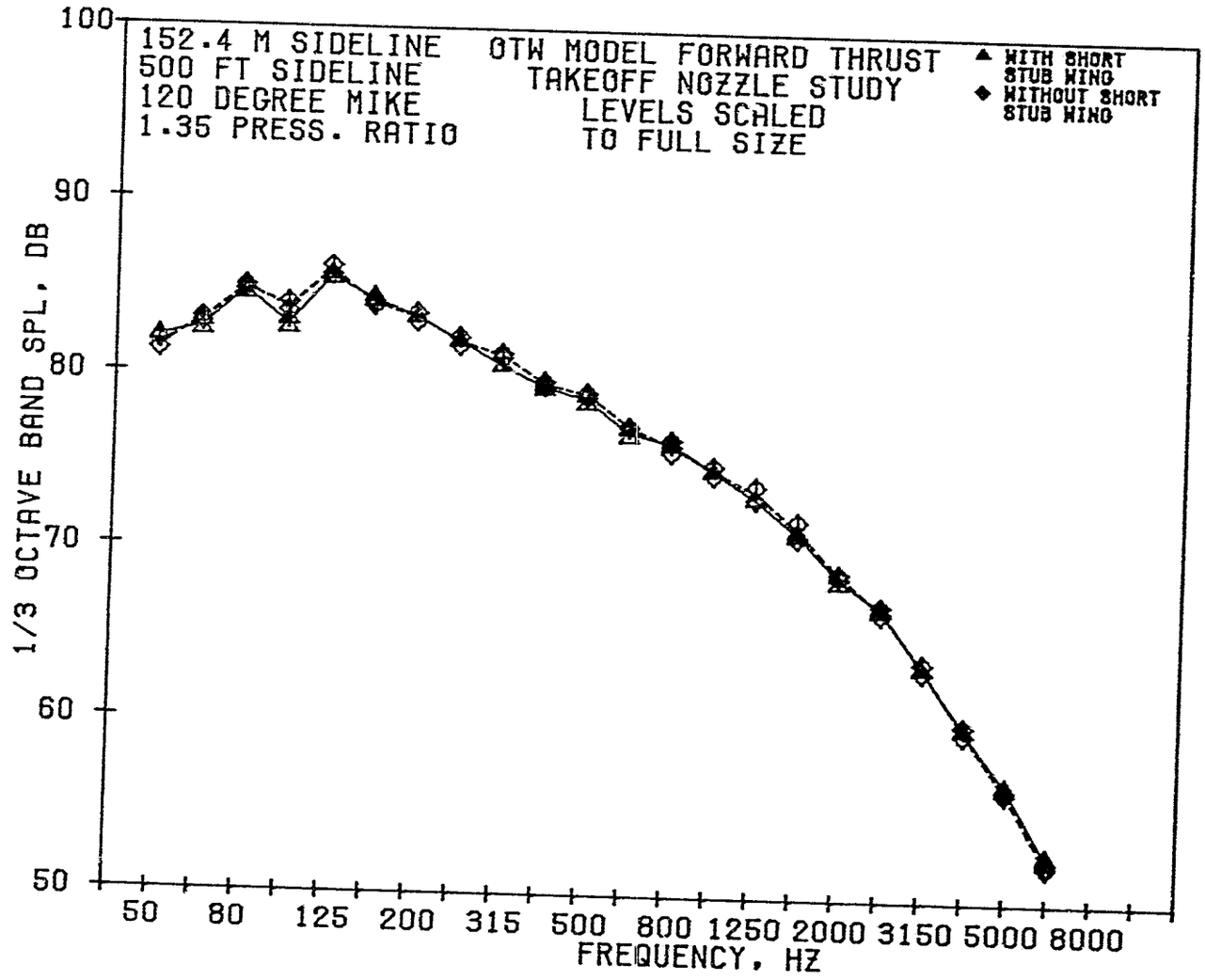

Figure 30. Takeoff Nozzle Spectra with and without Short Stub Wing.

- Forward Thrust
- 152 m (500 ft) Sideline
- Takeoff Nozzle
- Single Engine

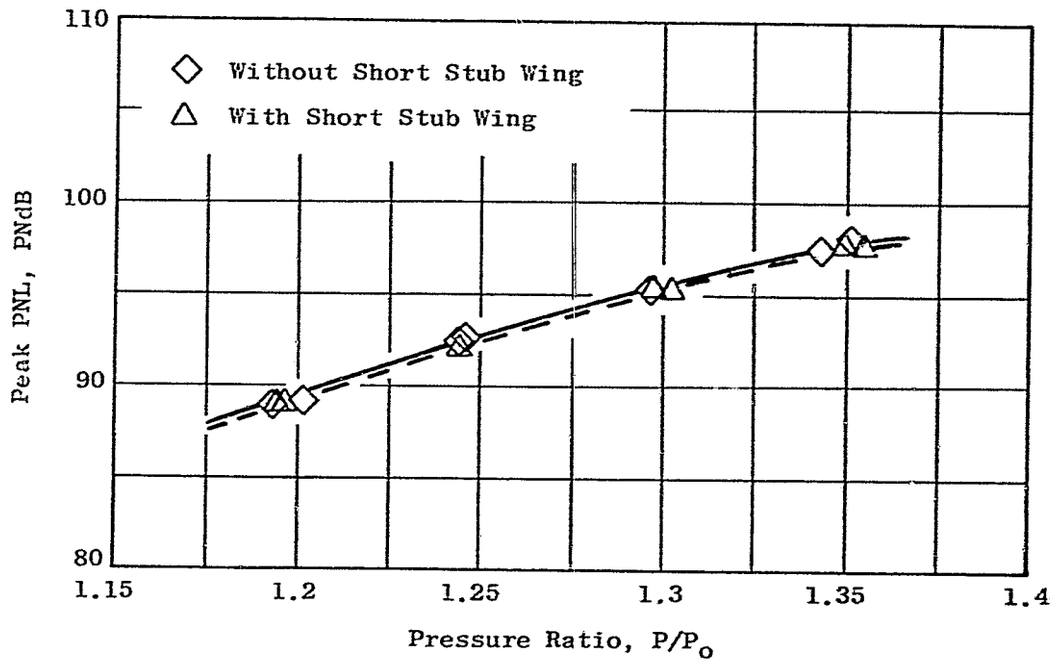

Figure 31. Takeoff Nozzle Peak PNL Variation with Pressure Ratio.

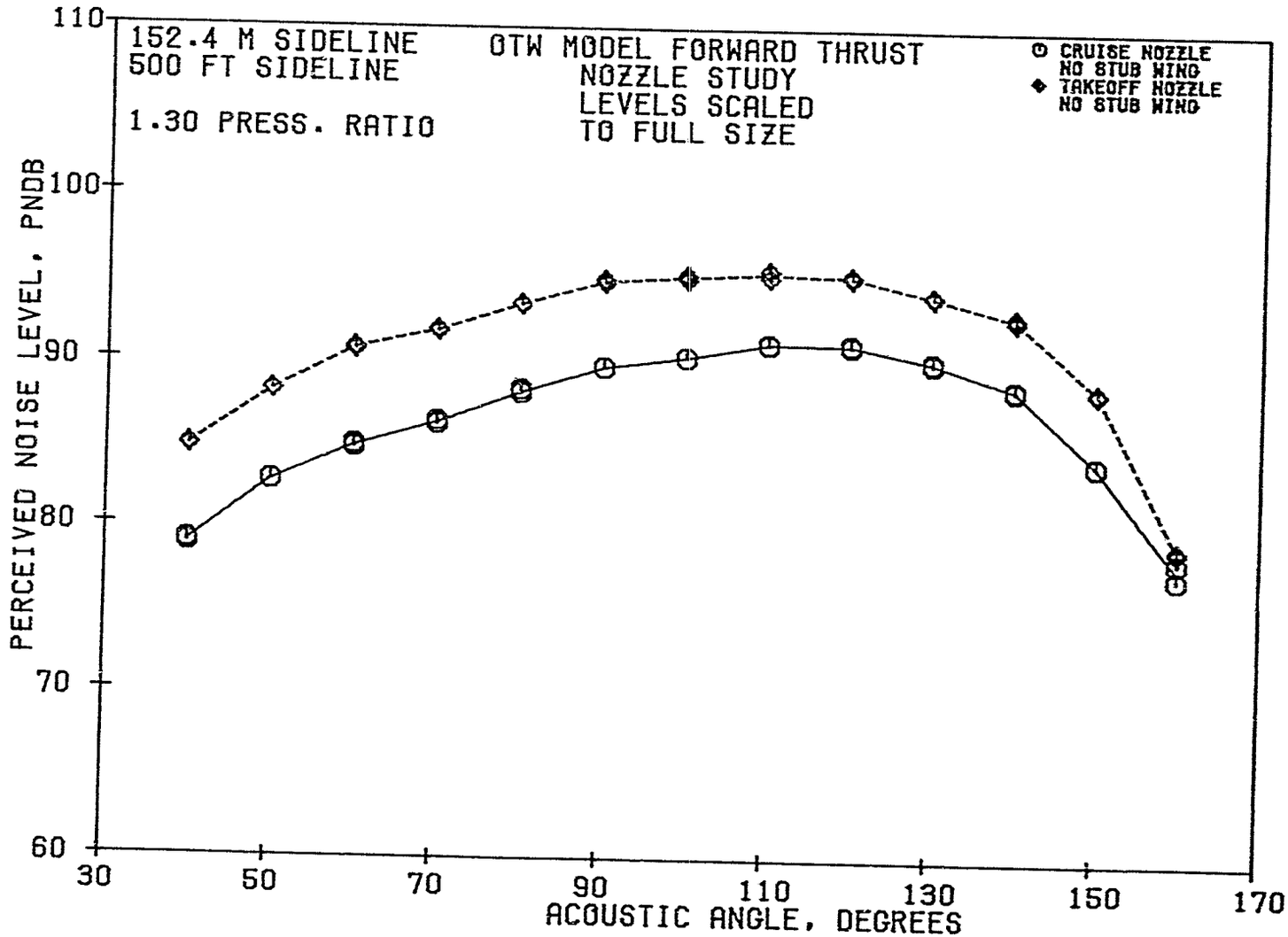

Figure 32. Cruise and Takeoff Nozzle PNL Directivity Comparison.

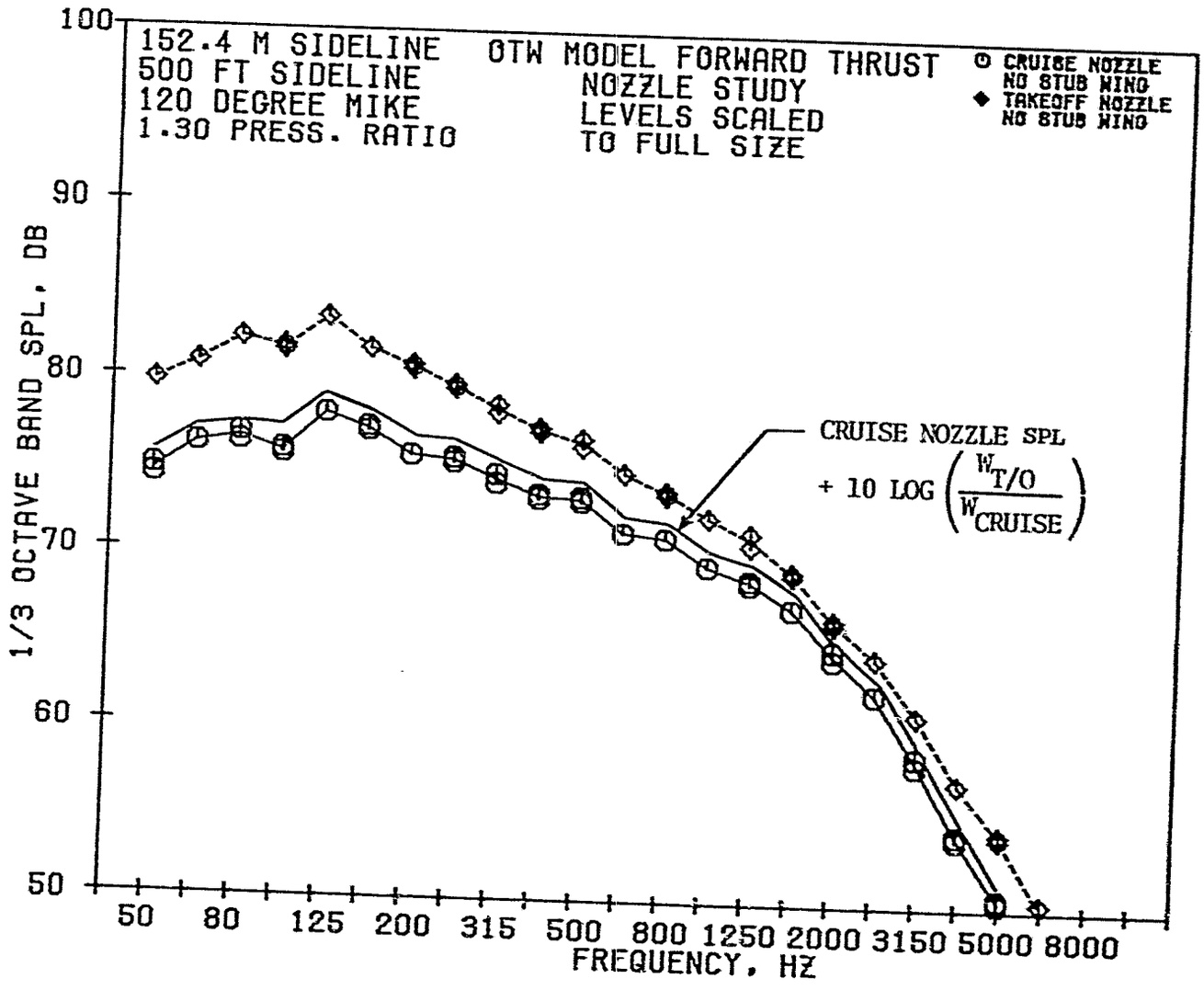

Figure 33. Cruise and Takeoff Nozzle Spectral Comparison at 120 Degrees.

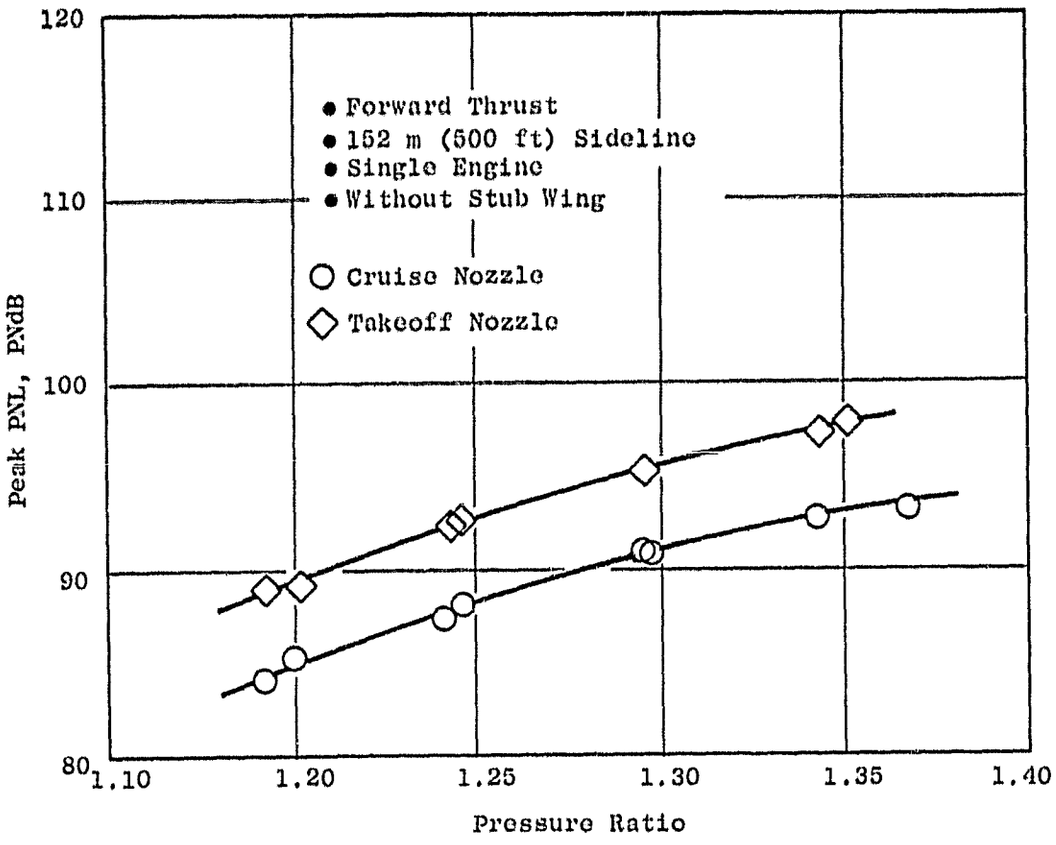

Figure 34. Cruise and Takeoff Nozzle Peak PNL Comparison as a Function of Pressure Ratio.

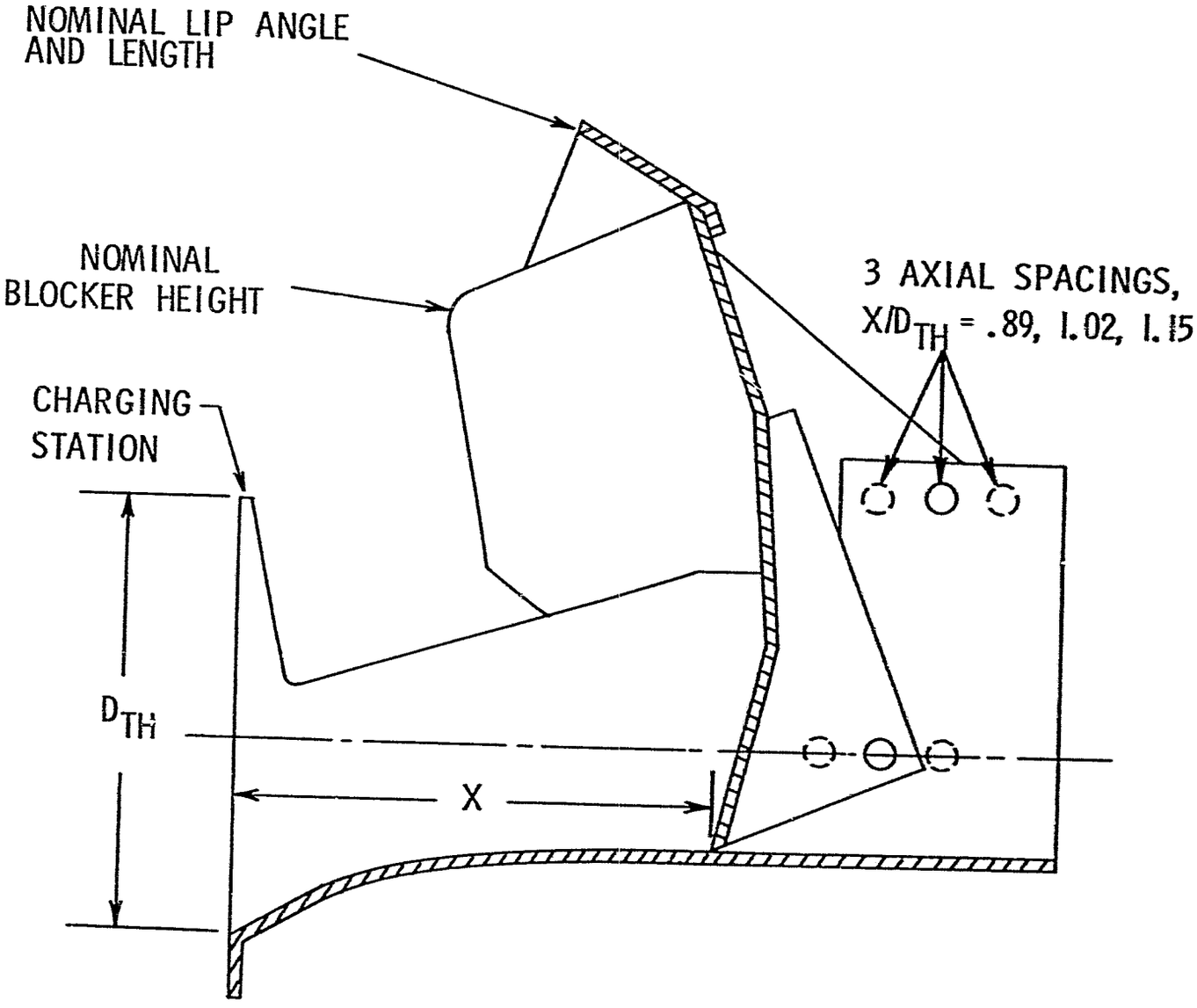

Figure 35. Reverse Thrust Spacing Variation.

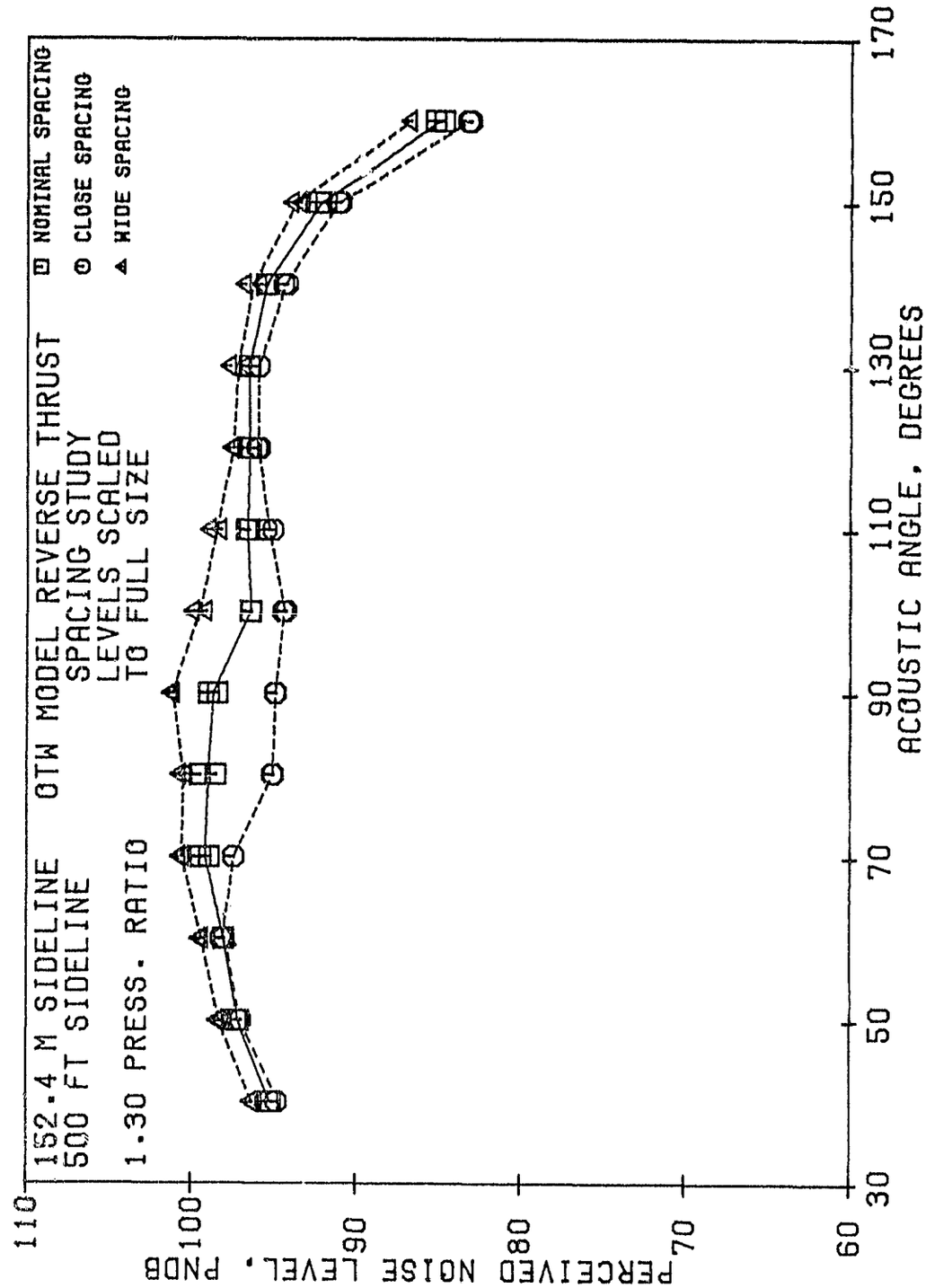

Figure 36. Reverse Thrust PNL Variation with Blocker Spacing.

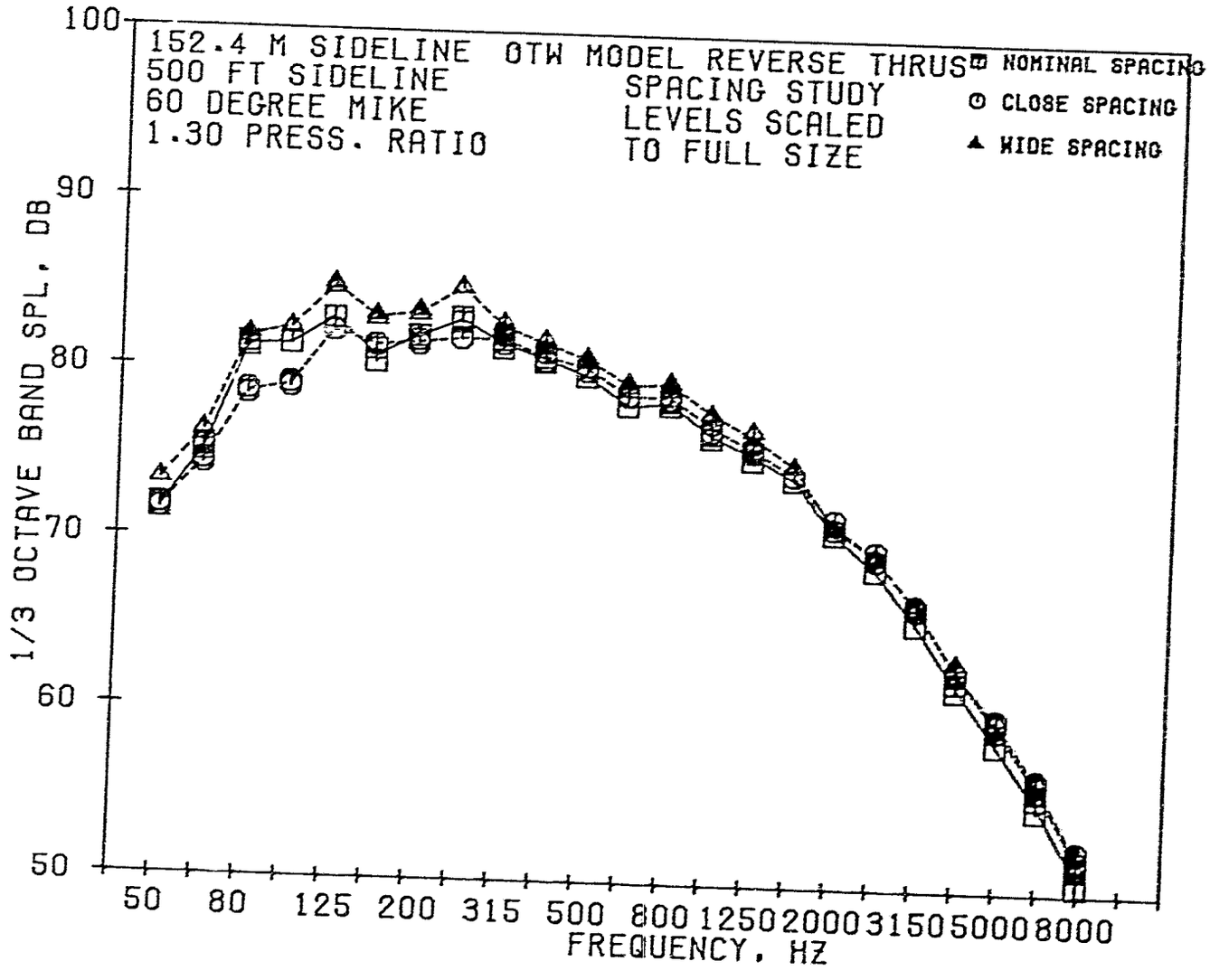

Figure 37. Reverse Thrust SPL Spectral Variation with Blocker Spacing at 60 Degrees.

effect noted in PNL at this angle in the preceding figure. At 80 degrees, in Figure 38, the effect of spacing is seen at all frequencies. The effect of pressure ratio variations on peak PNL are presented in Figure 39 which shows the wide spacing to be consistently higher and the close spacing the quietest.

2. Blocker Height Effects

Two different blocker heights were tested on the reverse thrust model. As shown in Figure 40, the height to the lip, H, was varied. A nominal height and an increased height were tested. Ratioed to charging station height, H/D_{TH} varied from 1.77 to 1.87. Spacing, lip angle, and lip length were nominal. There was 1 to 2 PNdB decrease in sideline PNL with the increased blocker height as shown in Figure 41. This difference holds at all angles larger than 50°. At the peak angle, Figure 42 shows that the increased blocker height is approximately 1 dB below the nominal blocker height at nearly all frequencies. At decreasing pressure ratio the peak PNL difference is about 0.5 PNdB with the increased length having the lower level as shown in Figure 43.

3. Lip Angle and Length Effects

Previous sections have discussed the effects of varying blocker spacing and height. This section involves variations of the lip itself, viz., angle and length while holding spacing and height nominal. The geometry is shown in Figure 44. Angle variation was from 30 degrees to 20 degrees with a nominal length lip. The lip length variation was done with the 20 degree lip and involved doubling the length from $L/D_{TH} = 0.26$ to $L/D_{TH} = 0.52$.

A comparison of the PNL directivities from the lip geometries is presented in Figure 45. The 20 degree extended lip had the highest PNL's over all angles and had a peak at 80 degrees. Both the 20 and 30 degree nominal length lip peaked at 70 degrees with the 20 degree lip being 0.5 PNdB higher. Spectral comparisons at 70 and 80 degrees in Figures 46 and 47, respectively, show that lip geometry changes affect the spectra from 100 to 4000 Hz with the 20 degree extended lip the highest. At 70 degrees the nominal length lips of 20 and 30 degrees differ only from 125 to 1000 Hz. This accounts for the small PNL difference between these two at 70 degrees. The peak 152 m (500 ft) PNL variation of these lip geometries with pressure ratio is shown in Figure 48. The 20 degree extended lip is 2 PNdB higher than both the nominal length lips. There is an increase of 0.5 PNdB for the 30° lip angle relative to the 20° lip angle for lips of nominal length.

4. Summary of Geometry Effects

Each of the thrust reverser geometry changes have been discussed individually in the preceding sections. Figure 49 presents the reverse thrust peak 152.4 m (500 ft) sideline PNL's as a function of pressure ratio. The levels shown have been scaled to full size and corrected to a four engine configuration with fuselage shielding and dirt/grass type of surface as specified in Reference 4. Highest levels were measured for the 20 degree extended lip while the lowest levels were for the close spacing configuration.

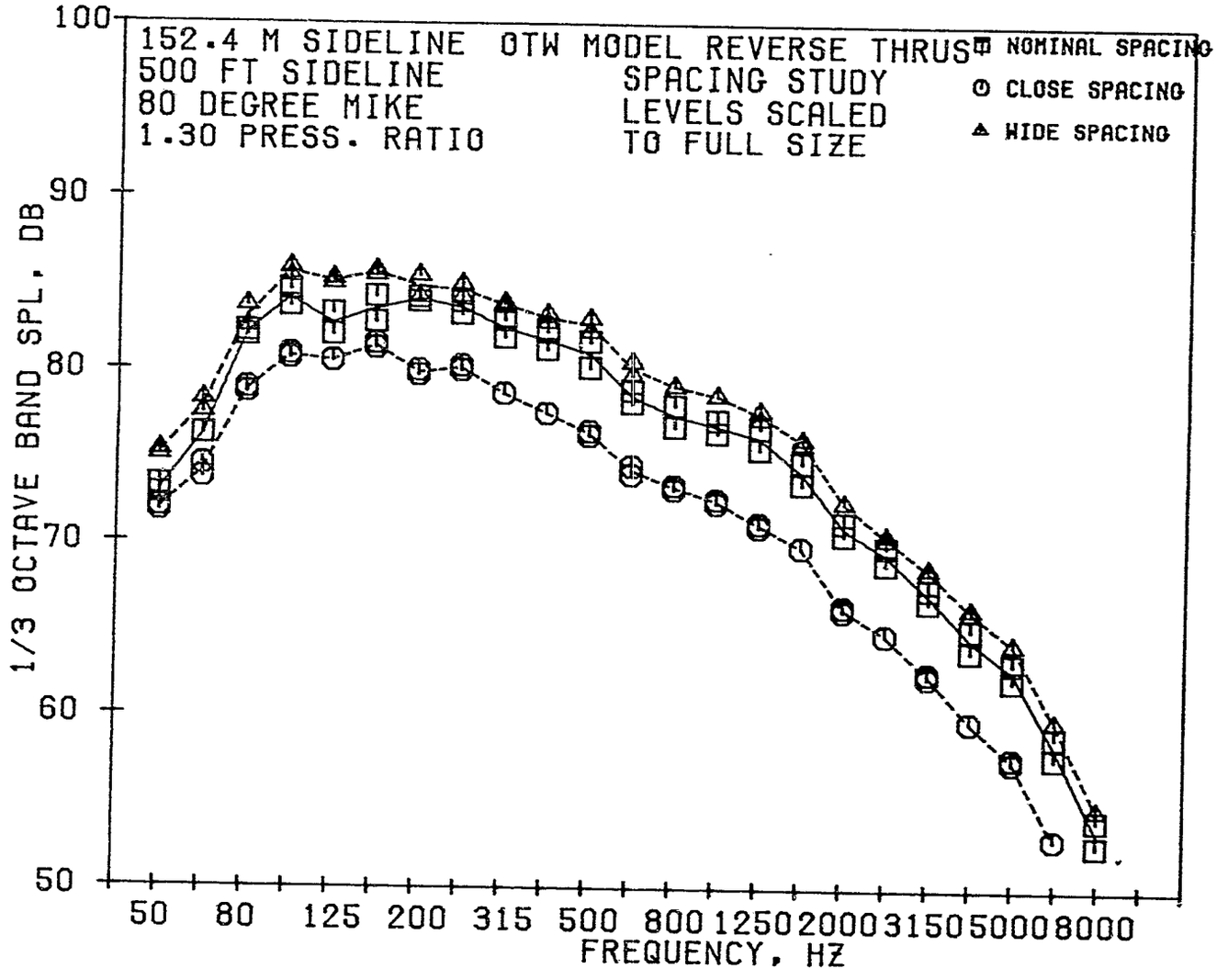

Figure 38. Reverse Thrust SPL Spectral Variation with Blocker Spacing at 80 Degrees.

- Reverse Thrust
- 152 m (500 ft) Sideline
- Nominal Blocker Height
- 30° Nominal Length Lip
- Single Engine

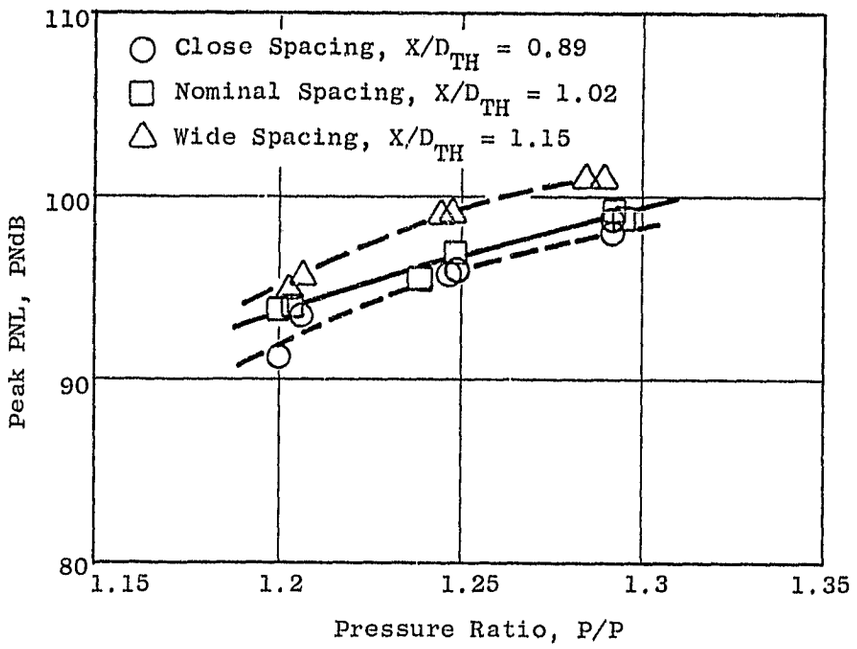

Figure 39. Reverse Thrust Peak PNL Variation with Blocker Spacing as a Function of Pressure Ratio.

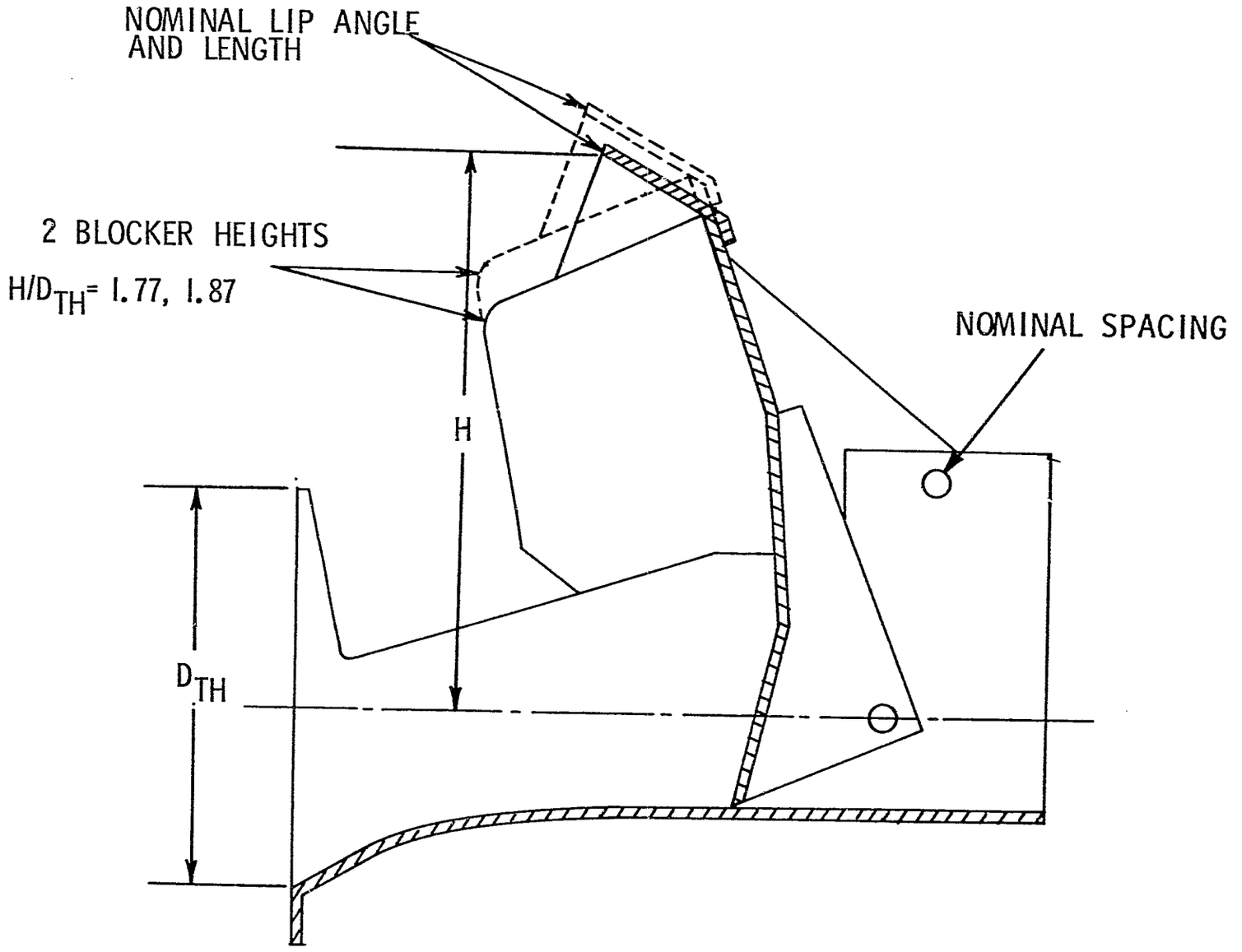

Figure 40. Reverse Thrust Blocker Height Variation.

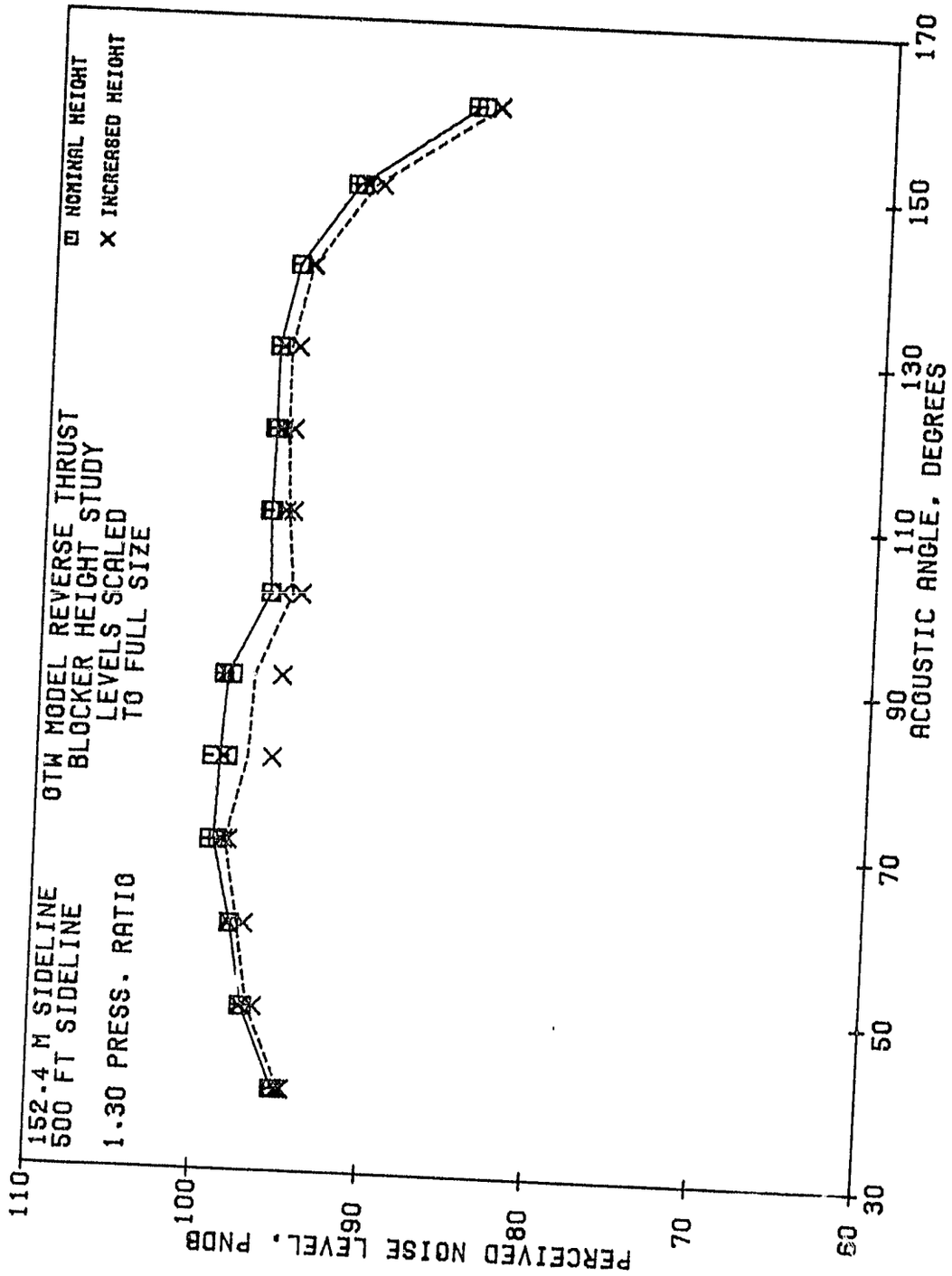

Figure 41. Reverse Thrust PNL Variation with Increased Blocker Height.

ORIGINAL PAGE IS
OF POOR QUALITY

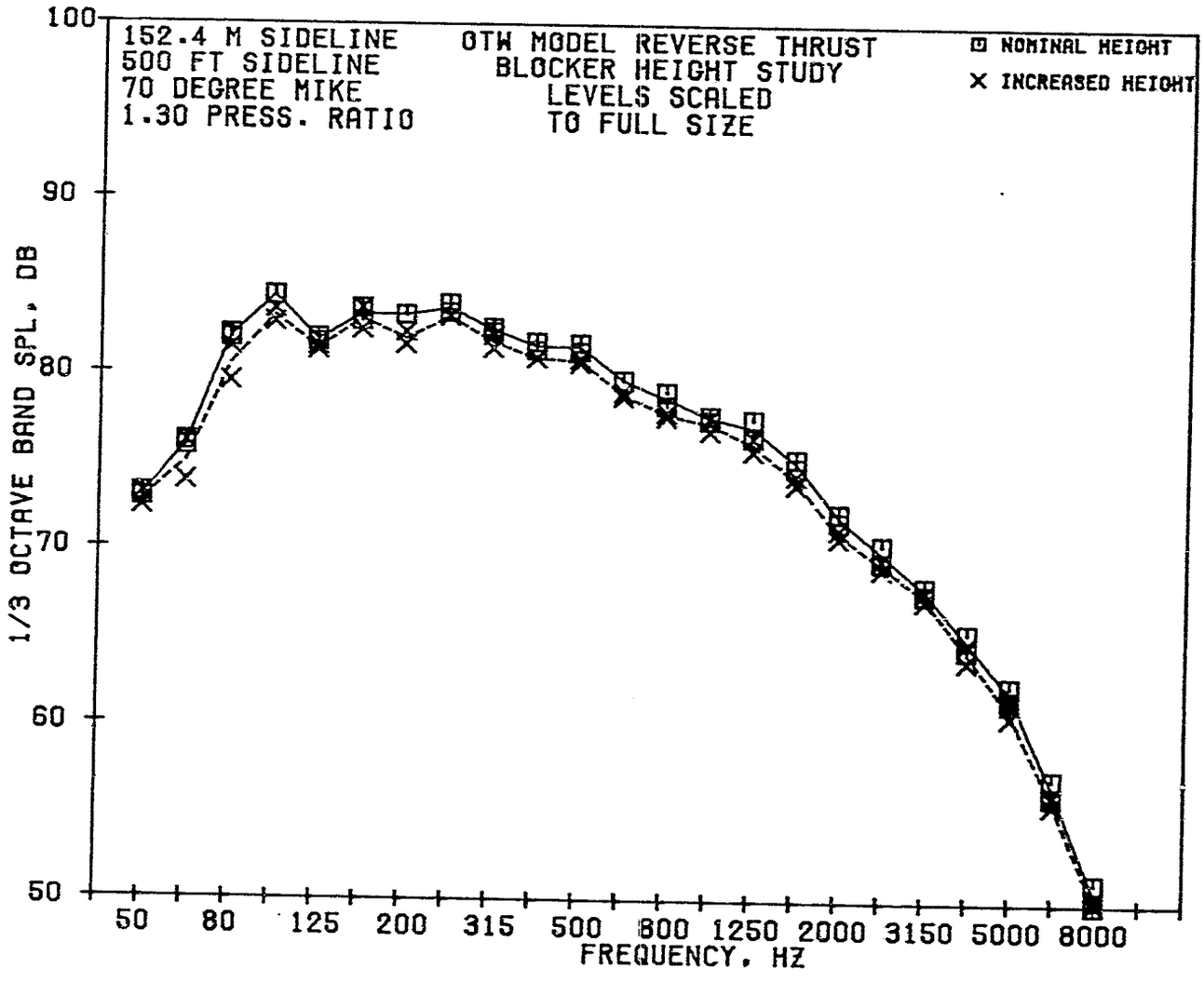

Figure 42. Reverse Thrust SPL Spectral Variation with Increased Blocker Height.

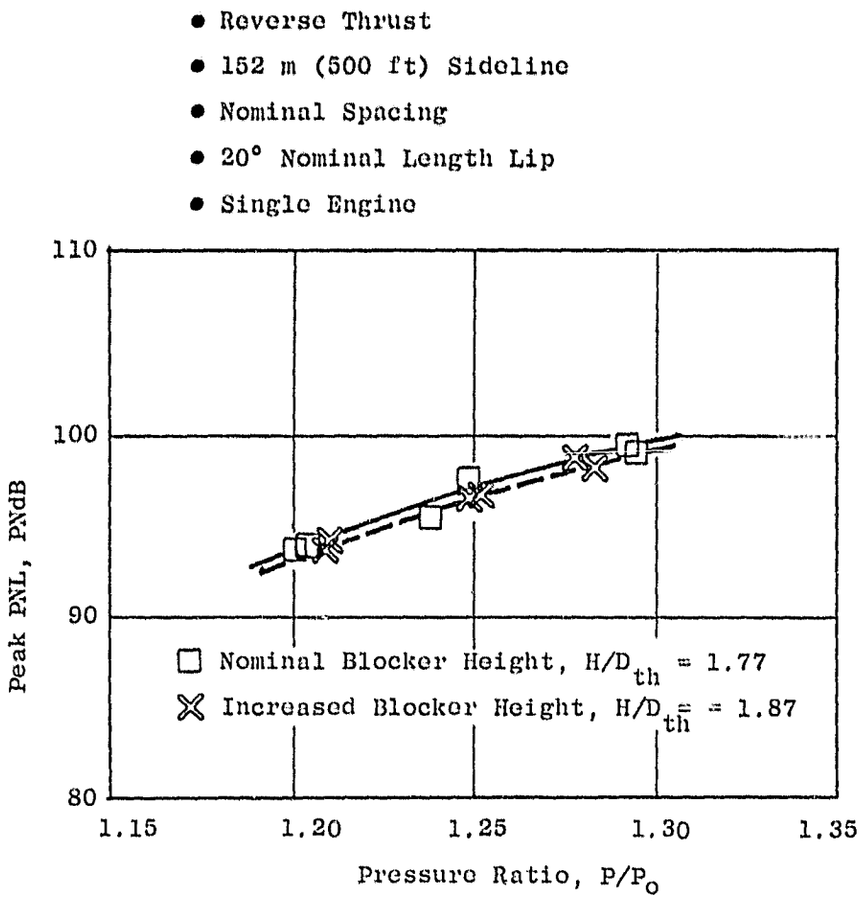

Figure 43. Reverse Thrust Peak PNL Variation with Increased Blocker Height as a Function of Pressure Ratio.

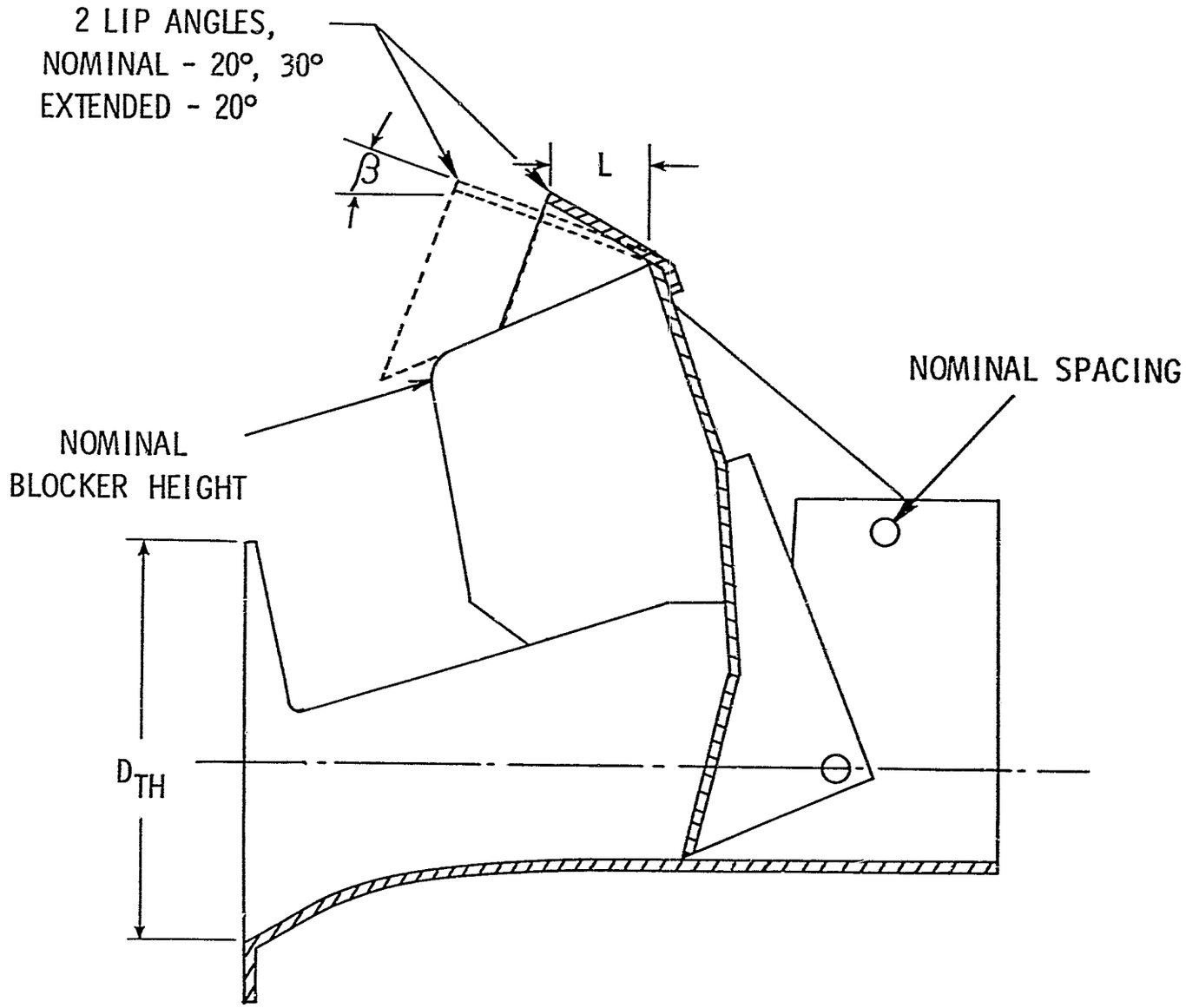

Figure 44. Reverse Thrust Lip Variation.

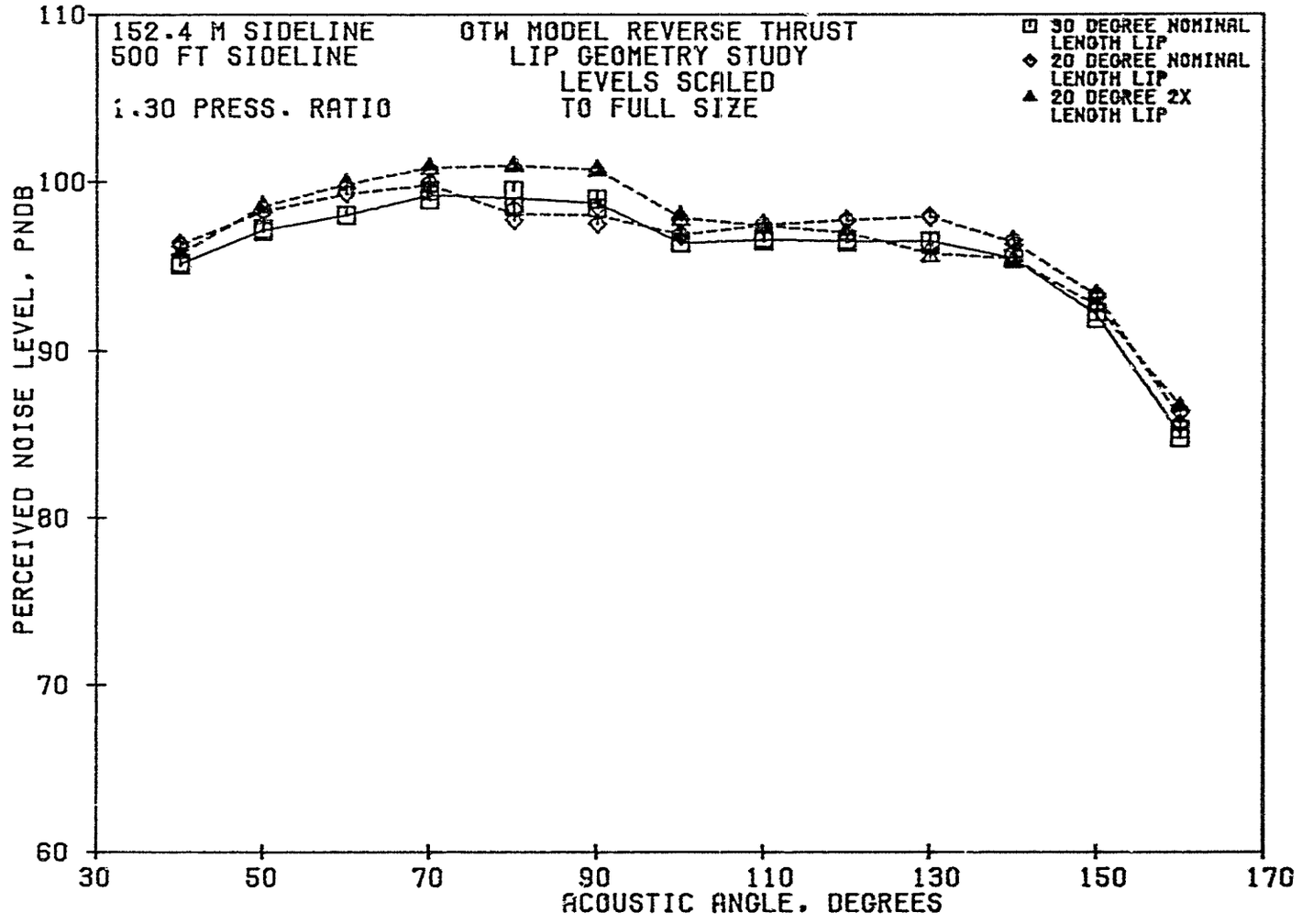

Figure 45. Reverse Thrust PNL Directivity Variation with Lip Geometry Changes.

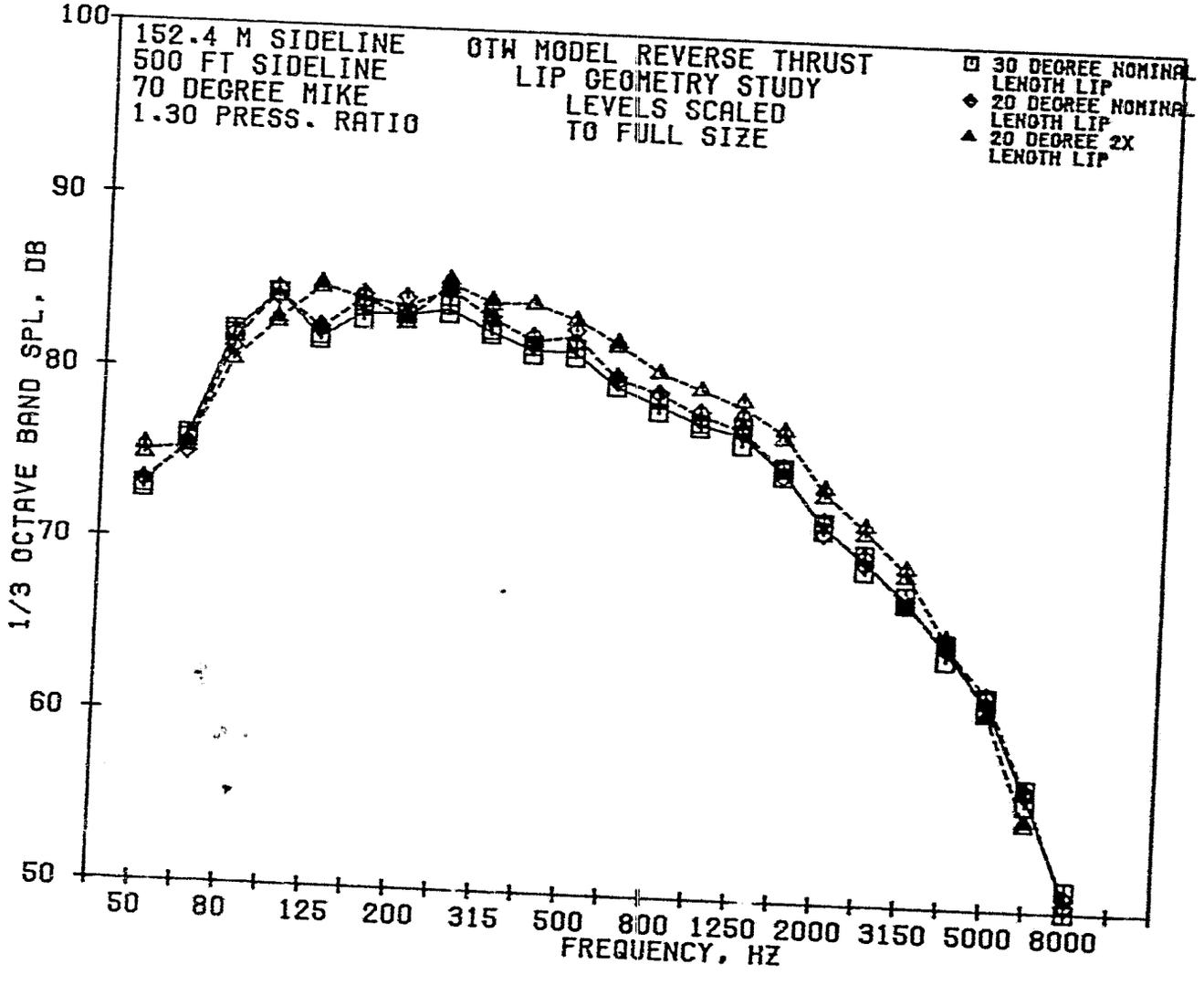

Figure 46. Reverse Thrust SPL Spectral Variations with Lip Geometry Changes at 70 Degrees.

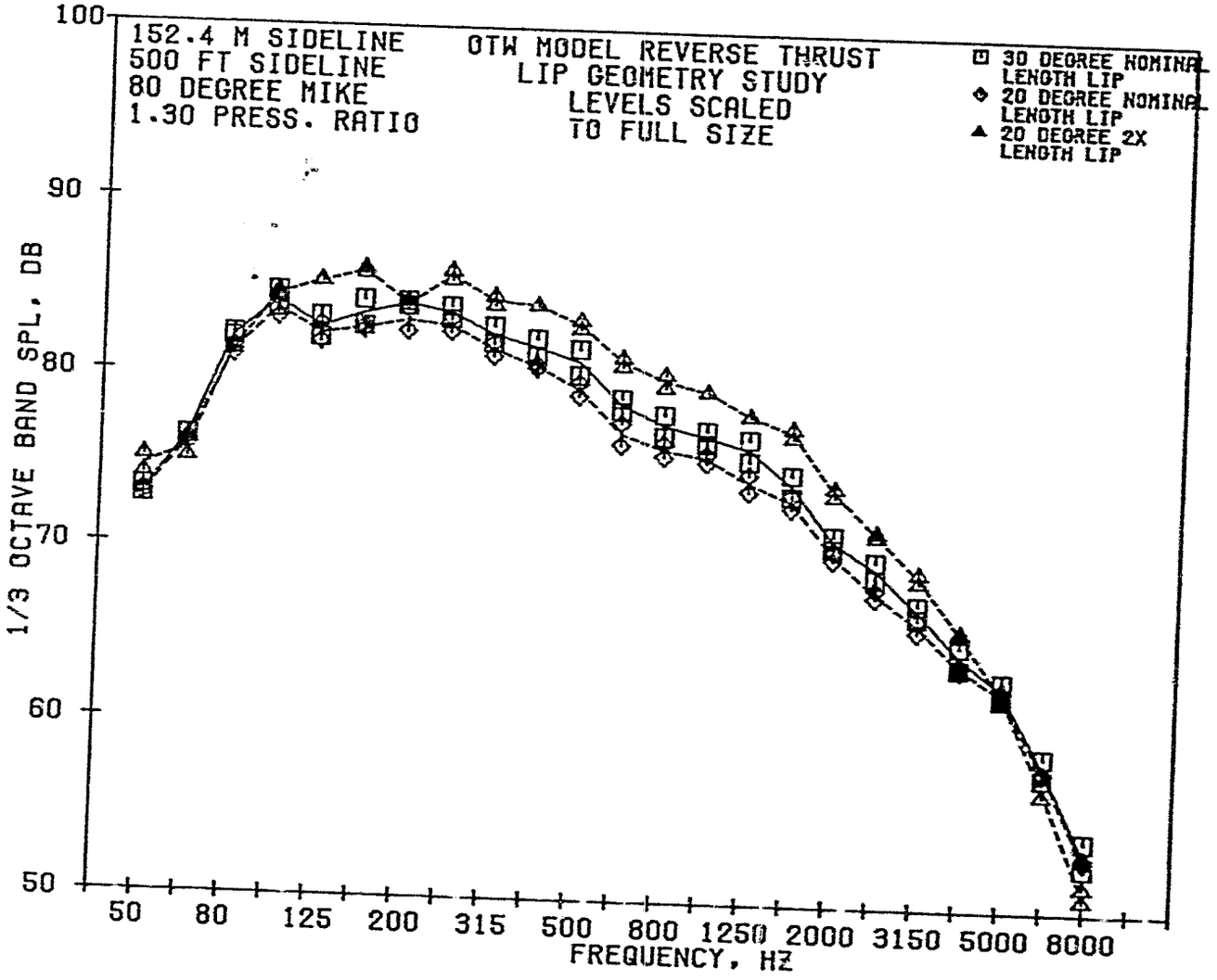

Figure 47. Reverse Thrust SPL Spectral Variation with Lip Geometry Changes at 80 Degrees.

- Reverse Thrust
- 152 m (500 ft) Sideline
- Nominal Spacing
- Nominal Blocker Height
- Single Engine

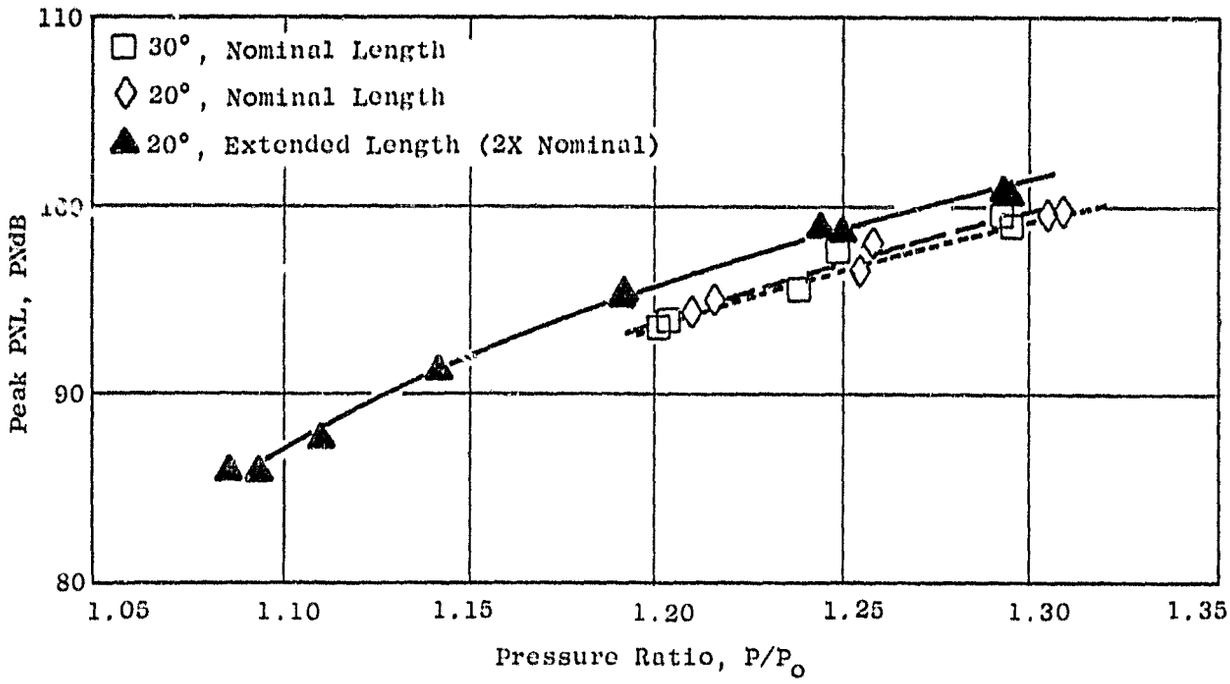

Figure 48. Reverse Thrust Peak PNL Variation with Lip Geometry Changes as a Function of Pressure Ratio.

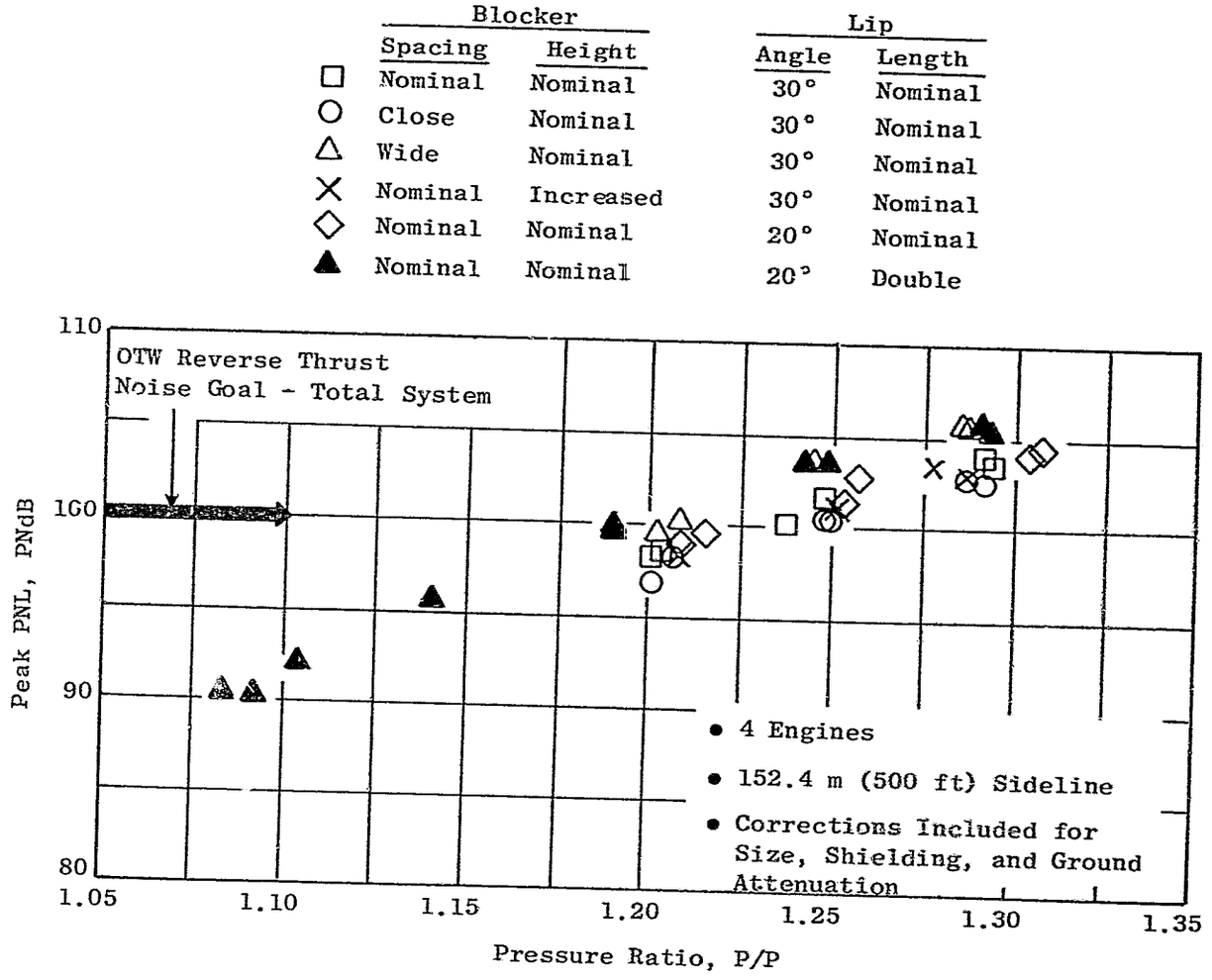

Figure 49. Summary of the Effect of Thrust Reverser Variations on Peak PNL as a Function of Pressure Ratio.

In reverse thrust, the total system noise goal including reverse thrust and other constituents is 100 PNdB on a 152.4 m (500 ft) sideline. This level is noted on Figure 49 and must be met at a reverse thrust level which is 35 percent or greater than the takeoff thrust. In preceding discussions of the reverse thrust levels, it was noted that the increased blocker height configuration would meet the reverse thrust level at the lowest pressure ratio of 1.20. The lowest pressure ratio is desirable because it minimizes the other noise constituents as well as reverse thrust noise; thus, the total system noise is the lowest. At this pressure ratio, the reverse thrust peak PNL is 98.0 PNdB. In order to meet the noise goal of 100 PNdB with this configuration at this pressure ratio, the other constituent noise levels (suppressed fan, core) must total not more than 93.8 PNdB. The empirical PNL adder curve shown in Figure 50 was used to calculate the allowable total of the other constituents.

This procedure can be used to estimate the maximum level of the other constituents for each thrust reverser configuration at the pressure ratio at which that configuration meets the thrust requirement.

b. Thrust Reverser Orientation

All of the preceding discussion on reverse thrust geometry variations was based on data taken with the reverser mounted conventionally as it would be on a wing with the exhaust gas flowing up and forward. Two alternate orientations were tested to provide a data base for possible mountings of the full-scale OTW engine when it is tested statically at the General Electric Peebles Test Operation. Here the engine is precluded from a conventional orientation because of the engine support structure located above the engine. Flow from a conventionally oriented thrust reverser would impact these supports and cause significant changes in the acoustic signature of the thrust reverser.

The first alternate mounting of the thrust reverser involved rotating the reverser 180 degrees so that the exhaust gas impinged on the ground. This is shown schematically in Figure 51. The ratio of the engine diameter to centerline height was held constant between the JENOTS test and the Peebles Test Operation. This required a simulated ground plane at JENOTS which is shown in Figure 52. With this orientation, there is a second sound source radiating to the far field, the jet impingement noise on the ground.

Thrust reverser geometry for the downward exhausting configuration was nominal spacing, nominal blocker height, and 30 degree nominal length lip. Figure 53 compares the 152 m (500 ft) sideline PNL directivities of the conventional and downward exhaust. At 70 degrees, which is the peak noise angle for both configurations, the downward exhaust levels are 1.5 to 2.0 PNdB higher than the conventional exhaust. In the aft quadrant, however, the downward exhaust levels are slightly lower. Similar results are observed at lower pressure ratios.

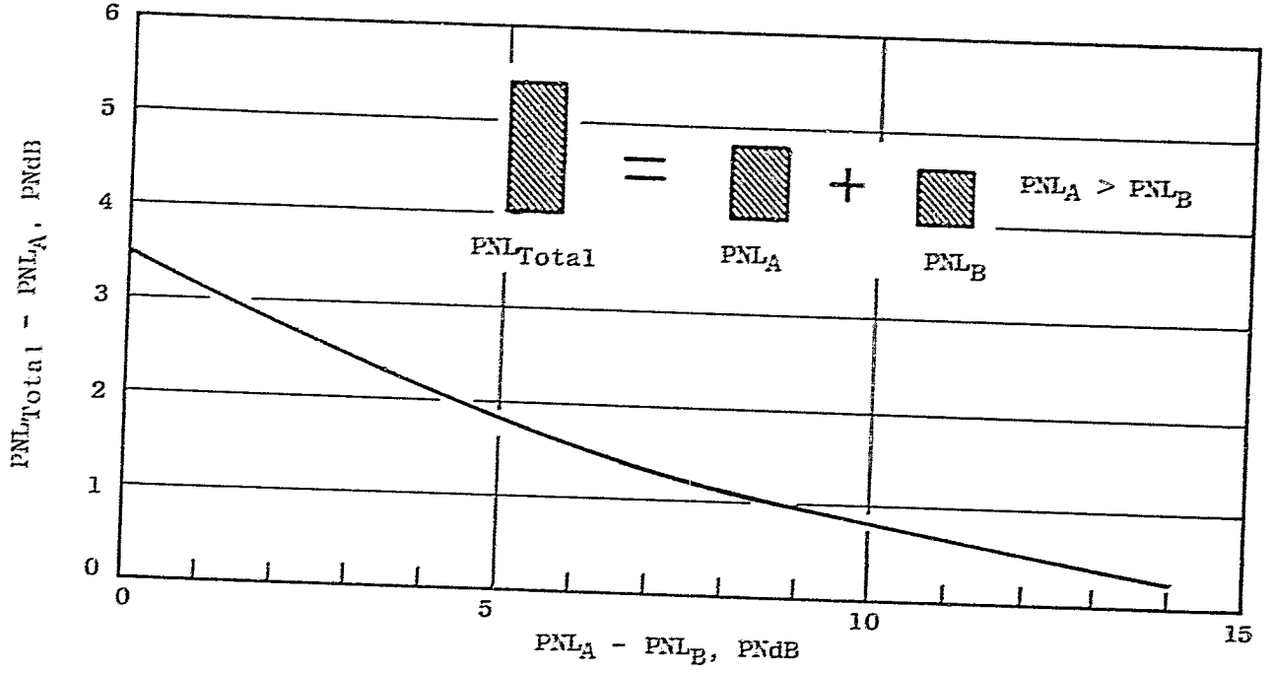

Figure 50. Empirical Curve for Adding Constituent PNL's with Non-Similar Spectra.

UPWARD AND DOWNWARD EXHAUSTING REVERSE THRUST CONFIGURATIONS

- NOMINAL BLOCKER SPACING
- NOMINAL BLOCKER HEIGHT
- 30^{0} NOMINAL LIP

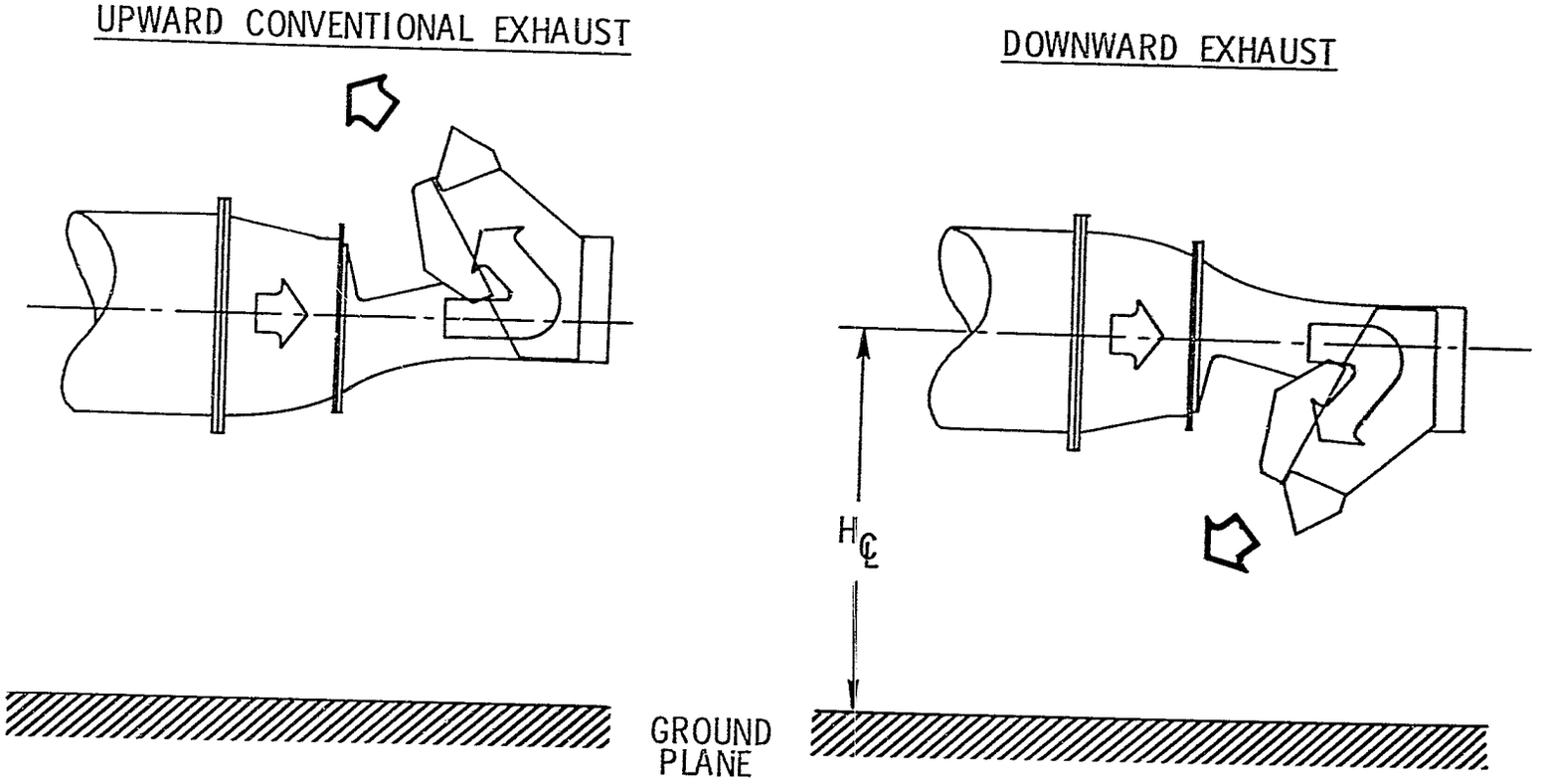

Figure 51. Upward and Downward Exhaust Reverse Thrust Configurations.

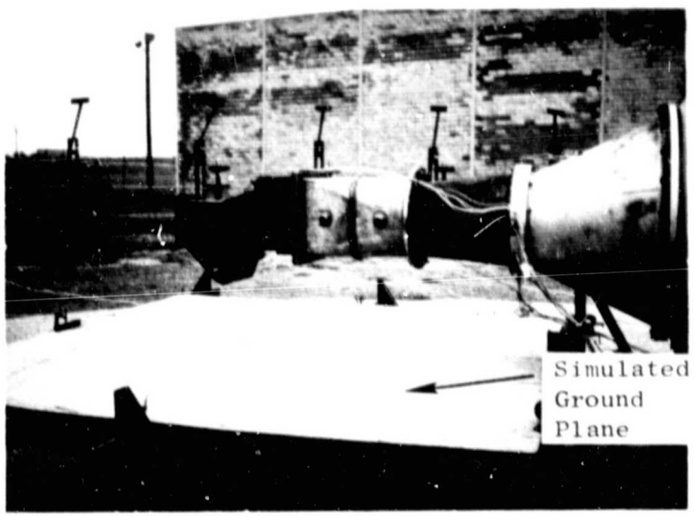

Figure 52. Photograph of Downward Exhausting Reverse Thrust Configuration.

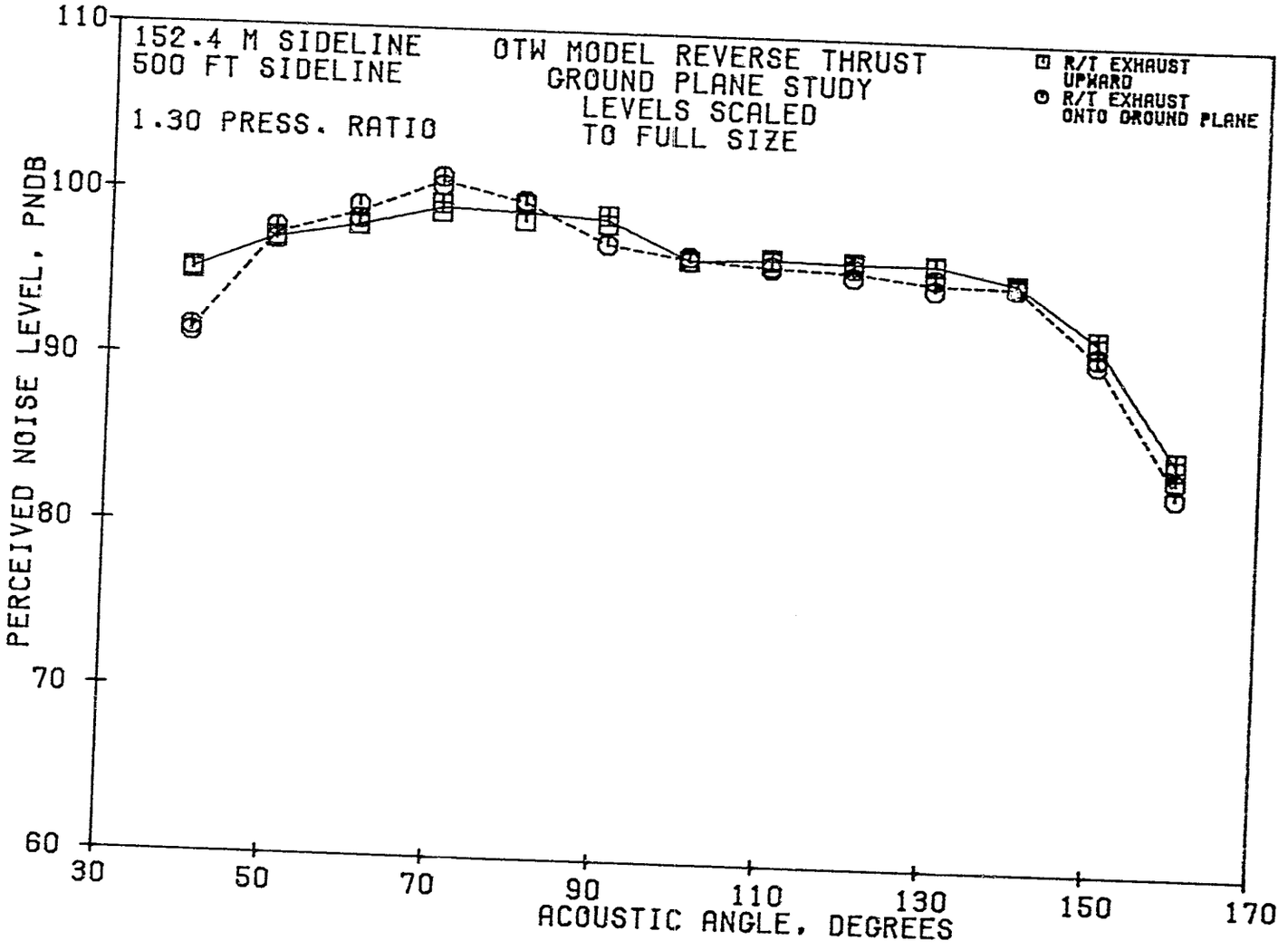

Figure 53. Reverse Thrust PNL Directivity for Upward and Downward Exhaust.

A spectral comparison of the two configurations is given in Figure 54 at the peak angle of 70 degrees. The low frequency SPL's are 5 to 7 dB higher for the downward exhausting orientation. Frequencies from 315 to 3150 Hz show a 1 to 2 dB increase over the conventional exhaust. The PNL difference between the two configurations at the peak angle is 1.5 to 2.0 PNdB as a function of pressure ratio as shown in Figure 55.

A correction procedure can be established for these two sets of data. For example, at the peak angle with the reverser exhausting downward the noise measured at the microphone is the totol of two sources - reverser noise and jet/ground interaction noise. Now the reverser noise is known from the conventional orientation; thus the jet/ground levels may be established by subtracting (antilogarithmically) the conventional levels from the total. These jet/ground interaction levels can then be removed from the levels measured on the downward exhausting full-size OTW engine at the Peebles Test Operation to give reverser noise only.

The second alternate orientation of the thrust reverser involved a rotation of 90 degrees so that the exhaust exited horizontal or parallel to the ground. This is shown in Figure 56. This type of orientation represents a "fly-under" measurement and not a true sideline.

For this orientation, the reverser geometry was nominal spacing, nominal blocker height, and 20 degree extended lip. A PNL directivity comparison between the conventional upward exhaust and the horizontal exhaust is shown in Figure 57. There is a significant difference in the directivity pattern of the upward and horizontal exhausts. This is most likely due to the asymmetry of the jet and the reorientation of the jet. These directivity differences could be applied to measured engine levels to obtain a sideline level should the engine be tested in a horizontally exhausting configuration.

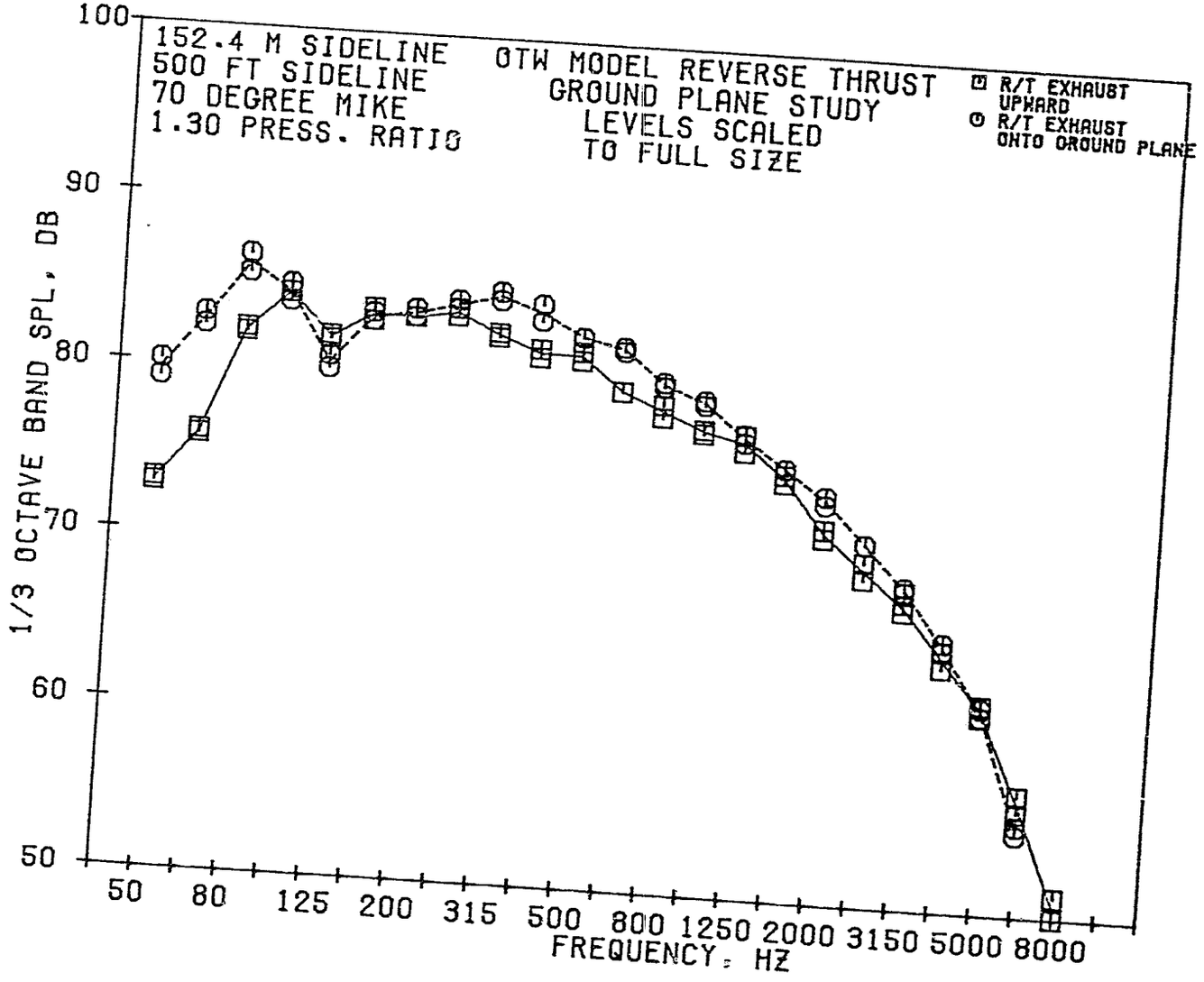

Figure 54. Reverse Thrust SPL Spectral Variation for Upward and Downward Exhaust.

- Reverse Thrust
- 152 m (500 ft) Sideline
- Nominal Spacing
- Nominal Blocker Height
- 30° Nominal Length Lip
- Single Engine

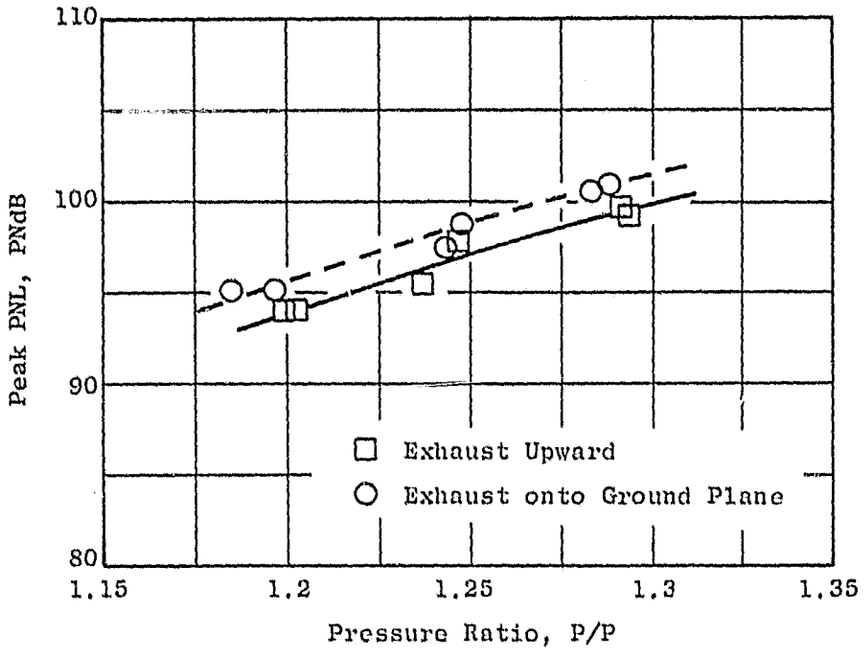

Figure 55. Reverse Thrust Peak PNL Variation for Upward and Downward Exhaust as a Function of Pressure Ratio.

- Nominal Blocker Spacing
- Nominal Blocker Height
- 20° Extended Lip

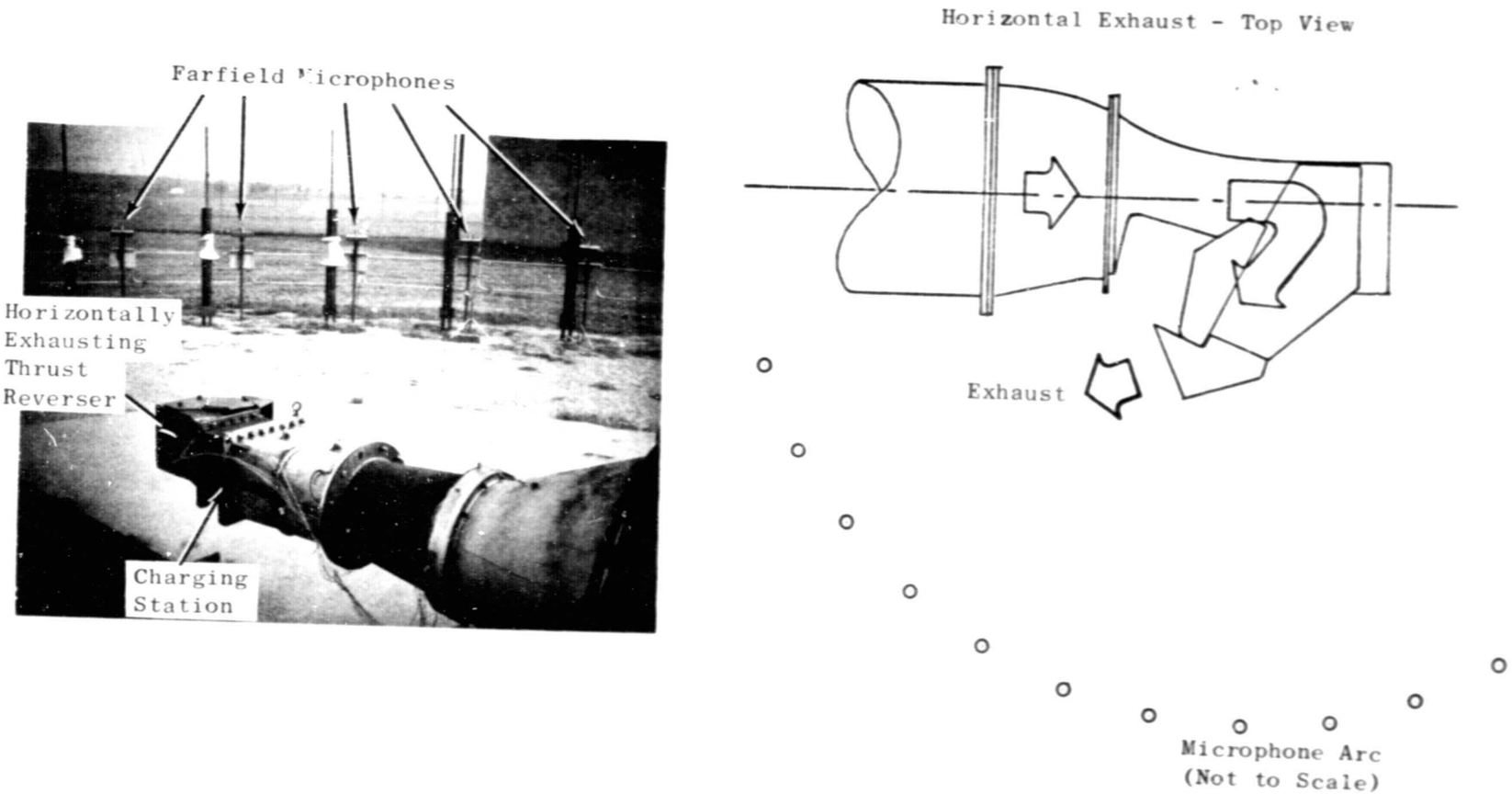

Figure 56. Horizontal Exhausting Reverse Thrust Configuration.

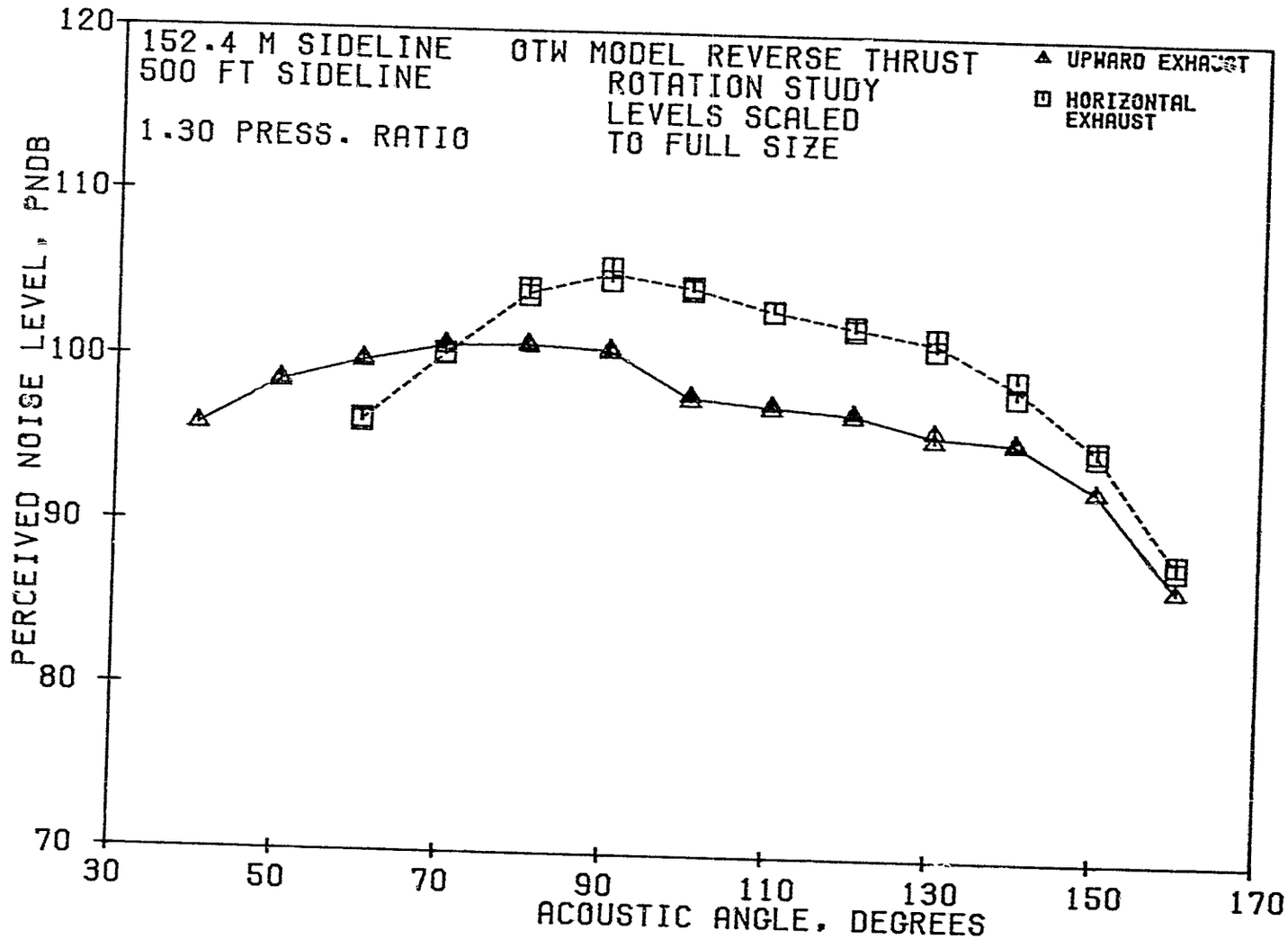

Figure 57. Reverse Thrust PNL Directivity Variation with Upward and Horizontal Exhaust.

SECTION VIII

CONCLUSIONS

1. The thrust reverser tests indicate the extended blocker height configuration with nominal blocker spacing and nominal length 30 degree lip meets the thrust goal of 35 percent of takeoff thrust at a 1.2 pressure ratio with a 152.4 m (500 ft) sideline noise level of 98.0 PNdB. However, the instrumentation and procedures used here are capable of yielding only approximate values of reverser weight flow and thrust.

2. Orienting the thrust reverser nozzle downward resulted in differences up to 1.5 PNdB in noise at sideline angles which must be accounted for in full scale engine tests.

3. Orienting the thrust reverser horizontal resulted in significant directivity changes which must be accounted for in full scale engine tests.

4. Installation of a long stub wing with the cruise nozzle resulted in a 2 to 3 PNdB increase in noise.

5. Installation of a short stub wing with the takeoff nozzle resulted in no change in the noise level or aerodynamic performance of the takeoff nozzle.

SECTION IX

NOMENCLATURE

Symbol or Abbreviation	Definition	Units
A	Blocker door offset	cm (in.)
BPF	Blade passing frequency	Hz
D_{TH}	Charging station height	cm (in.)
F_o	Thrust	N (lb)
h	Blocker tip spacing	cm (in.)
H	Blocker height to lip	cm (in.)
H_B	Blocker target height	cm (in.)
$H_{\mathcal{E}}$	Height of centerline above ground	m (ft)
l	Blocker door discharge slant height	cm (in.)
L	Axial lip length	cm (in.)
P_o	Ambient pressure	N/m^2 (psia)
P_T	Total pressure	N/m^2 (psia)
ΔP_T	Total pressure loss	N/m^2 (psia)
PNL	Perceived noise level	PNdB
q	Dynamic pressure	N/m^2 (psia)
S	Spacing to lip trailing edge	cm (in.)
SPL	Sound pressure level, re 0.0002 microbar	dB
T	Jet thickness	cm (in.)
T_T	Total temperature	K (° R)
W	Weight flow	kg/sec (lbm/sec)
X	Spacing to blocker door	cm (in.)
α	Blocker door inclination angle	degrees
β	Lip exit angle	degrees
$\beta_{effective}$	Effective blocker door discharge angle	degrees
θ	Charging station floor angle	degrees

SECTION X

REFERENCE

1. Adamson, A.P., "Quiet Clean Short-Haul Experimental Engine (QCSEE) Design Rationale," Society of Automotive Engineers, Air Transportation Meeting, Hartford, Connecticut, May 6-8, 1975, Paper Number 750605.

2. "Standard Values of Atmospheric Absorption as a Function of Temperature and Humidity for use in Evaluating Aircraft Flyover Noise," Aerospace Recommended Practice No. 866, SAE, August, 1964.

3. Ammer, R.C., Kutney, J.T., "Analysis and Documentation of QCSEE (Quiet Clean Short-Haul Experimental Engine) Over-the-Wing Exhaust System Development," NASA Contractor Report 2792, December, 1976.

4. "Quiet Clean Short-Haul Experimental Engine (QCSEE), Preliminary Analyses and Design Report," NASA Contractor Report Numbers 134838 and 134839, December 1974.